Simulating carbon stocks and fluxes of the Amazon rainforest: a journey across temporal and spatial scales

Dissertation

zur Erlangung des akademischen Grades
doctor rerum naturalium (Dr. rer. nat.)

Universität Osnabrück
Fachbereich Mathematik/Informatik

vorgelegt von
Edna Rödig
geboren in Heinsberg

Betreuer:
Prof. Dr. Andreas Huth
Dr. Matthias Cuntz

DANKSAGUNG

An dieser Stelle möchte ich mich bei all denen bedanken, die mich in den letzten Jahren auf verschiedenste Weise unterstützt haben. Ohne euch wäre die Erstellung dieser Arbeit nicht möglich gewesen.

Mein erster und besonderer Dank gilt meinen beiden Betreuern Andreas Huth und Matthias Cuntz, die mir die Möglichkeit gaben diese Arbeit anzufertigen. Andreas, dir danke ich für deine freundliche Art und deinen Enthusiasmus, die sich in einer tollen Arbeitsatmosphäre der Arbeitsgruppe wiederspiegeln. Du hast mir beigebracht die Wissenschaft nicht nur technisch zu betrachten. Außerdem danke ich für die vielen Möglichkeiten auf Konferenzen zu fahren, für die Dienstreise in den guyanischen Regenwald, für die ausführlichen Diskussionen über Conclusion-Folien und für die guten Weine bei den Weinproben. Matthias, dir danke ich für dein methodisches Wissen, dein unendliches Literaturwissen und die viele Zeit, die du dir genommen hast.

Ein großer Dank geht an die FORMIND-Gruppe: Franzi für dein photographisches Gedächtnis bezüglich des FORMIND Source Codes, die beste Konferenzbegleitung und die zahlreichen Kaffee- und Weinspaziergänge, Rico für deine aufmunternden Worte, dein offenes Ohr und dein Parametrisierungswissen, Friedrich für dein inspirierendes Chaos in zu viel Linie und deine Rückendeckung, Niko für deine Kenntnisse zur Fernerkundung und für deine Geduld beim Erlernen von Baumarten, Sebastian P. und Michael dafür, dass ihr FORMIND auf Linux zum Laufen gebracht habt, und eure erheiternde Art, Mateus für dein Amazonaswissen und deine brasilianischen Köstlichkeiten, Sebastian L. für deine Lektionen in Programmierung und Optimierung.

Desweitern danke ich dem BAE-Team dafür, dass ihr mir beigebracht habt, was es heißt Daten zu erheben und mit welchen Komplikationen zu rechnen ist. Insbesondere möchte ich mich bei dir, Corinna, bedanken, dass du mich in die Eddy-Kovarianz Methode eingeführt hast und mir stets bei Fragen zur Seite standst.

Niko und Sara - wir haben das tollste und hübscheste Büro am UFZ! Danke (auch an Meike), für die gute Laune im letzten Jahr – ich habe sehr viel mit euch gelacht. Unser Büro wäre natürlich nur halb so schön, wenn du nicht gewesen wärst, liebe Gaby. Danke auch, dass du einfach auf alles Bürokratische eine Antwort weißt und stets gut gelaunt bist. An dieser Stelle geht ein besonderer Dank an die gesamte OESA für die freundliche Atmosphäre. Ich danke natürlich auch dem OESA-Chor für die Motivation und die Gedanken-befreienden Proben.

Ich danke der ganzen CHS für die schönen Jahre in Gebäude 7, insbesondere euch, Martin und Benjamin, für den guten Start in unsere Promotionszeit, Jule für dein Kalibrierungswissen, Matthias für deine Eve-Kenntnisse und Rohini für deine anregenden Ideen.

Dir, Anja, möchte ich für die Unterstützung bei meinen Manuskripten danken und dir, Jens, für dein Statistikwissen und die inspirierenden Diskussionen zum Amazonas.

Danke an meine Korrekturleser: Lennart, Colin, Matthias und meine Eltern.

Ein großer Dank geht an meine Freunde und WG für amüsante und ablenkende Abende und Wochenenden. Meinen lieben Eltern möchte ich danken, dass ihr mich über so viele Jahre auf meinen (Um-)Wegen und bei meinen Entscheidungen unterstützt habt. Auch dir, Matthias, gilt ein besonderer Dank, dass du mich immer wieder aufheiterst und für mich da bist.

ABSTRACT

Global forests cover approximately 30% of land's surface storing around 45% of aboveground terrestrial carbon. This carbon storage is constantly endangered by anthropogenic activities. Especially, tropical regions like the Amazon rainforest suffer from deforestation taking a great share in global CO_2 emissions. In addition, forest dynamics are affected by climatic change like more frequent drought events. Quantifying the impact and feedback mechanisms of such climatic and anthropogenic changes on the global carbon cycle is still a great challenge.

In this thesis, we developed a regionalization scheme to apply a forest gap model on the entire Amazon rainforest. Such a forest model has the advantage that it calculates forest growth at the individual tree level. It considers different successional states, that evolve form natural forest dynamics and disturbances, including information on tree height and species. The regionalized forest model thereby allows for integrating forest structure and species compositions into large-scale carbon analyses. The approach is independent of spatial scale and the simulation results can be linked to measurements from field inventory, eddy covariance, and remote sensing at local to continental scales.

In a first study (chapter 2), we tested the capability of the forest model FORMIND to simulate gross primary production (GPP), respiration, and net ecosystem exchange (NEE) at daily and yearly time scales. The forest model was applied to spruce forests in Germany in order to analyze how the variability in environmental factors affects simulated carbon fluxes.

Simulation results were compared to 6 years of eddy covariance (EC) data at a daily scale. The analysis shows that the forest model described the seasonal cycle of the carbon fluxes correctly, but estimated GPP differed from the observed data on days with extreme climatic conditions. Based on these findings, we developed two new parameterizations. One resulted from a numerical calibration against EC data. The other parameterization resulted from a method where EC data is filtered to extract the limiting factors for productivity. Thereby, new parameter values and even a new function for the temperature limitation of photosynthesis were found. The adopted forest model was then tested successfully at another spruce forest for cross validation.

In general, the forest model reproduced the observed carbon fluxes of a forest ecosystem quite well. Although the overall performance of the calibrated model version was best, the filtering approach showed that calibrated parameter values did not necessarily correctly display the individual functional relations. The study has shown that the con-

cept of simulating forest dynamics at the individual tree level is a valuable approach for simulating the NEE, GPP, and respiration of forest ecosystems.

The focus of the second study (chapter 3) lied on the simulation of forest structure and above-ground biomass in the Amazon region with the forest model FORMIND. Estimating the spatial variation of biomass in the Amazon rainforest is challenging and, hence, a source of substantial uncertainty in the assessment of the global carbon cycle. On the one hand, estimates need to consider small-scale variations of forest structures due to natural tree mortality. On the other hand, it requires large-scale information on the state of the forest that can be detected by remote sensing. We, here, introduced a novel method that considered both aspects by linking the forest model and a wall-to-wall canopy height map derived from LIDAR remote sensing.

The forest model was applied to estimate above-ground biomass stocks across the Amazon rainforest. This allowed for the direct comparison of simulated and observed canopy heights from remote sensing. The comparison enabled the detection of disturbed forest states from which we derived a biomass map of the Amazon rainforest at 0.16 ha resolution.

Simulated biomass varied between 20 and 490 t (dry mass) ha^{-1} across 7.8 Mio km^2 of the Amazon rainforest (elevation < 1000 m). That equals a total above-ground biomass stock of 76 GtC with a strong spatial variation (coefficient of variation = 63%). The estimated biomass values fit estimates, that had been observed in 114 field inventories, well (deviation of only 15%). Beside biomass, the forest model allowed for estimating additional forest attributes such as basal area and stem density.

The linkage of a forest model with a canopy height map allows for capturing forest structures at the individual to large scale. The approach is flexible and can also be combined with measurements of future satellite missions like ESA Biomass or GEDI. Hence, the study sets a basis for large-scale analyses of the heterogeneous structure of tropical forests and their carbon cycle.

In a third study (chapter 4), we analyzed the interactions of productivity, biomass, and forest structure that are essential for understanding ecosystem's response to climatic and anthropogenic changes. We here applied the forest model on the Amazon rainforest, combined simulation results with remotely-sensed data as in chapter 3, and additionally simulated ecosystem carbon fluxes.

We found that the successional state of a forest has a strong influence on mean annual net ecosystem productivity (NEP), woody above-ground net primary production (wANPP), and net ecosystem productivity (NEP). These relations were used to derive maps of carbon fluxes at 0.16 ha resolutions (current state of the Amazon rainforest under spatial heterogenic environmental conditions). The Amazon was estimated to be a sink of atmospheric carbon with a mean NEP of 0.73 tC ha^{-1} a^{-1}. Mean wANPP equals 4.16 tC ha^{-1} a^{-1} and GPP 25.2 tC ha^{-1} a^{-1}. We found that forests in intermedi-

ate successional states are the most productive. Under current conditions, the Amazon rainforest takes up 0.59 PgC per year.

This third study shows that forest structure and species compositions substantially influence productivity and biomass, and should not be neglected when estimating current carbon budgets or climate change scenarios for the Amazon rainforest.

The findings of this thesis set a fundament for future analyses on carbon storage and fluxes of forests. Simulating at the tree level has the potential to investigate carbon dynamics from individual to continental scales. The regionalized forest model allows for the integration of different types of remotely sensed data in order to improve the spatial accuracy of estimates. The insights, we have gained from the eddy covariance study (chapter 2), help to investigate carbon dynamics of forests at continental scale also under changing climate. In combination with the regionalization approach (chapter 3 and 4), the findings of this thesis may be used to complement studies on drought events in forests and to understand feedback mechanisms caused by anthropogenic disturbances.

CONTENTS

1 INTRODUCTION

About 32% of CO_2 emissions are associated to deforestation of forests and land-use change (IPCC, 2013). In particular, tropical forests in developing countries are endangered (UN-REDD, 2011). The United Nations Framework Convention on Climate Change has expressed its concerns regarding the protection of forests (UNFCCC, 2010; Keenan et al., 2015) and founded an initiative for Reducing Emissions from Deforestation and forest Degradation (REDD+). Such international activities depend on reliable information on trends and states of global forests to inform and influence decision- and policymakers.

This thesis aims for a better understanding on the role of forests in the global carbon cycle (Fig. 1.1). It focuses on the assessment of forest's carbon pools and dynamics across temporal and spatial scales with a particular focus on the largest rainforest of the world – the Amazon.

1.1 THE ROLE OF FORESTS IN THE GLOBAL CARBON CYCLE

1.1.1 *The global carbon cycle*

The global carbon cycle describes the exchange of carbon between land, ocean, and the atmosphere including their responses to human activities and climatic changes. In a simplified description (Fig. 1.1), the cycle contains four major compartments: uptake of atmospheric carbon due to (1) vegetation and (2) the ocean, and carbon emission by (3) industries and fossil fuels, and (4) land-use change [Le Quéré et al., 2016].

Under current climate and human impact, carbon emissions are twice as large as carbon uptake [5.7 GtC a^{-1} uptake vs. 10.3 GtC a^{-1} emissions, Fig. 1.1, Le Quéré et al., 2016]. Hence, the concentration of CO_2 in the atmosphere is constantly increasing. The Mauna Loa Observatory in Hawaii records CO_2 concentration in the atmosphere since 1958. The carbon dioxide concentration has increased from below 320 parts per million (ppm, the ratio of the number of gas molecules to the total number of molecules of dry air) to above 400 ppm within the last 59 years [Tans and Keeling, 2017]. It is assumed that in preindustrial times, CO_2 concentration in the atmosphere oscillated in 100,000-year cycles by 100 ppm ranging between 180-280 ppm. Nowadays, it increases 10 to 100 times faster than in preindustrial times [Falkowski, 2000]. The latest Intergovernmental Panel on Climate Change (IPPC) reports a potential increase of CO_2 concentration of up

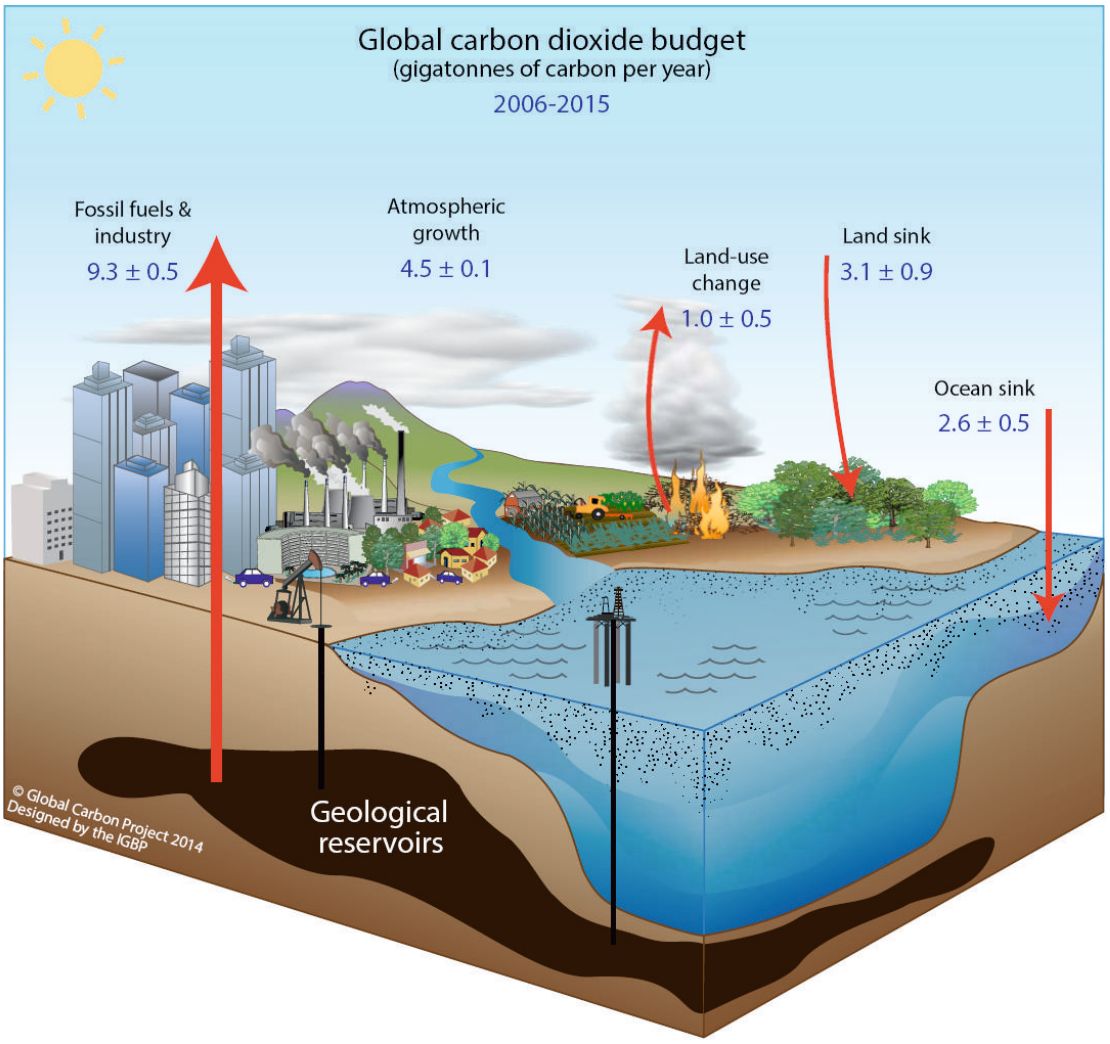

Figure 1.1: A simplified scheme of the global carbon cycle [Le Quéré et al., 2016].

to 800 ppm until the end of this century. Climate models project that this increase comes along with a temperature increase of up to 4.5°C [IPCC, 2013].

Processes of the global carbon cycle act on timescales that range from hours to millions of years. In oceans, the exchange of carbon acts on hours to millennia. Photosynthetic activities of algae take place permanently near the ocean's surface while the thermohaline ocean circulation (vertical deep water currents) can delay the exchange with the atmosphere by thousands of years [Mopper et al., 1991]. The exchange of carbon between vegetation and the atmosphere acts at hourly time scales to decades. Photosynthesis, plant respiration, and soil processes happen permanently; disturbances such as fires or land-use change take place on days to years. Turnover times of carbon in vegetation happen within decades and centuries [Falkowski, 2000]. Industries emit carbon constantly over days to decades and burn fossil fuels that are built up over millions of years [Berner, 2003].

Beside these differences in temporal scales, the global carbon cycle interacts with other biogeochemical cycles, e.g., the water and nitrogen cycle [Falkowski, 2000]. Additionally, complex feedback mechanisms have been detected which are still poorly understood [Schimel, 1995; Schimel et al., 2015]. This limited understanding leads to difficulties regarding the estimation of carbon fluxes, in particular within vegetation [Hoffman and Randerson, 2013; Friend et al., 2014], and at coastal oceans [Bauer et al., 2013] which are both exposed to anthropogenic disturbances. Thus, analyzing human impact on vegetation and coastal oceans remains an important task to increase the certainty of estimated shares in the global carbon cycle.

Vegetation is a component of the global carbon cycle that is challenging to estimate. Its contribution is mainly calculated as the residual of all other compartments taking their individual uncertainties along [Le Quéré et al., 2016]. Latest estimates state that with 3.1 GtC per year it is also the largest sink of atmospheric carbon [Le Quéré et al., 2016] of which around one third is associated to forests [$\sim$1.1 GtC a^{-1}, Pan et al., 2011].

1.1.2 *Global forests and the carbon cycle*

Forests cover around 30 Mio km^2 of land's surface of which 57% are assigned to the tropics, 16% to the temperate zones, and 27% to the boreal zone [Hansen et al., 2010]. Last decade's research has gained a lot of knowledge on the role of forests in the carbon cycle. For example, it has been explored how forests respond to climatic changes. Temperature and precipitation seem to correlate positively with gross primary production [Beer et al., 2010] and carbon turnover rates [Carvalhais et al., 2014]. Woody productivity of temperate forests increases with increasing CO_2 concentration in the atmosphere [FACE experiment where air enriched CO_2 is released to plants, Ainsworth and Long, 2005]. At the same time, climate responds to changes in forest ecosystems. A coupled-carbon-climate model predicts that deforestation of tropical forests could lead to an increase in evaporative cooling of the atmosphere while it might lead to warming at higher latitudes [Bala et al., 2007].

However, it is challenging to include such natural and human-induced processes in the assessment of global forest carbon stocks and dynamics. In large-scale vegetation models, carbon stocks and fluxes are often calculated for 'average' forest biomes which do not consider the variability of ecosystems, especially in the tropics [Houghton, 2005]. Hence, the following numbers are only rough estimates: Based on field observations and statistical and process-based models, the current amount of carbon stored in all forests of the world is estimated to be around 860 GtC. 55% are allocated to the tropics, 32% to the boreal zone, and 14% to the temperate zone [Pan et al., 2011]. A diagnostic model approach that extrapolates eddy covariance data into space, estimates total GPP of forests to be 59.0 GtC per year; tropical forests are the most productive with 40.8 GtC

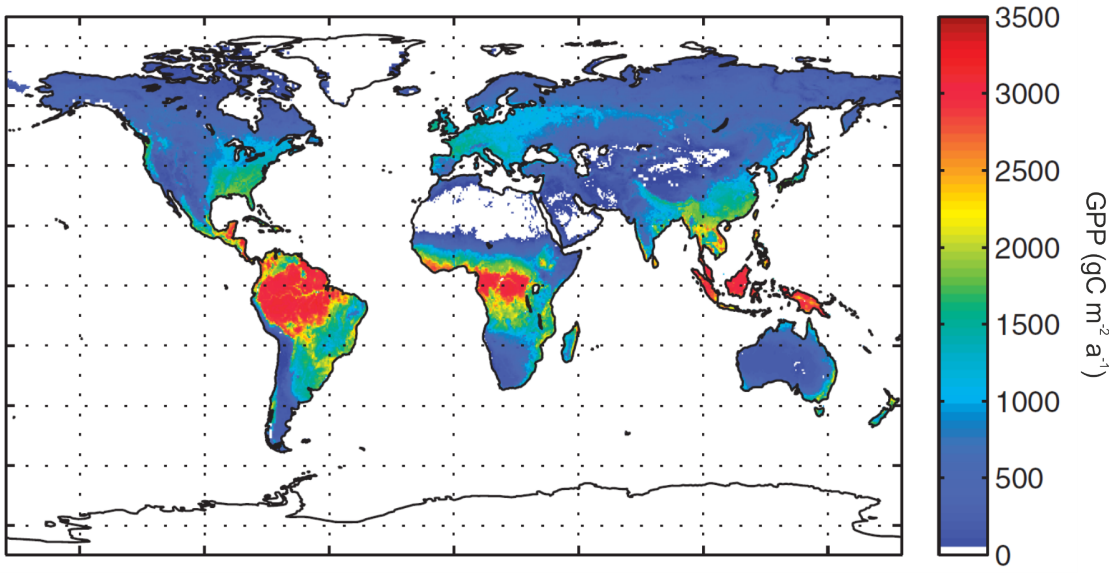

Figure 1.2: Spatial variation of annual gross primary production (GPP) extrapolated from eddy covariance measurements via a diagnostic model (gC m^{-2} a^{-1}) [after Beer et al., 2010]

.

per year (Fig. 1.1.2), compared to a GPP of 9.9 GtC per year in temperate forests and 8.3 GtC per year in boreal forests [Beer et al., 2010]. In summary, it is noticeable that in particular tropical forests take a great share in global vegetation dynamics. The main focus of this thesis lies on the Amazon rainforest – the largest intact tropical forest of the world [Hansen et al., 2010] which is introduced in more detail in the following.

1.1.3 *The Amazon rainforest*

The Amazon rainforest includes all lowland tropical forest of South America [Malhi et al., 2006] which is the largest area of tropical rainforest of the world. It is characterized by heavy rainfall (precipitation of 1000 mm per year in seasonal regions and up to 8000 mm per year in central Amazon), high temperatures (coldest monthly mean above 20°C), and high diversity [FAO, 2001], hosting around 16,000 tree species[ter Steege et al., 2013].

Estimates on the amount of carbon stored in the Amazon rainforest diverge strongly. Above-ground biomass estimates range from 38.9 to 93 GtC [Houghton et al., 2001; Malhi et al., 2006; Saatchi et al., 2007, 2011]. One reason for divergences in estimates is that processes, that drive spatial variations of carbon stocks and fluxes, are still poorly understood [Phillips et al., 2009; Malhi et al., 2015].

Field campaigns showed that mean wood density is lower in forests of the western Amazon than in the slower-growing forests of the eastern Amazon [Baker et al., 2004;

Figure 1.3: Evaporating Amazon rainforest (French Guyana) after a heavy rainfall.

Chave et al., 2006; Malhi et al., 2006]. This finding led to diverging assumptions on potential drivers for such a spatial variation in literature within the last years. Spatial variations in dynamics and stocks may be related to environmental conditions such as seasonality [Chave et al., 2006; Malhi et al., 2006]. A more recent study shows that soil properties may additionally influence forest dynamics [Quesada et al., 2012]. It seems likely that biomass patterns are driven by patterns of tree mortality rates [Galbraith et al., 2013; Malhi et al., 2015] and small-scale disturbances [Chambers et al., 2013b; Espírito-Santo et al., 2014].

Beside studies on the spatial variation of biomass across the Amazon rainforest, last decade's research has focused on understanding the response of the forest to climatic and human-induced changes. The drought events of the past decade gave insights on the vulnerability of trees to water and temperatures stress in the Amazon [Phillips et al., 2009]. It was found that the drought events of 2005 and 2010 reduced photosynthesis (0.38 GtC a^{-1} in 2010), but tree growth seemed unaffected. Net primary production (NPP) stayed constant throughout the extreme event compensating the reduction of GPP by an reduction in maintenance respiration [Doughty et al., 2015]. To the disadvantage of the trees' maintenance, the reduction of photosynthesis rather led to an increase in tree mortality [Brienen et al., 2015b]. It is expected that the Amazon might become a carbon source in the future due to an increase of drought events and drought-related

fires [Gatti et al., 2014]. Such events will intensify the additional carbon emission due to human-induced forest degradation such as fragmentation [Laurance, 1997; Numata et al., 2010; Pütz et al., 2014] and selective logging [Asner et al., 2002].

Future predictions on the behavior of the Amazon rainforest regarding climatic changes remain a challenge. Several global vegetation models project the potential of an Amazon forest 'dieback', a collapse of the Amazon as a consequence to climatic changes [Cox et al., 2000]. However, the intensity of an Amazon 'dieback' and sensitivities to climatic changes varies among vegetation models [Huntingford et al., 2008; Rammig et al., 2010; Cox et al., 2013]. A recent study even shows that carbon stocks in the Amazon rainforest might be resilient regarding climatic change due to a shift in plant trait diversity [Sakschewski et al., 2016].

1.2 MONITORING AND ESTIMATING CARBON BUDGETS AND FLUXES OF FORESTS ACROSS SCALES

Various methods have been developed to monitor and estimate carbon budgets and fluxes of forest ecosystems at different temporal and spatial scales (Tab. 1.1). Local estimates, derived from eddy covariance measurements or simulated with forest gap models, have proven to give detailed information on forest dynamics. Global estimates, derived from remote sensing or simulated with global vegetation models, give insights into the variation across biomes. Products of those tools are biomass, biomass increment, net primary production (NPP), gross primary production (GPP), respiratory pathways, and net ecosystem exchange (NEE)/net ecosystem productivity (NEP).

These methods come from different research disciplines which sometimes results in different terminologies. In this thesis, we handle the terms as followed (Fig. 1.4): Biomass of vegetation is described as the organic dry matter stored in vegetation (ODM, units in t ha^{-1}). In literature, biomass is also quantified as the amount of carbon deposited in vegetation (units explicitly contain C, e.g., tC ha^{-1}). Biomass of vegetation can be separated into above (stem, branches and leaves) and below-ground stocks (roots).

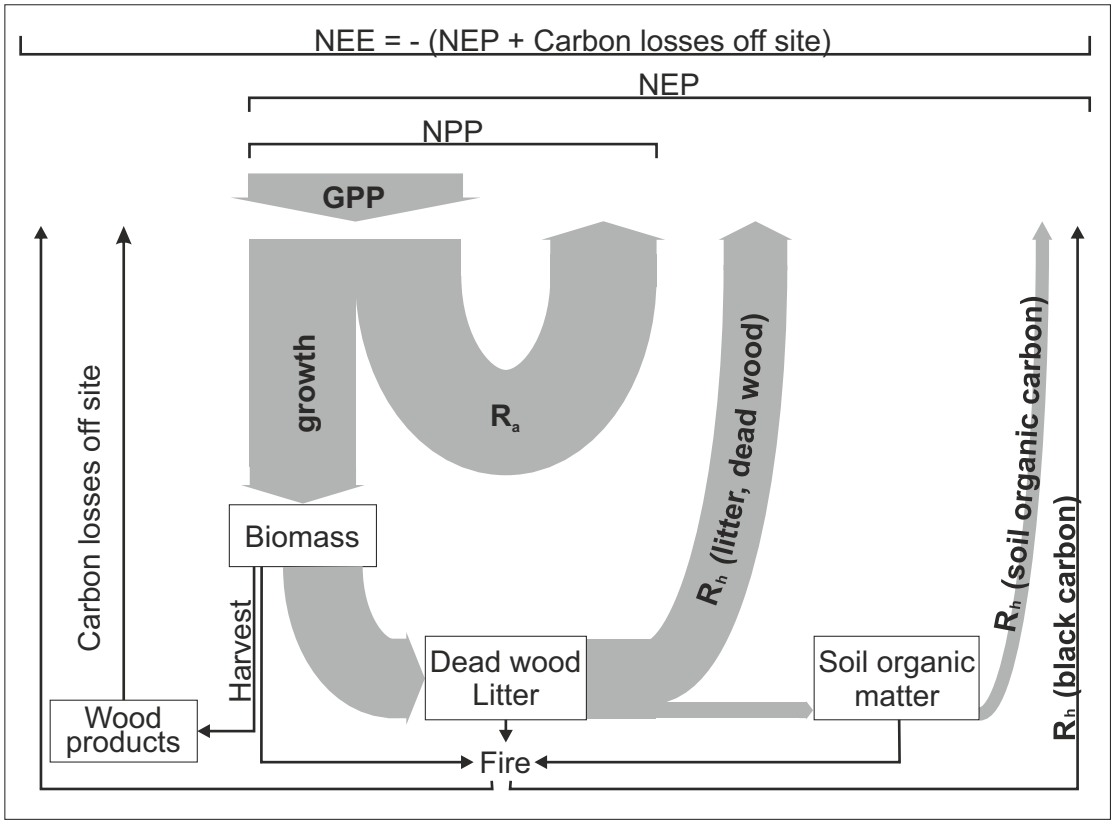

Figure 1.4: Flow chart of the terrestrial carbon cycle. Boxes indicate pools and arrows fluxes. NEP: net ecosystem productivity; NPP: net primary production; GPP: gross primary production; R_a: autotrophic respiration; R_h: heterotrophic respiration [modified from Schulze, 2000].

A number of methods measure carbon fluxes that go in and out of the forest ecosystem (the exchange of carbon over time). GPP is the gross uptake of carbon (per time) that is used for photosynthesis of vegetation. NPP is the net production of wood, branches, leaves, and roots. Biomass increment (often given in ODM) is often defined as the woody aboveground net primary production (wANPP).

Respiration can be separated into several pathways. The autotrophic respiration (R_a) is the respiration that includes growth and maintenance respiration (R_h) of trees; heterotrophic respiration describes the decomposition by microbial and animal activity [Luyssaert et al., 2007]. The sum of both is the ecosystem respiration. The difference between the GPP and ecosystem respiration then describes the NEP (Fig. 1.4).

The net ecosystem exchange (NEE) is the exchange of carbon from the ecosystem to the atmosphere. Note that the term NEE is often used in meteorology and describes the carbon exchange from the atmospheric point of view: a positive NEE is associated to a gain in atmospheric carbon. The term NEP, on the other hand, is mainly used in ecology and describes carbon fluxes from the forests' point of view: a positive NEP stands for a gain of carbon in the biosphere as we use it in this thesis. Strictly speaking, they do not only differentiate in their contrary algebraic sign (NEE=-NEP). As NEE is the total exchange of carbon, it also includes inorganic carbon that enters and leaves the ecosystem via, for example, ground water and rivers [Chapin et al., 2006].

Table 1.1: Overview over the spatial and temporal resolutions of different methods that estimate and monitor carbon fluxes and budgets. The information is gathered from literature introduced in chapter 1.2.

Tool	**Spatial resolution**	**Spatial extent**	**Temporal resolution** (time step)	**Temporal extent** (record length)	**References** (examples)
Field inventory	0.1-25 ha plots	local	hourly (dendrometer measurments) or census data	years-centuries	Cotta [1821]; Lopez-Gonzalez et al. [2011]; Anderson-Teixeira et al. [2015]
Eddy covariance	1-100 ha	local	1/2-hourly	few years	Friend et al. [2007]; Aubinet et al. [1999]
Remote sensing (passive sensors)	m to km, horizontal	local-global	hours–years	years-decades	Tucker et al. [1985]; Zhao et al. [2005]
Remote sensing (active sensors)	cm to m, horizontal and vertical	local-global	months-years	years-decades	Lefsky et al. [2005]; Saatchi et al. [2011]
Dynamic Global Vegetation Models	~0.5°-3°	regional-global	hours-year	centuries	Sitch et al. [2008]
Individual-based forest models	individual–0.1 ha	local-regional	hours-year	centuries	Bugmann [2001]; Fischer et al. [2016]

1.2.1 *Forest inventories*

Field inventory is the oldest technique to detect carbon stocks and analyze dynamics and development of a forest [e.g., yield tables, Cotta, 1821] by keeping records on changes in diameter of a tree at breast height (dbh, Fig. 1.5). Today, different networks exist compiling information on forest stands, for example, the CTFS-ForestGEO network with 63 sites [~25 ha each, Anderson-Teixeira et al., 2015] or the ForestPlots network with 2000 sites [~1 h, Lopez-Gonzalez et al., 2011].

Biomass stocks are often estimated via allometric relationships based on dbh and/or tree height [Chave et al., 2014]. NPP and GPP are indirectly assessed via monitoring biomass increment, root increment, and litter fall (Fig. 1.5 (b)) respiration [as in Malhi et al., 2015]. Aboveground processes, like biomass increment, are more frequently measured than belowground processes of fine and coarse roots which are difficult to access [Clark et al., 2001].

Although the number of assessable information on forest plots has increased, the number of sites in the tropics is still low compared to the temperate and boreal zones [Luyssaert et al., 2007; Schimel et al., 2015]. In addition, tropical inventories confront challenges in tree measurements, the determination of tree allometries and difficulties due to small sample sizes in highly heterogenic landscapes [Chave et al., 2004]. Regardless of these limitations, field inventories collect important and indispensable information. Long-term records provide insights into functional relations between forest attributes like biomass, productivity, and tree diversity. This information is a prerequisite for vegetation modeling and the ecological interpretation of eddy covariance and remote sensing measurements which are described in the following subsections.

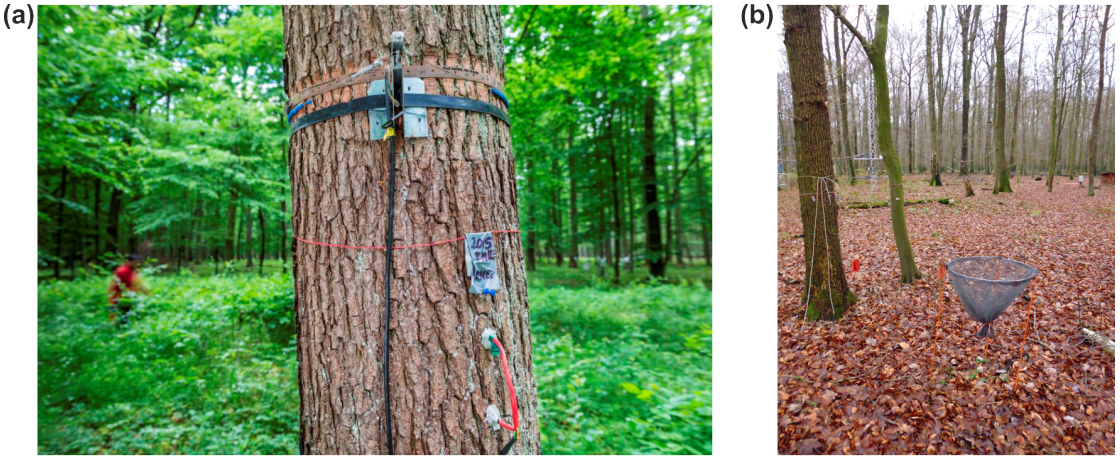

Figure 1.5: Measurements at Hohes Holz experimental site, Germany: (a) continuous measurements of diameter at breast height with a dendrometer (top) and of sap flow (below) (Foto: André Künzelmann, UFZ); (b) litter fall trap to estimate leaf turn over (Foto: Corinna Rebmann, UFZ).

1.2.2 *Eddy covariance method*

The eddy covariance method measures vertical turbulent fluxes of CO_2, heat, and water above vegetation. Fluxes result from the covariance of vertical wind velocity and its concentrations of, e.g., CO_2 [Baldocchi et al., 1988; Aubinet et al., 1999]. The technique enables monitoring inter-annual net fluctuation of sensible and latent heat fluxes, and net ecosystem exchange (NEE). Simultaneous recordings of meteorology allow for the partitioning of NEE into GPP and respiration. Night-time values of ecosystem respiration are extrapolated to daytime taking temperature sensibilities [Reichstein et al., 2005] and vapor pressure deficits into account [Lasslop et al., 2010].

In forests, the instruments are installed on a tower that emerges the top of the canopies (Fig. 1.6 (a)-(b)). The size of the footprint of an instrument depends on the height of the tower, the intensity and direction of the wind, and the surrounding terrain [Leclerc and Thurtell, 1990]. As a rule of thumb, it can reach areas around the tower that spread 100 times the height above the canopy [100-1000m, Baldocchi et al., 1996].

Today, more than 400 eddy-flux towers are installed worldwide. Most measurements are assessable in the global network FLUXNET [Fig. 1.6 (c), Baldocchi, 2014]. The highest density of towers is found in Europe and North America. Dense tropical forests are rather difficult to access and maintain, hence, only a few observations exist for the Amazon rainforest [Saleska et al., 2003; Bonal et al., 2008]. Currently, the FLUXNET network hosts data of 212 sites of which 23 are located in the tropics (23.5°S-23.5°N): 11 in Australia, 5 in Africa, 2 in Asia, 2 in Central America, and 3 in South America. Less than 50% (10 sites) of these are located in forests, the rest is placed in grasslands or savannas (counted from site list on `http://fluxnet.fluxdata.org/sites/site-list-and-pages/` on April, 1st 2017).

The eddy covariance method allows for investigating how the ecosystem responds to environmental conditions like light, seasonality, soil water, and temperature [e.g., Grace et al., 1996; Greco and Baldocchi, 1996; Saleska et al., 2003; Granier et al., 2007; Bonal et al., 2008], and anthropogenic disturbances [Baldocchi, 2014]. Eddy covariance measurements are used to validate global maps of GPP derived from remote sensing [Running et al., 2004] and validate and calibrate vegetation models [Krinner et al., 2005; Friend et al., 2007]. There have been first attempts to upscale flux measurements with the help of a diagnostic model approach [Beer et al., 2010] or remote sensing [Jung et al., 2011] to produce flux maps at the global scale at 0.5° resolution. These up-scaling approaches are challenging considering the fact that measurements are rare, in particular, in dense tropical forests. For example, 3 eddy covariance towers with a maximum footprint of 1 km^2 cover only $\sim$0.43μ% of the Amazon basin ($\sim$7 Mio ha). In order to fill these gaps and consider the effect of disturbances and climate into up-scaling approaches, it is promising to integrate vegetation modeling into large-scale estimates.

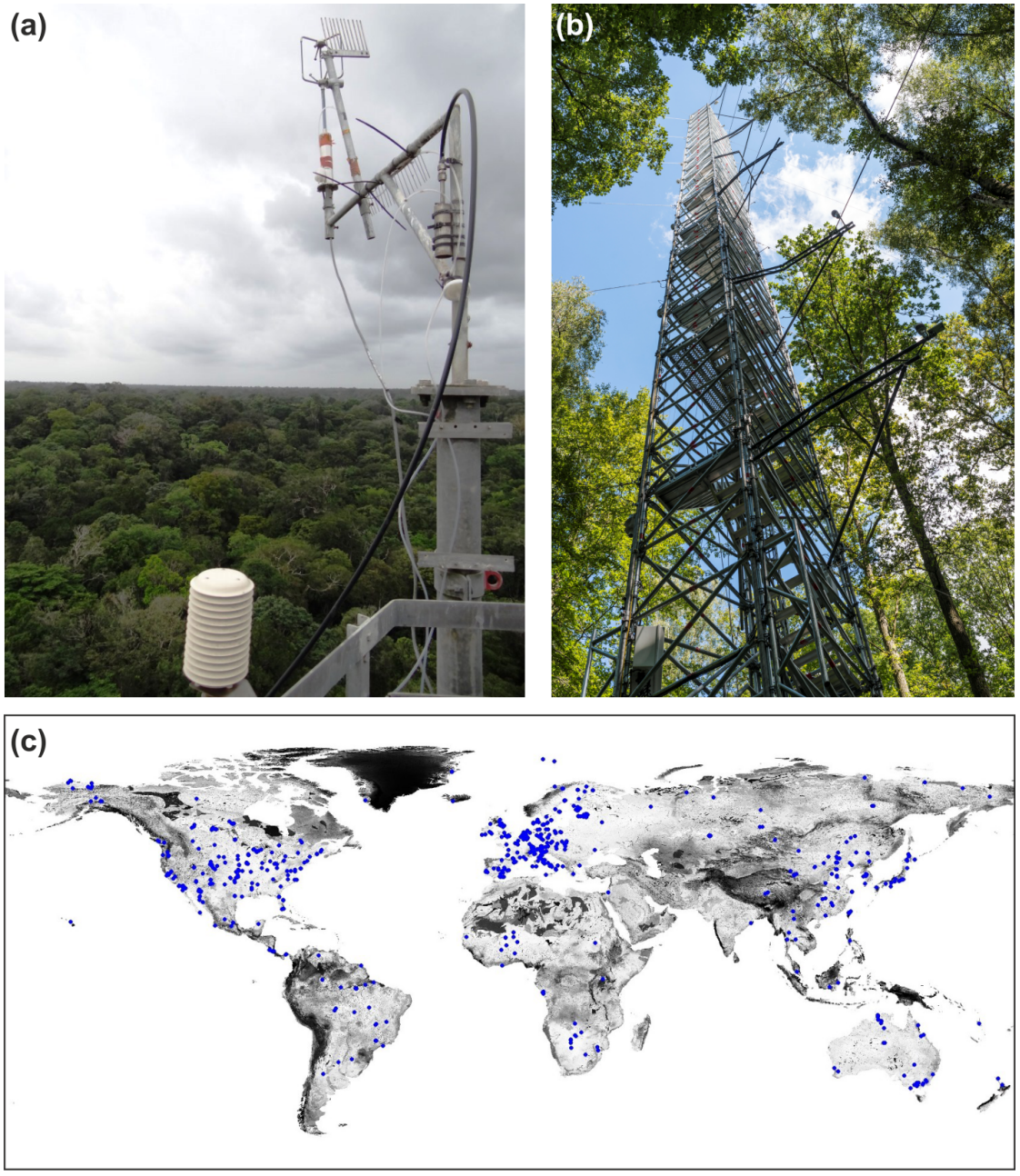

Figure 1.6: (a) Eddy covariance system with anemometer (measurement of wind velocity) and gas analyser (CO_2 concentration) on a 55m high tower in the tropics (Guyaflux, French Guyana). (b) Eddy covariance tower at a temperate forest (Hohes Holz, Germany, Foto: André Künzelmann, UFZ). (c) Locations of towers of the FLUXNET network (Figure: `http://fluxnet.fluxdata.org`, access date 02-21-2017).

1.2.3 *Remote sensing of vegetation*

Satellite-based remote sensing has revolutionized earth system monitoring in the 70s. Images from space enabled the detection of land-cover changes at a large scale. This new perspective from space helped to expand knowledge gained from ground observations to larger scales [COHEN and GOWARD, 2004; Jung et al., 2011].

Remote sensing sensors detect the intensity of radiation within wavelength bands [Turner et al., 2003]. Two types of sensors are used to explore vegetation from space: passive and active sensors. Passive sensors measure visible and infrared radiation that reaches the detector. Active sensors (Radio Detection And Ranging (RADAR) and Light Detection And Ranging (LIDAR)) actively send out signals and measure reflected energy.

One product of the passive sensor technique is the Normalized Difference Vegetation Index [NDVI Tucker et al., 1985] which detects differences in plant reflectance derived from satellite images (Fig. 1.7 (a)). In the 80s, it enabled to derive first biome-wide estimates of NPP [Fig. 1.7 (b), Goward et al., 1985; Tucker et al., 1985]. Deriving NPP from satellite images is based on the assumption that NPP and GPP are related to the NDVI and absorbed solar energy via a constant conversion factor [Running et al., 2004]. Modern technology allows for producing 8-day NPP and GPP maps at 1 km^2 resolution [Zhao et al., 2005] and analyzing last decade's trends of NPP [Fig. 1.7 (c), Zhao and Running, 2010]. The advantage of this approach is that it produces continuous maps at high temporal and spatial resolution. However, NDVI values tend to saturate in dense forest stands which can lead to, for example, an underestimation of leaf density and spatial heterogeneity in tropical regions [Myneni et al., 2001; Hall et al., 2011].

Another achievement of passive remote sensing are land cover maps [DeFries and Townshend, 1994; Hansen et al., 2000, 2013]. Vegetation types like grasslands, savannas, and different forest biomes are identified based on Landsat data. They serve to identify regions that are influenced by human activities which are known to have a strong influence on carbon dynamics [Houghton et al., 2012]. However, the extent of such influence is difficult to quantify and is one of the major challenges in the assessment of the global carbon cycle [Le Quéré et al., 2016]. One valuable information, that can contribute to a better understanding of carbon dynamics in forest ecosystems, is a three-dimensional perspective on forest structure which can only be provided by active remote sensing [Rosette et al., 2012]. Active sensors like RADAR and LIDAR can identify forest canopy heights that are related to forest biomass [Lefsky et al., 2005]. This relation was, for example, used to derive large scale maps of forest biomass from LIDAR measurements of the Geoscience Laser Altimeter System (GLAS) onboard Ice, Cloud and land Elevation Satellite (ICESat) [Saatchi et al., 2011; Baccini et al., 2012]. However, reflected signals of these sensors are discrete and the extrapolation of measurements to continuous maps

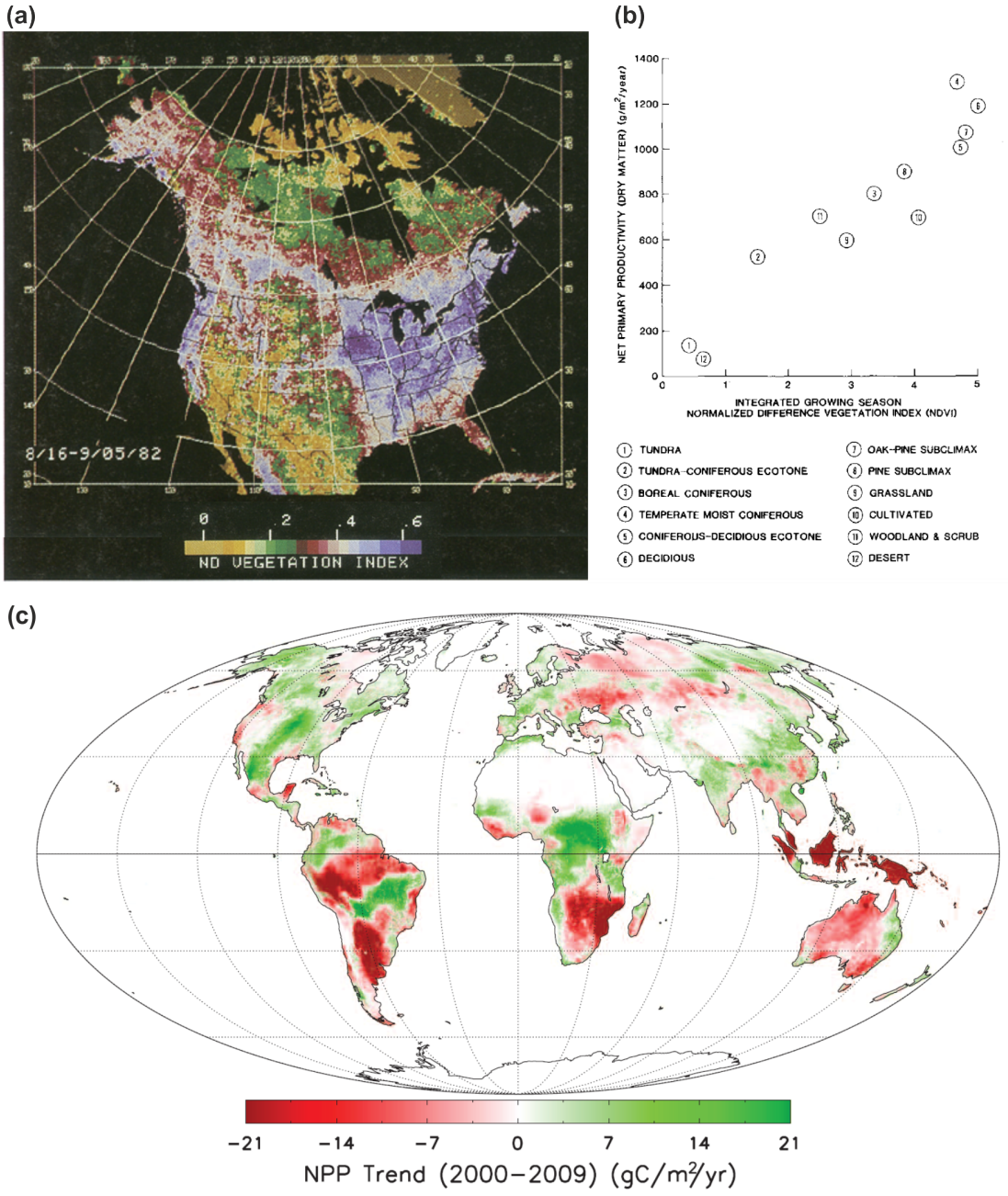

Figure 1.7: (a) Normalized difference vegetation index measurements (NDVI) for August 1982 for North America, and (b) derived biome-averaged net primary production (NPP) [both images from Goward et al., 1985]. (c) Linear trend of terrestrial NPP from 2000 through 2009 [image from Zhao and Running, 2010].

is challenging, especially in cloudy, tropical regions [Saatchi et al., 2011] where annual cloud cover exceeds 80% [Wilson and Jetz, 2016].

RADAR and LIDAR measurements of ongoing [Tandem-X and GEDI Krieger et al., 2007; NASA, 2017] and future satellite missions [Tandem-L, Moreira et al., 2015] will hopefully overcome this limitation. Although LIDAR measurements are easier to interpret for forest applications, satellite RADAR measurements provide spatially continuous and high-resolution data sets. Investigating the potential of RADAR for forest applications is therefore an issue of current research [Kugler et al., 2014]. Furthermore, sensors are installed on aircrafts in order to improve and develop new methods and to obtain the optimal relation between forest biomass or productivity and forest structure metrics [Dubayah et al., 2010; Asner and Mascaro, 2014]. Products of theses airborne measurements allow for deriving regional, high-resolution (~0.1 ha), continuous biomass maps [e.g., Asner et al., 2010; Marvin et al., 2014].

1.2.4 *Vegetation models*

Vegetation models simulate processes of the ecosystem that drive vegetation dynamics. Depending on the research question, they are applied at different temporal and spatial scales. Here, we introduce two types of vegetation models: dynamic global vegetation models that focus on forest biomes at regional to global scales, and forest gap models that focus on forest dynamics at the local scale.

1.2.4.1 *Dynamic global vegetation models*

Dynamic global vegetation models (DGVMs) simulate vegetation dynamics, hydrological processes, and its biogeochemical cycle in response to climatological input data [Sitch et al., 2008]. Commonly, they act at the scale of climatological input (0.5° (regional)-3°(global) resolution) and calculate mean processes for the entire grid cell. The spatial resolution varies depending on the spatial extend of the simulation area (e.g., 0.5° [Rammig et al., 2010] and 1° [Johnson et al., 2016] resolution for Amazon-wide simulations versus 3° [Sitch et al., 2008] for world-wide simulations). The temporal resolution varies among DVGMs and their internal processes: Photosynthesis and water fluxes are often calculated on half-hourly to daily time steps, climatological input data varies between daily to monthly time steps and tree growth is calculated on time steps up to one year [e.g., Sitch et al., 2003, 2008; Krinner et al., 2005; Sato et al., 2007]. Spatial and temporal resolutions depend on the research question and computational capacity.

Plant diversity is summarized in plant functional types (PFTs) that represent an average individual. PFTs compete for resources (e.g., light, water) and form biomes. Typical PFTs are broadleaf evergreen and raingreen trees for the tropics, needleleaf, broadleaf evergreen and broadleaf summergreen trees for the temperate and boreal zones, and different grasslands [<15 PFTs globally, Sitch et al., 2003; Sato et al., 2007]. Photosynthetic processes are often based on a model description of Farquhar [1989] and/or Collatz et al. [1991], a sub-model that describes the responses of carbon exchange by leaves under environmental conditions like CO_2 and oxygen concentration, temperature, and light [Farquhar, 2001].

DGVMs have been developed regarding particular research questions. The Lund-Potsdam-Jena (LPJ) model [Sitch et al., 2003], for example, has several modified versions: LPJ managed land (LPJml) includes crop functional types to analyze the effect of management on productivity [Bondeau et al., 2007]; the LPJml flexible functional traits [LPJml-FIT, Sakschewski et al., 2015] investigates the response of plant trait diversity under climatic changes [Sakschewski et al., 2016]. The Spatially Explicit Individual-Based (SEIB-) DGVM [Sato et al., 2007], LPJ-GUESS [Smith et al., 2008], and the Ecosystem Demography (ED-)Model [Moorcroft et al., 2001] combine the DGVM approach with concepts of forest gap models (see below).

Results of DVGMs depend on its climate input data and differ in patterns due to differences in its model structure. A model comparison of DGVMs has shown that simulated vegetation responses differently to drought in the tropics and to changing temperature and soil moisture in the boreal zone [Sitch et al., 2008]. Fig. 1.8 shows that DGVMs produce similar GPP estimates for the boreal and temperate zones, but strongly diverge in tropical regions [Beer et al., 2010]. Another limitation is that computational capacity is still a challenge. The individual-trait-based LPJ-mlFIT, for example, simulated 4 ha plots as a representative for each 0.5° grid cell in the Amazon (around 2000 grid cells in total) taking several days of simulation time [personal communication, Sakschewski et al., 2016].

DGVMs have been developed regarding particular research questions. The Lund-Potsdam-Jena (LPJ) model [Sitch et al., 2003], for example, has several modified versions: LPJ managed land (LPJml) includes crop functional types to analyze the effect of management on productivity [Bondeau et al., 2007]; the LPJml flexible functional traits [LPJml-FIT, Sakschewski et al., 2015] investigates the response of plant trait diversity under climatic changes [Sakschewski et al., 2016]. The Spatially Explicit Individual-Based (SEIB-) DGVM [Sato et al., 2007], LPJ-GUESS [Smith et al., 2008], and the Ecosystem Demography (ED-)Model [Moorcroft et al., 2001] combine the DGVM approach with concepts of forest gap models (see below).

Results of DVGMs depend on its climate input data and differ in patterns due to differences in its model structure. A model comparison of DGVMs has shown that simulated vegetation responses differently to drought in the tropics and to changing temperature and soil moisture in the boreal zone [Sitch et al., 2008]. Figure 1.8 shows that DGVMs produce similar GPP estimates for the boreal and temperate zones, but strongly diverge in tropical regions [Beer et al., 2010]. Another limitation is that computational capacity

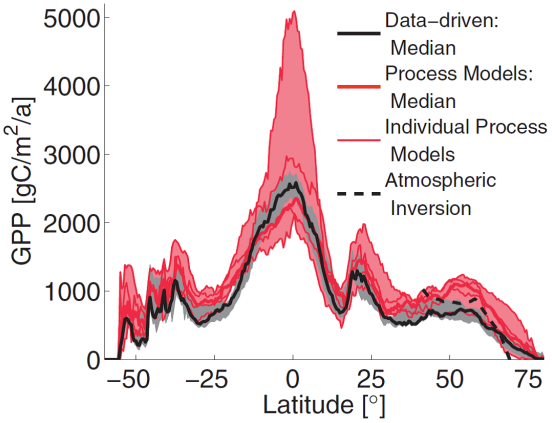

Figure 1.8: Annual GPP along the latitude. The red area shows the range of model output of different vegetation models. The gray area shows the range of the diagnostic models in combination with eddy covariance data. The thick lines represent the medians of both ranges [Beer et al., 2010].

is still a challenge. The individual-trait-based LPJ-mlFIT, for example, simulated 4 ha plots as a representative for each 0.5° grid cell in the Amazon (around 2000 grid cells in total) taking several days of simulation time [personal communication, Sakschewski et al., 2016].

Despite their limitations, DGVMs are valuable tools to analyze important research questions such as the potential response of vegetation to climate change [Cramer et al., 2001] like Amazon 'dieback' studies [Huntingford et al., 2008; Rammig et al., 2010; Cox et al., 2013]. DVGMs are used in earth system analyses where they are coupled to atmospheric and ocean models in order to investigate the climate-carbon feedback [Coupled Climate–Carbon Cycle Model Intercomparison Project C4MIP, Friedlingstein et al., 2006].

1.2.4.2 *Forest gap models*

The first forest gap model JEBOWA evolved in the early 70s [Botkin et al., 1972]. It provided a basis for the development of various forest gap models for forests worldwide [Shugart, 1984; Bugmann, 2001]. Forest dynamics are described on patches ('gap', Fig. 1.9). Within one patch, the growth of each tree is described (individual-based approach) without having an explicit spatial position. All trees within a patch compete for space and resources such as light, water, or nutrients. Main processes that are calculated at each time step are growth, mortality, establishment, and competition between trees.

Forest gap models have been used to address a variety of research questions on forest sites worldwide. The JEBOWA model was developed to analyze dynamics of a species-mixed forest in North America [Botkin et al., 1972]. The ForClim model was used, for example, to investigate differences in species compositions along a latitudinal gradient in North America [Bugmann and Solomon, 1995] and an elevation gradient in Europe [Switzerland, Heiri et al., 2006]. The FORMIND model investigates, for example, management strategies for logging [Huth et al., 2005, 2004], fragmented landscapes [Pütz

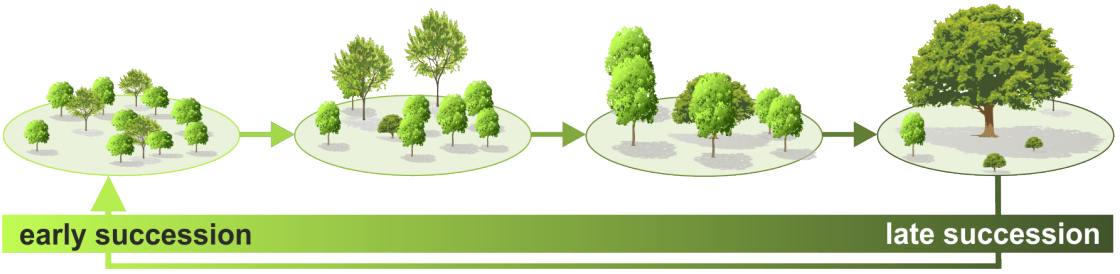

Figure 1.9: Different successional states of a forest ecosystem: light-demanding, fast-growing trees dominate the early successional stage and shade-tolerant, slow-growing trees dominate late successional stages. If a forest stand is disturbed (e.g. death of a large tree, fire event, or land slide), a gap occurs and succession starts again [image modified from Fischer et al., 2016].

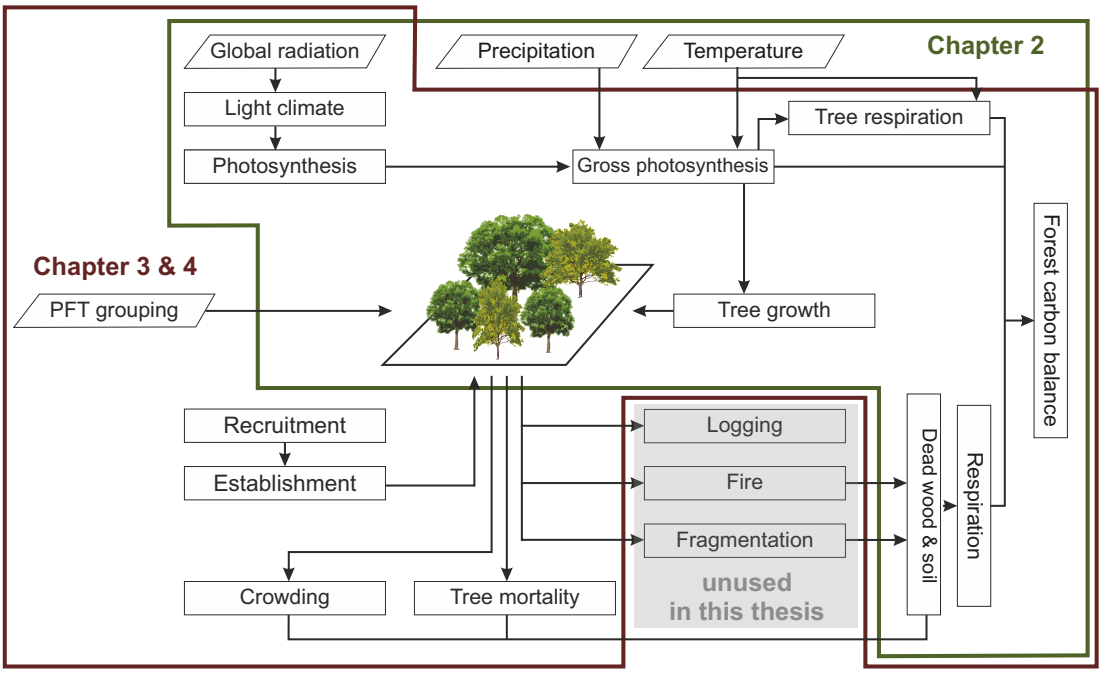

Figure 1.10: Conceptual framework of the forest model FORMIND [image modified from Fischer et al., 2016]: squares indicate processes, rhombuses indicate input. Processes that are used for the study linking the forest model and eddy covariance data (chapter 2) are framed in green, processes that are used for the study linking the forest model and remote sensing data (chapter 3 and 4) are framed in dark red. The logging, fire, and fragmentation modules are unused within the frame of this thesis.

et al., 2014], and the impact of landslides on species compositions [Dislich and Huth, 2012] in the tropics. These are just a few examples for the application of forest models at the local scale. The basic structure of forest gap models has been further developed and simplified. This allows for the investigation of forest dynamics at the landscape scale [e.g., the iLand model, Seidl et al., 2012].

The studies of this thesis are based on simulations with a forest gap model [FORMIND, Fig. 1.10, Köhler and Huth, 1998; Fischer et al., 2016]. It was developed to simulate dynamics of tropical, diverse forests [Köhler and Huth, 2004]. While traditional forest gap models often do not consider the carbon exchange of forests with the atmosphere [Bugmann, 2001], FORMIND simulates tree growth based on photosynthesis and respiration of the individual tree. The forest model calculates potential photosynthesis at the leaf level via a light-response curve. Temperature or water stress limits potential photosynthesis via a factor [ranging from 0 to 1, Bohn et al., 2014]. This is a more simple approach compared to the Farquhar [1989] model used in DGVMs, but clearly reduces computational time. Beside tree photosynthesis, FORMIND calculates decomposition of dead wood and soil. Therefore, it enables simulating carbon fluxes of the whole forest ecosystem.

Simulating carbon dynamics with an individual-based forest gap model has several advantages. First, species are grouped into plant functional types in order to differentiate tree species' characteristics (several PFTs per forest site, whereas DGVMs use one or two PFTs per biome). Thereby, the forest model detects carbon states and fluxes for different successional states and forest structures [Fischer et al., 2016, , Fig. 1.9]. This is a precious characteristic since forest structure and successional states determine the light conditions and productivity of a forest and are important factors to derive forest biomass of tropical forests [Marvin et al., 2014]. Second, forest gap models consider stem based mortality rates and thereby small-scale disturbances (gap-dynamics). It has been shown that small-scale disturbances have greater impact on the carbon cycle than large-scale disturbances [Espírito-Santo et al., 2014]. And third, the calculation of a forest stand simulation only takes a few seconds (e.g., for 10 ha over 1000 years).

One limitation of a forest gap model is that it relies on an extensive and time-consuming parameterization of species or plant functional groups. Such parameterizations depend on detailed observational data to describe processes and diversity [Hartig et al., 2012]. This observational data requirement limits the spatial extend of the model area [Jeltsch et al., 2008]. Normally, forest gap models are applied on areas of only a 1-1000 ha [Fischer et al., 2016; Jeltsch et al., 2008].

This thesis presents an approach that extends the FORMIND model to a larger region. We chose the Amazon rainforest to demonstrate this new approach and combine simulation results with field inventory, remote sensing, and eddy covariance data.

1.3 OBJECTIVES OF THIS THESIS

Field inventory, eddy covariance measurements, remote sensing ,and vegetation modeling are valuable methods to assess carbon dynamics of forest ecosystems. They give insights into the response of forests to environmental conditions, climatic changes, and disturbances. Anyhow, estimates on carbon dynamics of forest ecosystems still take a great share in the uncertainty of the global carbon cycle [Le Quéré et al., 2016]. The reason for this uncertainty is that tools have not been combined sufficiently, yet. In particular, studies miss out on considering forest structure and species compositions in their analyses. For instance, eddy covariance data has been used to identify the influence of variable climate in vegetation model processes [Verbeeck et al., 2011], however, only for 'mean' mature forest stands. LIDAR measurements were linked to forest modeling to simulate forest attributes [Hurtt et al., 2004; Dubayah et al., 2010], however, only for local forest stands. There is a clear need for combining approaches in order to include different forest structures, climatic conditions, and disturbances across temporal and spatial scales into the assessment of carbon dynamics of forest ecosystems [Saatchi et al., 2015; Shugart et al., 2015].

This thesis presents approaches for combining knowledge of all the above-mentioned methods. The central tool is an individual-based forest gap model (Fig. 1.10).

In a first study (chapter 2), FORMIND was enhanced to be applicable at a daily time step. Limiting factors for photosynthesis and respiration have been derived by linking simulation results with eddy covariance data. The main objectives of the first study are:

2. Investigating whether a forest gap model is capable of simulating carbon dynamics at the individual tree level under daily variable climate.
3. Identifying limitations of photosynthesis due to temperature and water stress using eddy covariance data.

The forest model is applied to two spruce forests in Germany where eddy covariance data are available. It is run on a daily time step in order to compare simulated and measured fluxes. The study shows that, in general, the forest model is capable of displaying carbon dynamics under variable climate. It is successfully linked to eddy covariance data which enables analyzing and improving individual model processes that describe the limitation of productivity due to temperature and water stress. The study demonstrates that forest gap models are valuable tools for investigations on carbon dynamics under the consideration of forest structure.

In a second study (chapter 3), the forest model is regionalized and combined with inventory and remote sensing data. The objectives of the second study are:

4. Implementing the local forest model FORMIND at the regional scale: the case study on the Amazon rainforest.
5. Deriving the spatial variation of biomass and forest structure of the Amazon rainforest by linking simulation results with satellite measurements.

We developed a regionalization approach to apply the forest model on the entire Amazon rainforest at the individual tree level. Simulation results are combined with a canopy height map derived from LIDAR remote sensing (ICESat satellite). This approach enables to produce high-resolution maps describing the distribution of above-ground biomass and other forest attributes in the Amazon rainforest that consider small- to large scale, natural, and human-induced disturbances. To our knowledge it is the first study that combines vegetation modeling and active remote sensing measurements at such a large scale. It sets a basis for analyses on the effect of forest structure and species compositions on carbon dynamics in the Amazon.

On the basis of this approach, further analyses on forest attributes in the Amazon rainforest are presented in chapter 4 with the following main objectives:

6. Deriving high-resolution maps of forest productivity and net carbon fluxes.
7. Investigating relations between forest structure, biomass, carbon fluxes and species compositions across the Amazon rainforest.

Simulating individual trees allows for analyzing forest structure and carbon dynamics at various spatial scales.

This thesis presents steps towards better estimates of carbon fluxes and budgets of forests. It provides insights and a basis for future studies on the Amazon rainforest across temporal and spatial scales under climatic and anthropogenic changes. In addition, the developed framework is transferable to other biomes around the world and applicable at the country-wide to continental scale.

2 ESTIMATING THE CARBON FLUXES OF FORESTS WITH AN INDIVIDUAL-BASED FOREST MODEL

This chapter is based on the publication Rödig et al. [2017b]:
Rödig, E., Huth, A., Bohn, F., Rebmann, C., Cuntz, M. (2017): Estimating the carbon fluxes of forests with an individual-based forest model, Forest Ecosystems, 4:4.

2.1 ABSTRACT

Background: Capturing the response of forest ecosystems to inter-annual climate variability is a great challenge. In this study, we tested the capability of an individual-based forest gap model to display carbon fluxes at yearly and daily time scales. The forest model was applied to a spruce forest to simulate the gross primary production (GPP), respiration, and net ecosystem exchange (NEE). We analyzed how the variability in climate affected simulated carbon fluxes at the scale of the forest model.

Results: 6 years were simulated at a daily time scale and compared to the observed eddy covariance (EC) data. In general, the seasonal cycle of the individual carbon fluxes was correctly described by the forest model. However, the estimated GPP differed from the observed data on the days of extreme climatic conditions. Two new parameterizations were developed: one resulting from a numerical calibration, and the other resulting from a filtering method. We suggest new parameter values and even a new function for the temperature limitation of photosynthesis.

Conclusions: The forest model reproduced the observed carbon fluxes of a forest ecosystem quite well. Of the three parameterizations, the calibrated model version performed best. However, the filtering approach showed that calibrated parameter values do not necessarily correctly display the individual functional relations. The concept of simulating forest dynamics on the individual base is a valuable tool for simulating the NEE, GPP and respiration of forest ecosystems.

2.2 BACKGROUND

Inter-annual climate variations can strongly influence the productivity of forest ecosystems. The heat wave of 2003, for example, caused a reduction of approximately 30% to the gross primary production (GPP) over Europe [Ciais et al., 2005]. This extreme event was followed by several studies to understand ecosystem responses and their underlying mechanisms [e.g., Zaitchik et al., 2006; Granier et al., 2007]. Models predict that such extreme events will become more frequent and intense in the future [Meehl and Tebaldi, 2004].

However, correctly capturing the responses of an ecosystem to varying climatic conditions with vegetation models is a major challenge [Keenan et al., 2012]. In this study, we test the potential of a forest gap model that considers forest structure at the local scale to estimate daily carbon fluxes and their response to climate variations in a spruce forest in Germany.

Forest models have a long tradition in ecological research [Botkin et al., 1972; Shugart, 1984; Pacala et al., 1993; Köhler and Huth, 2004]. They have been successfully ap-

plied to analyze forest succession, tree species composition, and biomass [e.g., Fischer et al., 2016]. Capturing the competition between individuals enables these types of models to reproduce reality better than vegetation models which operate at a larger scale [Smith et al., 2008]. Traditionally, studies using forest models have focused on forest structure and dynamics, but they often neglected carbon exchange with the atmosphere [Bugmann, 2001].

In this study, we used an individual-based forest gap model (FORMIND) that simulates the growth of individual trees by calculating its photosynthesis and respiration [Köhler and Huth, 1998]. In addition, a soil carbon module is included [derived from Sato et al., 2007]. These model characteristics established a base to capture carbon fluxes at the ecosystem level, in addition to biomass and tree-size distributions.

Up to now, the forest model FORMIND has mainly been used to reproduce the average forest conditions in long-term studies at yearly time scales [Gutiérrez et al., 2009; Fischer et al., 2014; Bohn et al., 2014]. The influence of short-term climate variability on individual model processes (GPP and respiration) has not yet been tested. Therefore, we here compared daily simulation output of the forest model with observed eddy covariance data of two spruce forests and analyzed the following two aspects. First, we wanted to test whether the local forest model is generally capable of displaying daily carbon fluxes. Second, we analyzed whether the model processes correctly respond to variable climate inputs. In this context, we evaluated the response of three different model parameterizations. We explored how we can use eddy covariance data to improve the simulation of carbon fluxes with an individual-based forest model. The simulation time also covered the heat wave of 2003 which enabled to include an extreme event in the analyses.

The following questions will guide us through this study: (1) How well does an individual-based forest gap model simulate the daily and yearly carbon fluxes of a temperate forest ecosystem? (2) How can EC data be used to improve the concept of limiting factors in forest gap models?

2.3 METHODS

2.3.1 *The study sites*

This study focused on a forest site located at Wetzstein Mountain, a part of the Thuringian Forest in central-east Germany where measured carbon fluxes and inventory data are available [Wetzstein flux tower, Rebmann et al., 2010]. Observed carbon fluxes were derived with the eddy covariance (EC) method, a technique that observes the local carbon flux dynamics of the vegetation and monitors inter-annual changes [Aubinet

Table 2.1: Site characteristics for Wetzstein [Rebmann et al., 2010, Martina Mundt, personal communication] and Tharandt [Grünwald and Bernhofer, 2007]. Climatological means were calculated from data obtained during the investigated time period.

	Wetzstein	**Tharandt**
Location	50°27'N, 11°27'E,	50°57'N, 13°34'E
Time period	2003-2008	1999-2008
Date of inventory	2004	1999
Stand age [a]	50	108
Stand density [ha^{-1}]	410	477*
Mean stem diameter (dbh) [m]	0.327	0.33
Leaf are index [m^2 m^{-2}]	7.0**	7.7
Elevation [m]	792	380
Annual mean temperature [°C]	6.5	8.8
Annual mean precipitation [mm a^{-1}]	810	673
Annual mean PPFD [μmol m^{-2} s^{-1}]	489	583

* In April 2002, the number of trees was reduced by approximately 30% due to tree cutting.

** Projected area, measured with LAI 2000 (LiCor)

et al., 1999]. The Wetzstein forest is dominated by even-aged Norway spruce (Picea abies) stands on clay loam. In addition, we analyzed another Norway spruce stand at Tharandt, a study site in the Ore Mountains in Germany where EC-data were available [Tharandt Anchor station, Grünwald and Bernhofer, 2007]. The stand characteristics of both sites are summarized in Tab. 2.1.

2.3.2 *The forest model FORMIND*

FORMIND [Köhler and Huth, 2004; Fischer et al., 2016] is an individual-based forest gap model in which growth is calculated for each tree individually. The approach uses patches to describe the vertical and horizontal forest structures. The main processes of the model include establishment, growth, mortality, and competition. Important driving factors are daily means of incoming light (photosynthetic photon flux density, PPFD), temperature, and precipitation (based on a model verison for temperate forests as in Bohn et al. [2014]). In this study, the model was applied to an even-aged spruce forest (1 ha). Establishment and mortality were deactivated for the short simulation time of 6 years. A full model description can be found in Fischer et al. [2016] and at `www.formind.org`.

The model runs with daily variable observed climate inputs of PPFD, day length, temperature, and precipitation measured onsite. PPFD and day length serve as the driving forces for forest productivity. The sum of the GPP over all trees thus equals the GPP of the ecosystem. The ecosystem respiration is the sum of the respiration of all trees

plus that of the soil and deadwood. The NEE is calculated as the difference between the ecosystem GPP and the ecosystem respiration [Fischer et al., 2014]. A positive NEE corresponds to increasing carbon stocks.

Gross primary production. Photosynthesis is calculated at the leaf level using a light-response function and is then integrated over the entire canopy [Thornley and Johnson, 1990]. The GPP of an individual tree under optimal climatic conditions [Huth and Ditzer, 2000] equals

$$GPP_{ptree}(I_{ind}(PPFD(t))) = \frac{p_{max}}{k} \cdot \ln\left\{\frac{\alpha k I_{ind}(PPFD(t)) + p_{max}[1-m]}{\alpha k I_{ind}(PPFD(t))e^{-kLAI} + p_{max}[1-m]}\right\} A_c \psi \tag{2.1}$$

in $\mu mol(CO_2)\ m^{-2}\ s^{-1}$, where p_{max} [$\mu mol(CO_2)\ m^{-2}\ s^{-1}$] is the maximum photosynthetic rate of the tree species (here, spruce), α is the initial slope of the light-response curve [$\mu mol(CO_2)\ \mu mol(photons)^{-1}$], k is the light extinction factor, and m is the transmission coefficient of the leaves. I_{ind} is the fraction of the PPFD at daily time step t that reaches the top of the individual tree. A_c [m^2] is the crown area, and ψ [s] the photosynthetically active period of the time scale. Under non-optimal climatic conditions, GPP_{ptree} is limited by the available soil water (SW) and temperature (T) [Bohn et al., 2014]:

$$GPP_{tree}(t) = GPP_{ptree}(t) \cdot \varphi_{SW}(t) \cdot \varphi_T(t) \tag{2.2}$$

where φ_{SW} is the water reduction factor ([0,1]), and ψ_T the temperature reduction factor ([0,1]). The temperature reduction factor φ_T is derived from the LPJ-model [Sitch et al., 2003] which includes two ramp functions [Gutiérrez et al., 2012]:

$$\varphi_T(t) = \left(1 + e^{\frac{2\ln(0.01/0.99)\cdot(0.5(T_{CO_2,l}+T_{cold})-T(t))}{T_{CO_2,l}-T_{cold}}}\right)^{-1} \cdot \left(1 - 0.01e^{\frac{\ln(0.99/0.01)\cdot(T(t)-T_{hot})}{T_{CO_2,h}-T_{hot}}}\right) \tag{2.3}$$

where T [°C] is the daily mean air temperature at time step t. $T_{(CO_2,h)}$, $T_{(CO_2,l)}$, T_{cold} and T_{hot} [°C] are species-specific parameters representing the higher and lower temperature limits for CO_2 assimilation and the monthly mean air temperatures of the warmest and coldest months when production can still occur.

In this study, we also tested a new temperature reduction curve φ_T^*. It is distributed around the optimal temperature for photosynthesis T_{opt} [°C] and the width T_{sig} [°C] [June et al., 2004, , reduction of the electron transport rate with n = 2] since Eq. 2.3 could not be properly fitted to the observed data. We suggest fitting this bell-shaped curve because it only relies on two parameters instead of four parameters (Eq.2.3):

$$\varphi_T^{\star}(t) = e^{-\left(\frac{T(t)-T_{opt}}{T_{sig}}\right)^n}. \tag{2.4}$$

We use a water reduction factor, φ_{SW}, as proposed by Granier et al. [1999]:

$$\varphi_{SW}(t) = \begin{cases} 0 & : SW < SW_{pwp} \\ \frac{SW(t)-SW_{pwp}}{SW_{msw}-SW_{pwp}} & : SW_{pwp} < SW(t) < SW_{msw} \\ 1 & : SW(t) > SW_{msw} \end{cases} \tag{2.5}$$

where SW_{pwp} is the permanent wilting point, $SW_{msw} = SW_{pwp} + 0.4(SW_{fc} - SW_{pwp})$ is the minimum soil water content for maximum photosynthesis, and SW_{fc} is the field capacity. Available soil water is calculated from the daily precipitation, interception by leaves, above- and below-ground water runoff, and transpiration of trees [Fischer et al., 2014].

Respiration. The respiration of a tree is the sum of its maintenance respiration, R_m, and its growth respiration, R_g, a constant fraction of $(GPP - R_m)$.The maintenance respiration is calculated as follows:

$$R_m(t) = R_b(t)\kappa(T(t)), \tag{2.6}$$

where R_b is a base respiration, a fraction of standing biomass of the tree (Bohn et al. 2014, detailed description in supplementary information A3). $\kappa(T)$ describes the influence of the daily mean air temperature T on respiration [Prentice et al., 1993]:

$$\kappa(T(t)) = Q_{10}^{\frac{T(t)-T_{ref}}{10}}, \tag{2.7}$$

with constants T_{ref} and Q_{10} [Bohn et al., 2014].

2.3.3 *Field data and data filtering*

We compared the simulation results of the forest model with the EC data of the Wetzstein site (Tab. 2.1). For the Wetzstein site, the EC data were pre-processed as described in Rebmann et al. [2010]. The net ecosystem exchange (NEE) was gap filled since the data are compared at daily time scales and partitioned into GPP and respiration. We use an algorithm that extrapolates day-time ecosystem respiration from night-time respiration considering temperature sensitivities [Reichstein et al., 2005].

We filtered the EC data to identify days that are affected by specific limitations. Optimal temperature or soil water conditions were defined for days when the daily mean GPP was maximal (98th percentile for the years 2003 to 2008). We assumed that on those days the GPP is not affected by any limitation. The filtered range of the optimal temperature (daily daytime mean) conditions was identified at $7.3°C < T < 18.0°C$, and the threshold for non-limiting soil water conditions at $SW > 16.0\%$. Optimal light conditions were defined for days when values rise above the monthly 80th percentile. We define night-time as time periods when PPFD < 20 $\mu mol(CO_2)$ m^{-2} s^{-1}. When we use normalized GPP values in our analyses, we normalize GPP values yearly by its annual 98th percentile.

2.3.4 *The model setup*

The forest model was run with daily time steps for three different parameterizations: literature-based (M1), numerically calibrated (M2), and filter-based (M3) parameterizations (Tab. 2.2). The literature-based parameterization (M1) is based on Bohn et al. [2014] for a spruce forest where the parameter values are derived from inventory data and the literature. The soil parameter values were adapted to the clay loam soil type as in Maidment [1993]. The calibrated parameterization (M2) is based on parameters derived from a numerical calibration against the NEE, GPP, and respiration data [Lehmann and Huth, 2015, , see A for details]. The filter-based parameterization (M3) arose from filtering the EC data (same data as used for calibration of M2) for optimal climatic conditions (see Observational data and data filtering) to isolate individual processes. Model functions were directly fitted through filtered data to derive new parameter values and a new temperature reduction curve (Eq. 2.4).

All model setups were initialized according to the inventory data for Wetzstein and Tharandt (Tab. 2.1). Trees were spread equally over the 25 patches of the 1 ha model area (at Wetzstein, 410 stems ha^{-1} with a mean stem diameter of 0.33 m). The deadwood pool was filled with 4.14 tC ha^{-1} (Wetzstein inventory, personal communication from Martina Mund, University of Goettingen). The fast-decomposing soil stock was initialized with 2.0 tC ha^{-1}, and the slow-decomposing soil stock with 1.5 tC ha^{-1} (means in the climax stage of long-term simulations). The simulation period at the Wetzstein site was from 2003 to 2008 and at Tharandt from 1999 to 2004. All model simulations were deterministic since none of the model setups included recruitment or stochastic mortality.

2.4 RESULTS

2.4.1 *Simulation of daily carbon fluxes at Wetzstein forest*

The measured and modeled (parameterization M1) GPP and respiration at Wetzstein forest for the dry year 2003 are shown in Fig. 2.1. The forest model performed well for daily GPP. It reproduced the seasonal cycle and the daily fluctuations showed similar magnitudes to those observed. Differences were observed during times of low soil water availability, very low and high temperatures and bright days. In late summer (July-September), the simulated respiration diverges from the observational data. In general, simulated respiration shows stronger fluctuations than the observed respiration.

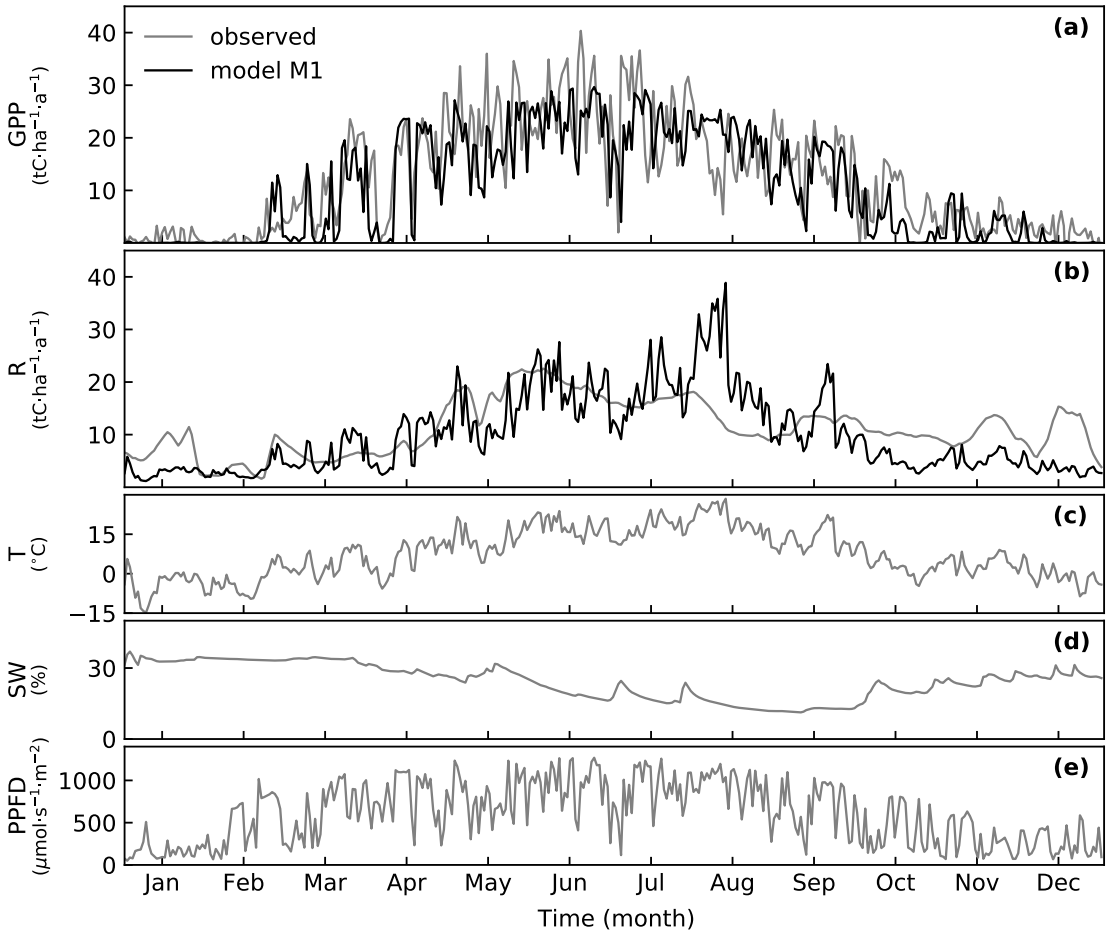

Figure 2.1: Time series of the daily observed and simulated data for 2003 at Wetzstein. Observed (grey line) and modeled (M1, black line) (a) GPP and (b) respiration (R) of the ecosystem with the literature-based parameterization. Time series of the observed (c) daytime temperature (T), (d) soil water content (SW), and (e) daytime PPFD.

2.4.2 *Simulation of carbon fluxes at Wetzstein forest for three different parameterizations*

We compared the simulations of all three model versions with the observed fluxes at Wetzstein at the daily time scale (Tab. 2.3, Fig. 2.2). The correlation is best for the numerically calibrated parameterization (M2), closely followed by the filter-based parameterization (M3). Simulated respiration correlates with the observed values with an R^2 of 0.44-0.54, NEE with an R^2 of 0.63-0.66. Simulated and observed GPP values match best with an R^2 of 0.73-0.82. High GPP values above 30 tC ha^{-1} a^{-1} can only be reached with the filter-based parameterization (M3, Fig. 2.2).

In a second step, we calculated annual GPP, NEE, and respiration for the Wetzstein forest (Fig. 2.3a). The simulated annual NEE values fit the observed annual values best for the calibrated parameterization (M2, deviation from observed data by 3.5% for average values throughout the simulation years). The simulated annual GPP fits quite well and only diverges from the observed data by 0.8% for the calibrated (M2) and 2.6% for

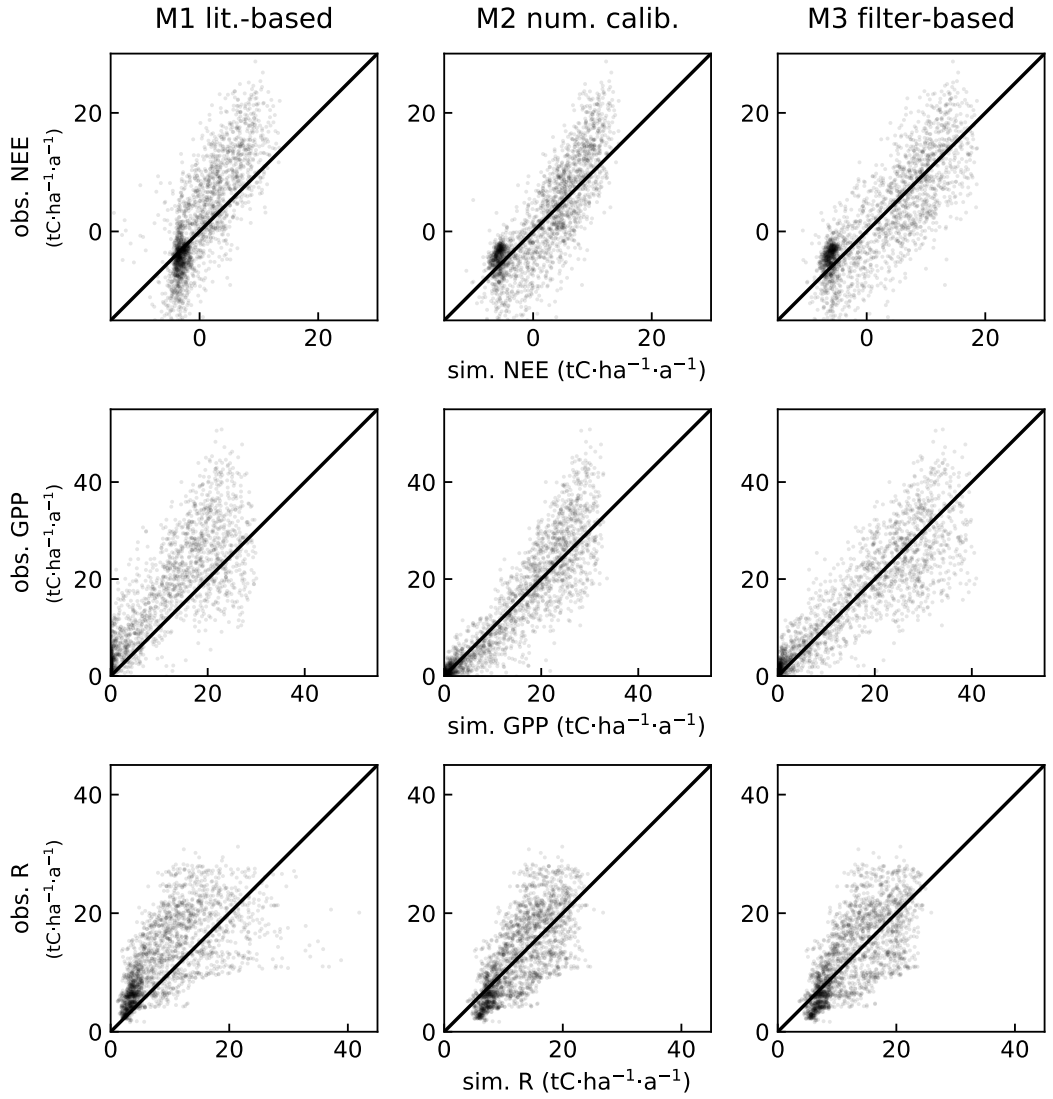

Figure 2.2: Simulated vs. observed ecosystem carbon fluxes (NEE, GPP, and respiration) at Wetzstein for the three parameterizations for 2192 simulated days.

the filter-based (M3) version, simulated respiration by 0.3% (M2) and 0.9% (M3). The literature-based model version clearly underestimates all ecosystem fluxes.

2.4.3 *Simulation of carbon fluxes at another spruce forest*

We applied the forest model to another spruce forest (Tharandt) for the years 1999-2004 (Fig. 2.3 b). The model parameters were the same as at Wetzstein. Only the climate input and the initialization of the forest model (forest state based on inventory data) were adapted to the site.

Both, the filter-based (M3) and calibrated (M2) model version, performed well for the daily GPP (R^2 = 0.61 (M2), R^2 = 0.61 (M3), RMSE = 8.83 tC ha^{-1} a^{-1} (M2), and

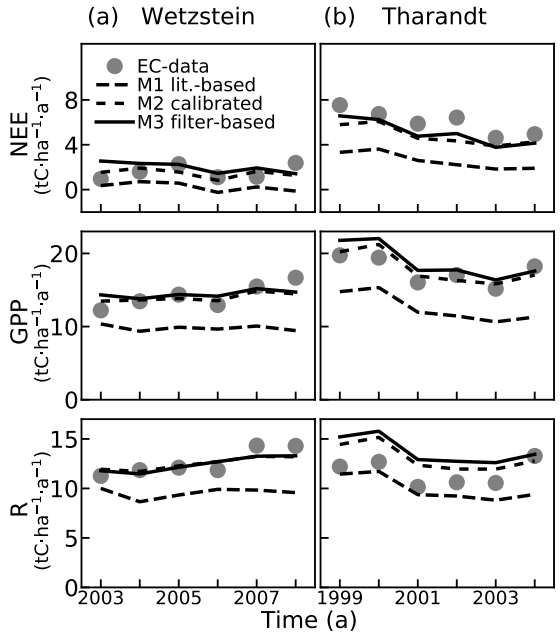

Figure 2.3: Annual ecosystem carbon fluxes (NEE, GPP and respiration) for the three parameterizations: literature-based (M1, dashed), calibrated (M2, dotted) and filter-based (M3, solid), and the observed data (circles) for (a) the Wetzstein site and (b) the Tharandt validation site.

RMSE = 9.57 tC ha^{-1} a^{-1} (M3), Tab. 2.3). The simulated respiration was even better than at Wetzstein, at the daily scale (R^2 = 0.62), the NEE performed worse at Tharandt than at Wetzstein (R^2 = 0.38).

The annual simulated GPP is best for the calibrated (M2) and filter-based (M3) parameterizations (2% and 7% deviations). In April 2001, the tree density was reduced by 30% (at Tharandt and in the forest model), which is reflected in the lower GPP values after 2001. In the dry year 2003, the simulated annual GPP is 0.47 tC ha^{-1} lower than in the previous year for the calibrated model version (M2) and 1.37 tC ha^{-1} lower for the filter-based (M3). The observed GPP in 2003 is 1.87 tC ha^{-1} lower than in 2002. The annual carbon budget (NEE in Fig. 2.3 (b)) matches the observed budget well (M2: mean deviation of 20% from observations, M3: deviation of 16%). Note that NEE is the balance between GPP and respiration and the bias is consequently more sensitive. Respiration is partly overestimated for the model versions M2 and M3 (deviations of 14% and 19%).

2.4.4 *Limiting factors for productivity*

As an example, we analyze here the GPP limitation due to temperature (Fig. 2.4). Daily GPP values were normalized and filtered for optimal soil water conditions and sunny days to distinguish them from days with other limitations. Filtered, normalized data thus represent the reduction factor due to temperature.

On colder days, the literature-based model (dashed line) shows a reduction in GPP which seemed stronger than the observed. For example, at the freezing point, the observed GPP was reduced to 20% of its optimum, whereas the model reduced the GPP to nearly 0. For higher temperatures, the observed data show a reduction of photosynthesis starting at 20°C, whereas the literature-based parameterization barely showed a reduction in photosynthesis until 30 °C was reached. For the calibrated model version, the reduction curve showed a steep slope at 0 °C, attained its highest values between 3°C and 20°C and reached zero at 30 °C. The solid black line shows the best fit of the bell-shaped curve (Eq. 2.4) through filtered EC-data.

We further analyzed the relationships between the PPFD and productivity, temperature and respiration, as well as the soil water and productivity (see Appendix and Tab. 2.1 for the derived filter-based parameter values).

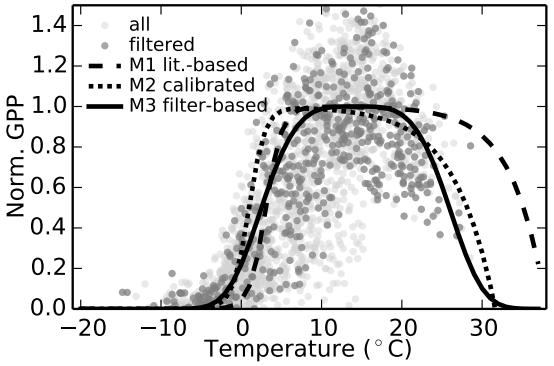

Figure 2.4: Temperature limitation of photosynthesis at Wetzstein. Parameter values are listed in Tab. 2.2. The three parameterizations are the literature-based (dashed) and the calibrated (dotted) parameterizations with the original function (Eq. 2.3), and the filter-based parameterization with the new formulation (Eq. 2.4). The observed, daily mean temperature values of the Wetzstein site were filtered for optimal soil water and light conditions and normalized (see section 2.3.3).

Table 2.2: Model parameter values for the literature-based (M1) with references (ref.), calibrated (M2), and filter-based (M3) model version.

Parameter		M1	ref.	M2	M3
Productivity					
p_{max}	maximum photoproducitvity of leaf [µmol(photons) m^{-2} s^{-1}]	8.9014	[Bohn et al., 2014; Sonntag, 1998]	5.67	10.98
α	slope of light response curve [µmol(photons) m^{-2} s^{-1}]	0.0402	[Bohn et al., 2014; Sonntag, 1998]	0.15	0.08
Temperature					
T_{CO_2low}	min. temperature for photosynthesis [°C]	−2	[Bohn et al., 2014; Sitch et al., 2003]	−7.82	-
T_{CO_2high}	max. temperature for photosynthesis [°C]	38	[Bohn et al., 2014; Sitch et al., 2003]	31.59	-
T_{cold}	mean temperature of coldest month [°C]	10	[Bohn et al., 2014; Sitch et al., 2003]	8.47	-
T_{hot}	mean temperature of warmest month [°C]	18.9	[Bohn et al., 2014; Sitch et al., 2003]	12.0	-
T_{opt}	optimal temperature for photosynthesis [°C]	-	-	-	14.22
T_{sig}	width of new temperature curve [°C]	-	-	-	12.83
Q_{10}	constant for temperature dependent respiration	2.3	[Bohn et al., 2014; Piao et al., 2010]	1.52	1.52
T_{ref}	reference temperature [°C]	10.1	[Bohn et al., 2014]	12.61	15.06
Water					
SW_{pwp}	permanent wilting point [vol-%]	19.7	[Maidment, 1993]	14.0	9.5
SW_{fc}	field capacity [vol-%]	31.8	[Maidment, 1993]	40.0	20.7

Table 2.3: R^2 and root mean square error (RMSE, in tC ha^{-1} a^{-1}) at the calibration and validation sites. Simulated fluxes are compared to observed values at the daily time scale (scale of the simulation output).

	Wetzstein (calibration site)		**Tharandt (validation site)**	
	R^2	*RMSE*	R^2	*RMSE*
GPP				
lit.-based (M1)	0.73	7.91	0.59	10.47
calibrated (M2)	0.82	5.39	0.61	8.83
filter-based (M3)	0.80	5.72	0.61	9.57
Respiration				
lit.-based (M1)	0.44	6.31	0.58	5.14
calibrated (M2)	0.54	4.64	0.62	4.92
filter-based (M3)	0.53	4.73	0.62	5.12
NEE				
lit.-based (M1)	0.63	6.25	0.30	7.90
calibrated (M2)	0.66	5.43	0.38	6.87
filter-based (M3)	0.65	5.42	0.38	7.62

2.5 DISCUSSION

2.5.1 *Simulating carbon fluxes at daily and yearly time scales*

We analyzed the overall model performance for three parameterizations at the daily scale (Tab. 2.3, Fig. 2.2) and the annual scale (Fig. 2.3). At the Wetzstein site, the forest model performed best for the numerical calibration. This performance is not surprising since the calibration method aims for the least error [Lehmann and Huth, 2015]. In any case, it is satisfying that we found a parameter combination that reproduces the observations with such good performance at the daily and annual time scales. This shows that the simplifications assumed in this forest model are sufficient to reproduce the complex interactions of climate and ecosystem fluxes even with the literature-based model version (M1). By comparison, LPJ-Guess simulated daily GPP with a similar performance (RMSE of 6.50-8.94 tC ha^{-1} a^{-1} and R^2 of 0.62-0.72) for a pine stand in the Netherlands in a similar study [the range results from different model setups, Vermeulen et al., 2015].

Simulated respiration shows a stronger bias than GPP. The deviation from the observed data can be explained in several ways. On the one hand, respiration is strongly coupled to GPP in the forest model. Consequently, strong GPP fluctuations induce strong fluctuations in respiration which is also seen at Tharandt. On the other hand, observed respiration shows a rather smooth curve (Fig. 2.1 b), which is a consequence of the flux-partitioning method that derives respiration from the measured NEE [Reichstein

et al., 2005]. Respiration data thus arise from a modeling approach. The forest model additionally uses a simplified soil module [as in SEIB-DGVM, Sato et al., 2007]. Some of the rhizosphere processes are neglected, such as the release of organic compounds by roots [Nguyen, 2009]. Rhizomicrobial respiration might have effects on short-term CO2 efflux but should have no effect on the long-term carbon stock in the soil [Kuzyakov, 2006]. Also, note that different forest histories, such as different forest management at Wetzstein and Tharandt, might thus lead to different soil pools and respiration rates. The fact that the soil carbon pool of the forest model was initialized with a soil pool in a steady state might lead to an overestimation of ecosystem respiration at Tharandt.

The simulation results of Tharandt after the dry year 2003 show that the filter-based version (M3) reproduced the drought and heat event of 2003 better than the calibrated version (M2). Hence, parameter values of individual processes of the filter-based version (M3) might be more appropriate than the calibrated ones (M2) although the overall performance of M2 is better than the performance of M3 (Tab. 2.3). This might indicate that the numerical calibration compensates individual processes of extreme events to achieve an overall best performance throughout all simulation years while the filter-based version aims for the best parameterization of individual processes.

The overall performance of all parameterizations let us conclude that carbon fluxes of forest ecosystems can also be modeled with individual-based models. The characteristic of simulating each individual tree has the advantage to investigate in plant-population dynamics, forest structure, and their interaction with carbon dynamics in future studies.

2.5.2 *Analyzing limiting factors for productivity with the help of EC data*

To test whether the parameter values (M1, M2) correctly describe the limiting factors of photosynthesis and respiration in the forest model, we filtered the EC data. The filtering singled out time steps that are mainly influenced by a single constraint such as temperature or water stress. This approach resulted in an additional parameterization of the forest model for which the functional relations between the variable climate and model processes were directly fitted through the filtered data (M3). As an example, we here discuss the relationship between temperature and productivity. The other relationships are discussed in detail in appendix A.

The relationship between the measured GPP and temperature (Fig. 2.4) showed that the literature-based parameterization, which was validated for long-term simulations [Bohn et al., 2014], underestimated GPP for low and overestimated it for high temperatures. The function was taken from the LPJ model [Sitch et al., 2003]. In LPJ, the function was applied as a “bulk” temperature-response function for different plant functional types in temperate forests to reproduce the current vegetation distribution (Stephan Sitch, personal communication). In FORMIND, this function seems to be sufficient to estimate the

current mean carbon budgets from long-term simulations [Bohn et al., 2014], but the model version is not able to display inter-annual changes correctly. A similar study, that tested the temperature-response curve in LPJ-Guess in a pine stand, concluded that the curve needs to be shifted to lower temperatures [Vermeulen et al., 2015]. This finding also agrees with the fact that trees can photosynthesize down to a temperature of about -5 °C (root zone temperature), while growth seems to stop at approximately 0 °C [Körner and Paulsen, 2004]. The numerical calibration experiment also shows that shifting the curve towards lower temperatures results in a better fit to the observed data. The EC data indicate photosynthetic activity down to about -10 °C. This is plausible considering that the air temperature is generally lower than temperature in the root zone during winter. In addition, the trees at the Wetzstein site are adapted to low temperatures and cold winter conditions due to the elevation. Note, that positive ecosystem GPP does not necessarily implicate tree growth since respiration compensates for GPP at low temperatures and low PPFD in the forest model.

GPP was not limited due to high temperatures with the literature-based parameterization (M1). High temperatures might go along with a vapor pressure deficit limitation [Körner, 1994; Lasslop et al., 2010], which is not considered in our model approach. This assumption is supported by the results of the numerical calibration (the limiting factor is 0 at 31.6 °C). This reduction in temperature might compensate for the missing vapor pressure deficit limitation.

Since the original reduction curve did not fit the filtered data, we introduced a new functional relationship for the temperature reduction factor (Eq. 2.4, methods). The new curve originates from a normal distribution that describes the temperature dependence of the photosynthetic electron transport rate [June et al., 2004]. A completely normal distribution (n = 2) led to a very small plateau in the temperature reduction function, which means a small range of optimal temperature conditions. n = 4 led to a much wider range of optimal conditions. An advantage of the introduced function is that it uses only two instead of four parameters. We therefore suggest using the less complex bell-shaped curve for future studies.

The fact that the original temperature curve could not be fitted through filtered data properly supports the assumption that a pure calibration against ecosystem fluxes does not necessarily result in optimal parameter values of the individual model processes. We can conclude that eddy covariance data and the filtering-approach can give important insights into the correct parameterization of model processes (the limiting factors).

2.5.3 *Sources of uncertainty*

This study comes with a variety of uncertainties from various sources that must be considered. The first source of uncertainty comes from the EC data. NEE is measured at a

half-hourly scale. However, it comes with data gaps that are filled to compare the observed data with the simulated data at a daily time scale. The gap-filled NEE is based on a modeling procedure [Reichstein et al., 2005]. At the Tharandt site, for example, the uncertainty of the gap filling methods is up to 10% [Grünwald and Bernhofer, 2007]. In addition, GPP and respiration are not directly measured, but are partitioned from the NEE, which is based on another modeling procedure [Reichstein et al., 2005]. When we analyzed the drought event of 2003 at Tharandt, we found that GPP was 1.87 tC ha^{-1} less than in the previous year. A multi-site study on the event in 2003 reported a reduction of 2.08 tC ha^{-1} at Tharandt [Ciais et al., 2005]. These deviations demonstrate the uncertainties implied by gap filling and the partitioning of EC data, especially at the annual time scale.

The second potential source of uncertainties comes from the filtering method and the concept of limiting factors. The forest model, and thus also the filtering method, consider only temperature and water as limiting factors. The vapor pressure deficit and its influence on productivity (as in BIOME-BGC [Kimball et al., 1997], 3PG [Landsberg and Waring, 1997]), for example, is not considered. However, we still assume that the filtered data are reasonable for singling out different constraints in forest productivity.

2.6 CONCLUSION

The model version, that is only based on literature values [M1, Bohn et al., 2014], is capable of reproducing the seasonal cycle and daily fluctuations of carbon fluxes. However, this model version underestimates carbon fluxes at both spruce stands on the annual time scale. The calibrated model version (M2) derived from a numerical calibration [Lehmann and Huth, 2015] against the observed NEE, GPP, and respiration performs best at the daily and annual time scales. Deviations of the individual processes from the observed data seem to compensate each other, so that, in sum, they reproduce the observed net fluxes well. The third parameterization resulted from a fit through filtered data (M3). We identified a new functional relationship between temperature and GPP. Its mean performance at both sites differs only slightly from the calibrated parameterization, but it shows a closer match to observations for the extreme event at Tharandt in 2003. This shows that we should not blindly trust in a numerical calibration, although its overall performance is best.

The presented filter method improved carbon flux estimates for both spruce stands by improving the model processes. The consideration of the individual limiting factors for productivity (Fig. 2.4, Fig. A1) is essential to correctly reveal the impact of inter-annual climate variations on carbon fluxes. Therefore, we favor the filter-based model version for future studies. We can conclude that an individual-based forest model is a valuable

tool that allows analyses of daily and yearly carbon fluxes in addition to the traditional analyses of forest successions and biomass.

ACKNOWLEDGEMENTS

Measurements were supported by the CarboEurope-IP (European Commission, Directorate-General Research, Sixth Framework Programme, Priority 1.1.6.3: Global Change and Ecosystem (Contract No. GOCECT-2003-505572)) of the Max Planck Institute for Biogeochemistry in Jena. We thank Martina Mund of the Georg-August-University of Goettingen for the inventory information at the Wetzstein site. EC data at the Tharandt site were kindly provided by the Department of Meteorology at TU Dresden. We thank Rico Fischer, Sebastian Paulick, and Franziska Taubert for their support and discussions.

3 SPATIAL HETEROGENEITY OF BIOMASS AND FOREST STRUCTURE OF THE AMAZON RAINFOREST: LINKING A FOREST GAP MODEL, REMOTE SENSING AND FIELD INVENTORY

This chapter is based on the publication Rödig et al. [2017a]:
Rödig, E., Cuntz, M., Heinke, J., Rammig, A., Huth, A. (2017): Spatial heterogeneity of biomass and forest structure of the Amazon rain forest: Linking remote sensing, forest modelling and field inventory. Global Ecology Biogeography, 26:1292–1302

3.1 ABSTRACT

Aim: Estimating the current spatial variation of biomass in the Amazon rainforest is a challenge and remains a source of substantial uncertainty in the assessment of the global carbon cycle. Precise estimates need to consider small-scale variations of forest structures resulting from local disturbances, on the one hand, and require large-scale information on the state of the forest that can be detected by remote sensing, on the other hand. In this study, we introduce a novel method that links a forest gap model and a canopy height map to derive the biomass distribution of the Amazon rainforest.

Location: Amazon rainforest.

Methods: An individual-based forest model was applied to estimate the variation of above-ground biomass across the Amazon rainforest. The forest model simulated individual trees and hence, allowed for the direct comparison of simulated and observed canopy heights from remote sensing. The comparison enabled the detection of disturbed forest states and the deviation of a simulation-based biomass map at 0.16 ha resolution.

Results: Simulated biomass values ranged from 20 to 490 t (dry mass) ha^{-1} across 7.8 Mio km^2 of Amazon rainforest . We estimated a total above-ground biomass stock of 76 GtC with a coefficient of variation of 45%. We found mean differences of only 15% when comparing biomass values of the map with 114 field inventories. The forest model enables to derive additional estimates such as basal area and stem density.

Main conclusions: Linking a canopy height map with an individual-based forest model enables to capture the spatial variation of biomass in the Amazon rainforest at high resolution. The study demonstrates how this linkage also allows for quantifying the spatial variation in forest structure caused by tree-level to regional-scale disturbances. It thus provides a basis for large-scale analyses on the heterogeneous structure of tropical forests and their carbon cycle.

3.2 INTRODUCTION

Observing the dynamics of terrestrial biomass is a great challenge and one of the major sources of uncertainties in the global carbon cycle [Le Quéré et al., 2016]. In particular, tropical forests are sensitive to anthropogenic disturbances such as deforestation or logging that cause large-scale forest degradation [van der Werf et al., 2009]. The Amazon rainforest is the largest intact tropical forest with a share of around 18% of global forest area [Hansen et al., 2010]. Robust estimates of its above-ground biomass (AGB) and forest structure are essential to correctly budget carbon emissions. However, above-ground biomass (AGB) estimates diverge by a factor of two for the Amazon rainforest, ranging

from 38.9 to 93 PgC [Houghton et al., 2001; Malhi et al., 2006; Saatchi et al., 2007, 2011].

The large spread of the above-ground biomass estimates arises from diverse methodological approaches at different spatial and temporal scales: ground-based measurements, remote sensing, a combination of both, and modeling. On the one hand, ground-based measurements (forest inventories that are mostly at the plot scale of ~1ha and census intervals of one year or more) are interpolated in order to display spatial distribution of biomass [Malhi et al., 2006; Johnson et al., 2016]. Since the number of observations is limited, it is uncertain how representative these samples are for the whole basin [Chave et al., 2004; Marvin et al., 2014; Réjou-Méchain et al., 2014]. Therefore, ground-based measurements are often linked with remote sensing products that capture the state of forests, in order to derive static maps of above-ground biomass [e.g. 1 km^2 resolution in Saatchi et al., 2011; Avitabile et al., 2016]. Modeling approaches, on the other hand, such as dynamic global vegetation models (DGVMs), simulate the temporal dynamics of biomass at regional scales [e.g., Sitch et al., 2003]. Such models are applied for, e.g., investigating the impact of climate change on Amazon rainforest ecosystems [e.g., Huntingford et al., 2008; Rammig et al., 2010] and can be useful to provide hypotheses for the underlying mechanisms that drive biomass distribution and dynamics [e.g., Hofhansl et al., 2016]. Depending on the resolution of the climate input, these models mostly cover large-scale patterns of mature forests at a spatial resolution of more than 10 km^2. Thus, they may not capture forest structures and dynamics at small scales, e.g., the individual tree level and effects of logging. This may be a reason for the divergence [simulated maps in Johnson et al., 2016] from maps that combine remote sensing and ground observations [Saatchi et al., 2011; Baccini et al., 2012; Avitabile et al., 2016].

There is clearly a need of combining remote sensing products and vegetation models in order to broaden our knowledge on the dynamics, structures and carbon stocks in the Amazon rainforest. Here, we present a method to bridge this gap by linking remote sensing data with an individual-based forest gap model [FORMIND, Köhler and Huth, 2004; Fischer et al., 2016].

Individual-based forest gap models are normally applied at the local scale to reproduce successional dynamics and forest structures [e.g., Botkin et al., 1972; Shugart, 1984; Bugmann, 2001; Shugart et al., 2015]. In contrast to DGVMs, forest gap models simulate processes of tree growth, establishment and mortality for each tree individually. This concept enables the projection of forest succession, vertical and horizontal heterogeneity, competition between individuals, and disturbances due to stem-based mortality. Individual-based forest models thereby depict forest structure more closely than area-based models [Smith et al., 2008].

In the present study, we expand the forest gap model FORMIND from the local scale (stand level) to the regional scale (entire Amazon rainforest). This regionalization im-

plies some model adaptations. First, we adapt the model's mortality parameters that influence tree species composition across the Amazon. We find that annual precipitation and clay fraction is a potential proxy for tree mortality rates in our forest model. This relation is supported by observations made in the field [Quesada et al., 2012; Galbraith et al., 2013; Malhi et al., 2015]. The adapted individual-based forest gap model is then applied across the Amazon to simulate all potential successional stages and related tree heights.

Second, we assume that canopy height is a good indicator for the successional stage of a forest site [Dubayah et al., 2010]. We use remotely sensed canopy heights from a high resolution (1 km^2) wall-to-wall map derived from spaceborne LIDAR [Simard et al., 2011] as a proxy for the successional state of the forest [inspired by Ranson et al., 2001; Hurtt et al., 2004]. We then link the observed with the simulated canopy height and successional stage of our forest gap model to derive the amount of above-ground biomass stored at each location. Combining both tools results in a new, high-resolution, simulation-based AGB map of the Amazon rainforest that takes natural and anthropogenic disturbances into account.

The following research questions will guide us through the study:

(1) What is the benefit of linking remote sensing data and a forest model?

(2) How well does simulated AGB represent ground observations?

(3) How does forest structure influence the spatial distribution of AGB in the Amazon rainforest?

3.3 METHODS

3.3.1 *The individual-based forest gap model*

The individual-based, forest gap model FORMIND [Köhler and Huth, 2004; Fischer et al., 2016] was developed specifically for the simulation of tropical forests. Tree species are assigned to plant functional types (PFTs) in order to represent forests of high diversity. Forests can thereby develop through different successional stages. In FORMIND, tree growth is mainly driven by light (photosynthetic photon flux density (PPFD)). Four main processes are calculated for each tree individually in each time step: establishment, competition for light, growth and mortality (Fig. 3.1, for more details see B1). An individual tree can establish if there is sufficient space and light. Since a tree grows individually, each tree competes for space and light. Growth of each tree results from its carbon balance including photosynthetic production and respiratory losses. Mortality of a tree is stem diameter-dependent and is determined stochastically. Traditionally, a forest gap

model is applied at the local scale (< 50 ha). The forest site is divided into equally distant 20m x 20m patches ('gaps'). Within each patch, trees have no explicit position.

As a first step, FORMIND was applied to local forest stands in central Amazon where detailed forest inventory data were available (stem size distributions of different successional stages in the Amazon basin [Brondizio and Moran, 2009]; in climax stage near Manaus [Kunert et al., 2015]. Species were assigned to three plant functional types (early, mid and late successional trees). FORMIND was found to reproduce observed biomass and stem size distributions of the different successional states (see Appendix B1, Tab. B2 and Fig. B3 for parameterization of the basic forest model).

3.3.2 *The regional individual-based forest gap model*

Expanding the forest model from the local scale (stand level) to the regional scale (entire Amazon rainforest) implied some model adaptations. Preliminary tests showed that driving the model by spatially variable PPFD [WFDEI Forcing Data, Weedon et al., 2014] alone is not sufficient to reproduce different species (here PFTs) compositions across the Amazon rainforest. Supported by literature [Castanho et al., 2013; Galbraith et al., 2013; Malhi et al., 2015], we found that we can adapt the forest model's mortality parameter of shade tolerant, late successional trees to reproduce inventory data correctly. This key parameter was calibrated [Lehmann and Huth, 2015, , see B1 for calibration method and objective function] to simulate above-ground forest biomass, mean wood density and basal area information of 180 mature forest sites [based on data of Lopez-Gonzalez et al., 2011; Mitchard et al., 2014]. The mortality rate of the shade tolerant species (PFT3) was the most dominate driver for structural differences so that we calibrated only this mortality parameter to simplify the procedure. The calibration resulted in 180 different parameter sets (one mortality parameter for PFT3 (late successional trees) per site). The calibrated mortality parameters were correlated to local characteristics such as climatic conditions (precipitation, length of dry season, climatic water deficit) and soil properties (classification and chemical properties) which were derived from global maps (Tab. B6).

We investigated intensively linear (Appendix Tab. B4) and multivariate (Appendix Tab. S. B5) linear regressions between calibrated parameters and 40 local conditions. The calibrated mortality parameters were best replicable with a linear function driven by precipitation and clay fraction (as a representative for soil type). This relation is supported by field observations which state that tree mortality might be related to drought characteristics [Malhi et al., 2015] and soil physical properties [Quesada et al., 2012]. Note, that the analysis was restricted to climatic and soil conditions that were available as Amazon-wide, continuous maps. Nutrients in soils were not considered in the analysis. FORMIND was extended by the input annual precipitation [derived from WFDEI,

Weedon et al., 2014] and clay fraction [Wieder et al., 2014] as a proxy for mortality. Mortality is reduced with rising precipitation and clay fraction (see Appendix B1 for function and parameter values). Our regionalization method was inspired by regionalization techniques commonly used in hydrology where model parameters are linked with land surface properties [Blöschl and Sivapalan, 1995; Samaniego et al., 2010].

3.3.3 *Large scale simulations of the Amazon rainforest*

We applied the adapted forest model on the entire Amazon rainforest as is defined by the following criteria [as in Malhi et al., 2006]: all forest plots are located at an elevation below 1000 m; they are categorized as rainforest or moist deciduous rainforest (according to the FAO definition) and have an annual mean temperature above 18 °C. In this study, we considered additionally only forest plots that have a mean maximum canopy height above 10 m. Global and regional datasets (climate, soil properties, canopy height map, Appendix Tab B6) used in this study were processed with the Climate Data Operators [CDO, 2015].

In order to reduce computational efforts, we classified the study region into regions of similar environmental conditions: mean annual precipitation (8 classes: [0-500,500-1000,...,3500-4000] in mm a^{-1}), clay fraction (10 classes: [0-0.1,0.1-0.2,...,0.9-1]) and mean annual PPFD (13 classes: [670-690 , 690-710, ..., 970-990] in μmol m^{-2} ha^{-1}). This resulted in 1040 regions in total, to which we refer as 'response units' (Appendix Fig. B13). The assumption is that forest dynamics are similar within each response unit due to similar input conditions [inspired by the concept of 'hydrological respose units' in Flügel, 1995]. FORMIND was used to simulate forest succession from bare ground to climax stage over 1000 years on an area of 1 km^2 (100 ha) for each response unit. In total, we simulated growth of more than 50 Mio individual trees (stem diameter $\geqslant$ 10 cm) spread over 1040 km^2 of forest. The calculations were performed in parallel (per 1km^2) on a Linux-based computer cluster (simulation time $<$ 20 min on 1000 cores). According to local environmental and soil conditions, we assigned the simulation results of the response units to each 1km^2 grid cell of the Amazon rainforest.

3.3.4 *Linking remote sensing data and the forest gap model to identify forest successional states*

After 300-500 years of simulation, the simulated forests in all regions within the Amazon rainforest reach climax stage where dynamics are driven by tree mortality caused by tree fall or crowding. In the following, we refer to simulations in climax stage as the 'undisturbed scenario'. We linked our simulation results and a wall-to-wall canopy height

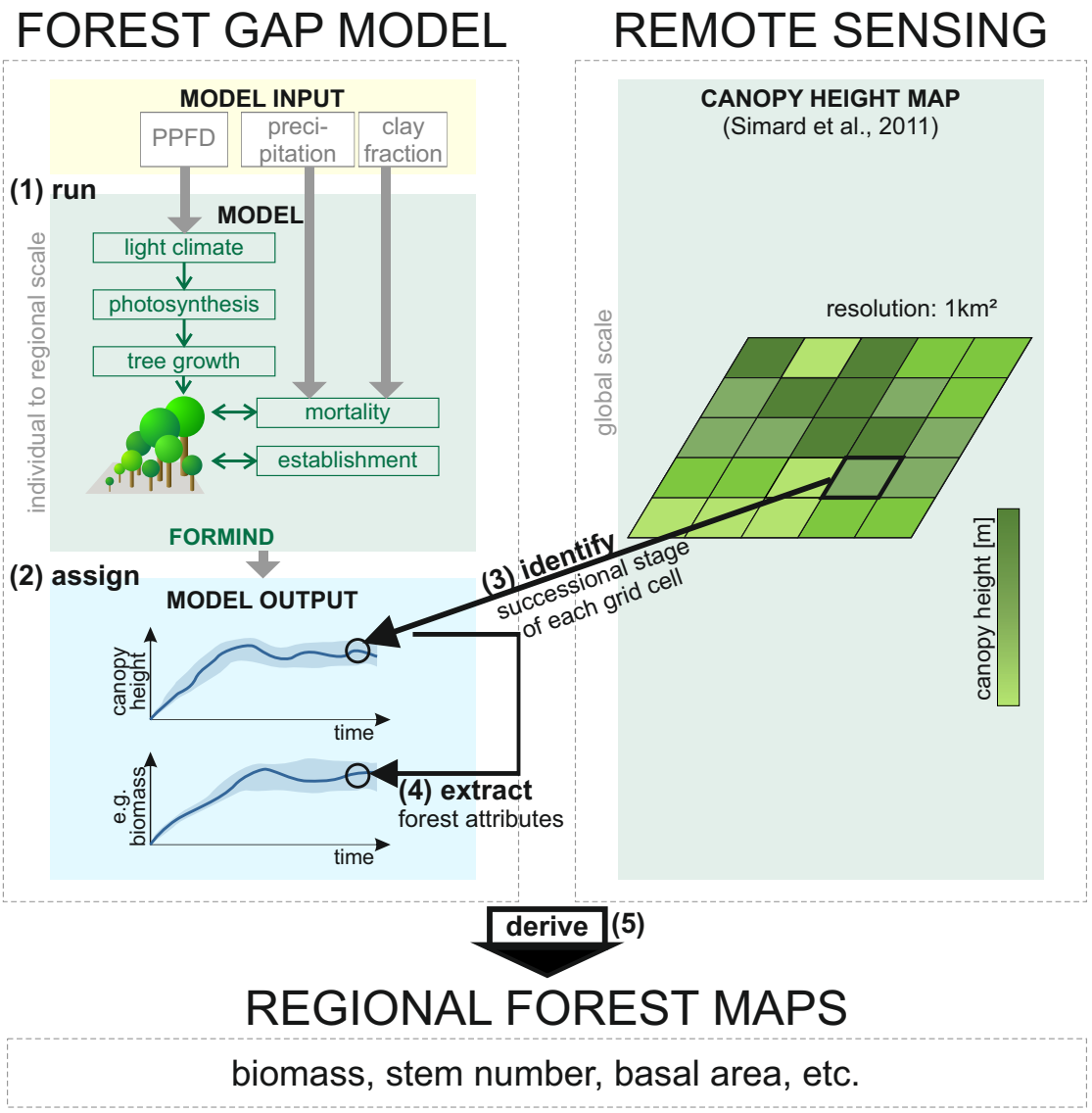

Figure 3.1: The five working steps to derive regional maps from an individual-based forest gap model in combination with remote sensing data: (1) run the forest model on 1 km^2 to equilibrium driven by local photosynthetic photon flux density (PPFD), precipitation and clay fraction, (2) assign the simulations to the grid cells of the Amazon rainforest according to similar input, (3) link canopy height of remote sensing data at each location with the forest simulations to identify the successional stage, (4) extract other simulated forest attributes at the same successional state (e.g., above-ground biomass). (2)-(3) is performed for every 1 km^2 grid cell within the Amazon rainforest to finally (5) derive forest maps.

map [Simard et al., 2011] in order to identify the actual successional state of forests caused by larger disturbances such as logging, deforestation, or blow-downs (Fig. 3.1). The canopy height map was derived from remotely-sensed LIDAR data (2005 data from the Geoscience Laser Altimeter System (GLAS)) and has a resolution of 1 km^2.

For each grid cell, we identified the time steps (within simulation years 0-1000) of the forest simulation when simulated canopy height was equal to the observed, static value

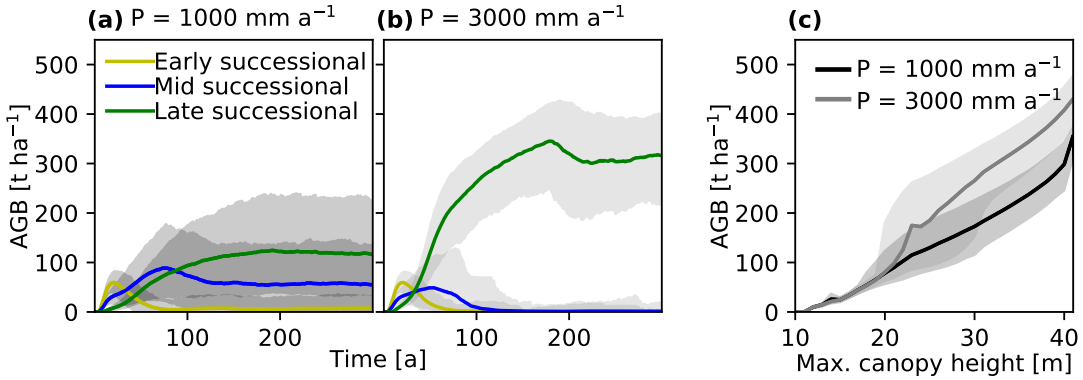

Figure 3.2: (a,b) Exemplary, mean above-ground biomass (AGB) of 1 km^2 over time (solid lines) for the three plant functional types (early, mid and late successional trees) from bare ground to climax stage for: (a) annual precipitation (P) of 1000 m a^{-1}, clay fraction of 30% and photosynthetic photon flux density PPFD = 720 µmol m^{-2} ha^{-1}, (b) annual precipitation of 3000 m a^{-1}, clay fraction = 30% and PPFD = 720 µmol m^{-2} ha^{-1}. Mortality is driven by precipitation and clay fraction which results in different forest structures. The shaded range around mean AGB shows the spatial variation (95% quantile) of 100 ha plots (100 individual 1 ha plots in 1 km^2). (c) Total AGB of all 40 m x 40 m plots within 1 km^2 (simulation time of 1000 years) over its maximum canopy height, exemplary for two response units. The shaded range around AGB results from the different time steps when the maximum canopy height is reached.

of the canopy height map. The simulations then provide additional forest attributes at the identified time steps such as AGB (Fig. 3.2 (c)), basal area or tree density. It is hence possible to derive regional maps of, for example, AGB for the Amazon rainforest. In the following, we refer to this simulation as 'disturbed scenario'. The 'disturbed scenario' describes the current state of the Amazon, while the 'undisturbed scenario' describes the potential biomass of the Amazon under current mean climate (Fig. 3.4, Appendix Fig. B14). The potential biomass of the 'undisturbed scenario' is derived by calculating the mean biomass over years 500-1000 of the simulation (forest in mature state). We also tested a model version for which we hold the mortality rates constant throughout the entire Amazon rainforest, we refer to as 'disturbed scenario with constant mortality'. The AGB map was validated with data of 114 independent field inventories of different successional states [Houghton et al., 2001; Mitchard et al., 2014; Poorter et al., 2015].

3.3.5 *Spatial resolution of the approach*

The smallest resolution of the approach is the individual tree which grows within a 40m x 40m patch. From this, we can derive frequency distributions for AGB for the Amazon at different spatial resolutions (0.16 ha, 1 km^2). The derived AGB map is shown at 1 km^2 resolution which corresponds to the resolution of the used remote sensing product

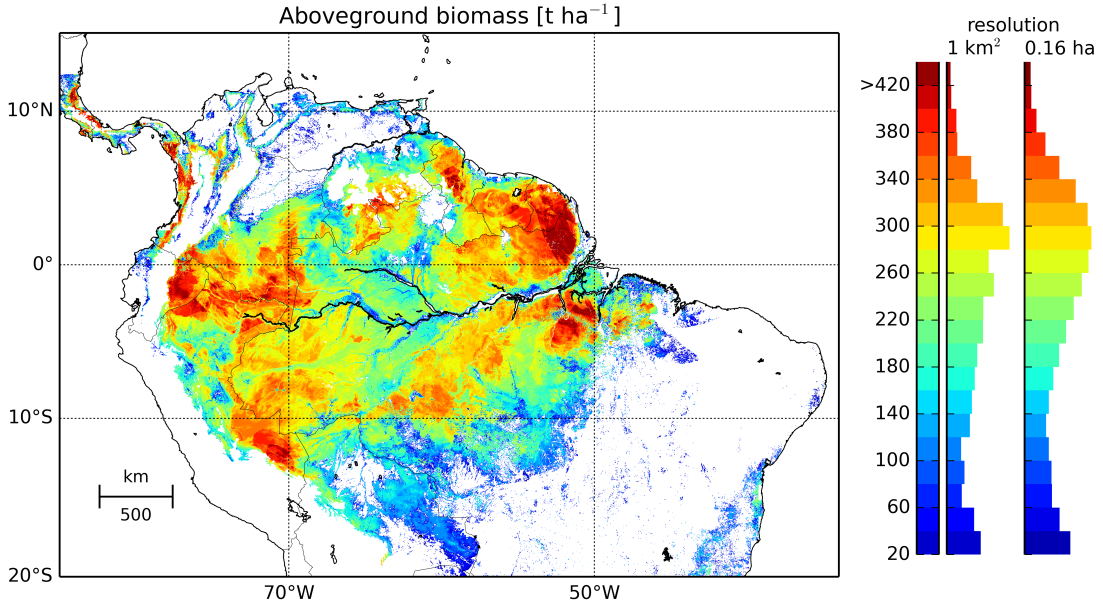

Figure 3.3: Map of aboveground biomass (stem diameter > 10 cm) in the Amazon rainforest (South American rainforest with elevation < 1000 m) and relative frequency distributions (right) at 1 km^2 resolution and at 20 m x 20 m resolution (smallest resolution of forest model) simulated with an individual-based forest model. Successional stages within the simulation were identified via a canopy height map.

(canopy height map). Hence, it represents the simulated AGB values at 1 km^2 resolution by taking the mean over all 40 m x 40 m patches (625 patches which correspond to 100 ha = 1 km^2). We identify the forest state at which the three highest trees within 40m x 40m (~footprint size of LIDAR) equal the height of the canopy height map [the canopy height map was validated with the three highest trees in 20 m radius in Simard et al., 2011].

3.4 RESULTS

The individual-based forest gap model enabled the simulation of forest dynamics and succession over time. Different environmental conditions have an influence on tree mortality rates. This causes different species compositions across the Amazon rainforest which can be represented by the ratio between early, mid and late successional trees (Fig. 3.2 (a,b)). In the forest simulations, late successional trees clearly dominate the forest in regions of high precipitation/clay fraction while species composition is more balanced in regions of lower precipitation/clay fraction.

Linking simulated data with the canopy height map of Simard et al. [2011] resulted in an AGB map at 0.16 ha to 1 km^2 resolution (Fig. 3.3, coefficient of variation in

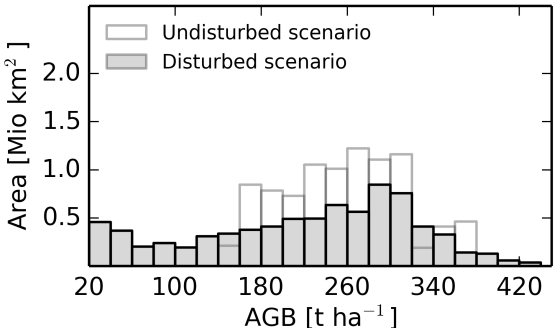

Figure 3.4: Frequency distribution of simulated aboveground biomass (AGB) for the simulated undisturbed scenario (mature forests, steady state of simulations) and disturbed scenario (linked to canopy height map).

Fig. B5). The mean simulated AGB (dry mass) stored in South American tropical rainforests (elevation $<$ 1000 m) is 222 t ha^{-1}; in total 76 PgC on 7.8 Mio km^2. Our AGB map (Fig. 3.3) shows a pronounced gradient between regions of high biomass density in northeastern and lower in southern Amazonia. Highest values are estimated for the north-eastern Guiana Shield and around the east Amazon delta with AGB up to 490 t ha^{-1}. AGB is slightly lower in central Amazon rainforest along the Amazon river. In western Amazon, biomass distribution strongly varies with peaks of up to 44 t ha^{-1}. At the northern and southern edges, biomass is reduced due to deforestation. We estimated mean AGB values (and standard deviation) for four regions across the Amazon basin [regions according to Feldpausch et al., 2011]: Western Amazon 239$\pm$99 t ha^{-1}, Brazilian Shield 170$\pm$102 t ha^{-1}, East Central Amazon 226$\pm$77 t ha^{-1} and Guiana Shield 264$\pm$82 t ha^{-1}.

Our AGB map considers human-induced and natural disturbances identified via canopy heights. Across the Amazon basin, biomass ranges from 20 to 490 t ha^{-1} (mean 222 t ha^{-1} with a standard deviation of 100 t ha^{-1}). If we do not relate the canopy height map to our simulation results, we analyze the simulated forest in an undisturbed, mature state (Fig. 3.4, 'undisturbed scenario', see methods for details). In this scenario, mean biomass is higher with 264 t ha^{-1} and the variability of biomass is lower with a standard deviation of 54 t ha^{-1} since natural (e.g. flooding) or anthropogenic disturbances are not considered. In the undisturbed case, total AGB is 15 PgC higher than in the disturbed scenario.

The new AGB map was tested with observed biomass from field inventories [Houghton et al., 2001; Lopez-Gonzalez et al., 2011; Mitchard et al., 2014; Poorter et al., 2015, ; Fig. 3.5]. On average, our model approach underestimates observed biomass by about 15% (R^2=0.41). If several inventories were located within one grid cell (1 km^2) they were summed up to larger sample sizes. Note that these samples are not necessarily connected to each other's. Values of sample sizes greater than 4 ha [suggested size of field calibration plots in Réjou-Méchain et al., 2014] match particularly well with a root

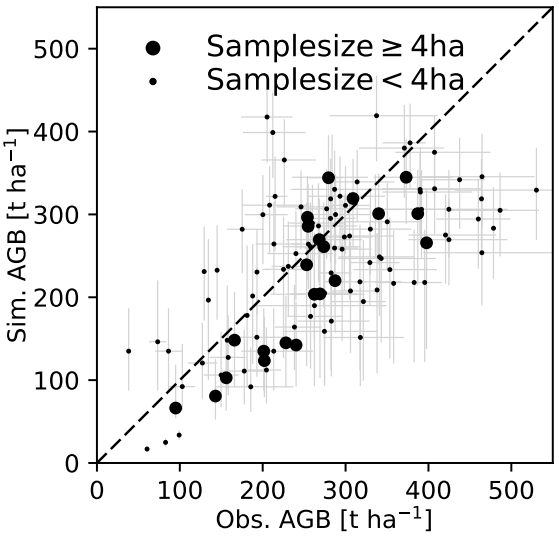

Figure 3.5: Comparison of simulated above-ground biomass (AGB, closest location to inventory in AGB map, Fig. 3.3) and observed AGB at 114 field inventories [Houghton et al., 2001; Lopez-Gonzalez et al., 2011; Mitchard et al., 2014; Poorter et al., 2015].The ranges of observed AGB (horizontal grey error bars) come from different allometries used in Mitchard et al. [2014]. The error bars for the simulated biomass (vertical grey error bars) result from different time steps at which the observed canopy height matches the simulated canopy height. The dashed line is the 1:1 line. R^2=0.41; root mean square error (RMSE) and normalized (nRMSE) for samples of sizes >4 ha and for all points: $RMSE_{samplesize>4ha}$= 61 t ha^{-1}, $nRMSE_{samplesize>4ha}$=0.12, $RMSE_{all}$= 73 t ha^{-1}, $nRMSE_{all}$=0.15.

mean square error $RMSE_{samplesize>4ha}$=61 t ha^{-1} (normalized $RMSE_{samplesize>4ha}$=0.12) while all together (all points in Fig. 3.5) have a $RMSE_{all}$=73 t ha^{-1} ($nRMSE_{all}$ = 0.15).

We also tested a third model version ('disturbed scenario with constant mortality') in which mortality was kept constant throughout the Amazon (Fig. B9). In this scenario, mean AGB is lower with 199 t ha^{-1} and model performance is weaker with R^2 = 0.37 (Fig. B10). The model version does not reach AGB values above 350 t ha^{-1} (Fig. B11).

The forest model delivers additional forest attributes such as basal area, tree densities or stem size distributions. Fig. 3.6 (a) shows the spatial distribution of basal area (stem diameter > 10 cm) within the Amazon rainforest with a mean of 26 m^2 ha^{-1} and a range between 0 and 48 m^2 ha^{-1}. Tree densities (Fig. 3.6 (b)) range in between 0 and 920 stems ha^{-1} (mean is 484 stems ha^{-1}). Fig. 3.6 (c) shows the stem diameter distribution for the entire Amazon rainforest.

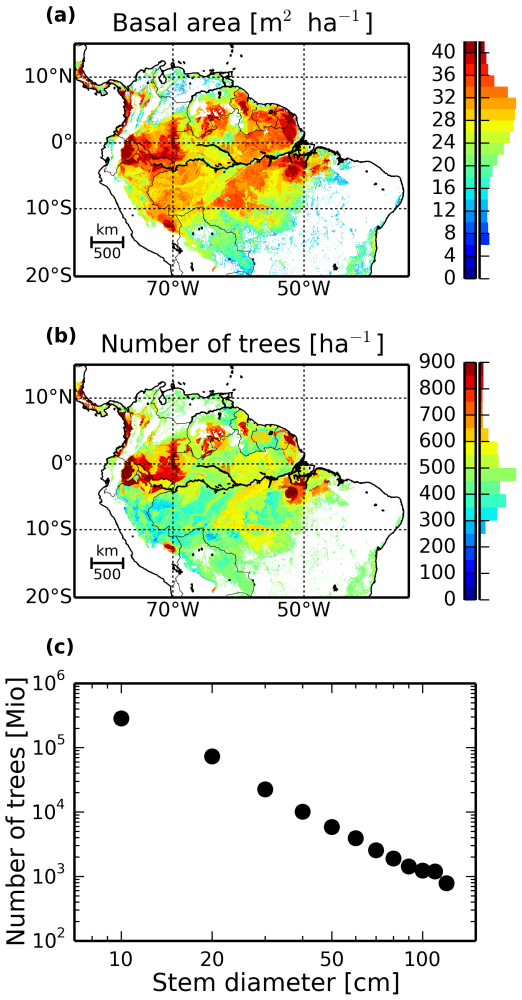

Figure 3.6: Maps and relative frequency distributions of (a) basal area [m^2 ha^{-1}] and (b) number of stems [ha^{-1}] (stem diameter $>$ 10 cm) simulated for the Amazon rainforest (elevation $<$ 1000 m) with the forest model linked to a canopy height map. (c) Stem diameter distribution of the entire Amazon rainforest on a log-log scale.

3.5 DISCUSSION

The estimated above-ground biomass varies between 20 and 490 t ha^{-1} across the Amazon. This range is a result of a new regionalization approach and the combination of ground data, a remote sensing product and a forest gap model. In the following, we discuss the potentials and limitations of combining such information.

3.5.1 *The regionalization approach*

We developed a regionalization approach to transfer the local forest model to the regional scale. In this approach, we analyzed the potential drivers for biomass variations in the Amazon. Studies agree that mortality rates drive the spatial variation of AGB

within the Amazon rainforest [Delbart et al., 2010; Castanho et al., 2013; Galbraith et al., 2013; Malhi et al., 2015]. We tested 40 relations between mortality rates and environmental factors (Tab. B4, Tab. B5). We obtained the best results with precipitation and clay fraction as a proxy for mortality (regarding standard error and R^2). Previous studies support the assumption that a combination of climatic and soil physical conditions could drive turnover rates in the Amazon [de Castilho et al., 2006; Malhi et al., 2006, 2015; Quesada et al., 2012]. We detected a decrease of mortality with increasing clay fraction. This relation might arise from the fact that water retention is higher in clay-rich soils as hydraulic conductivity decreases with clay fraction [Maidment, 1993].This means that a higher clay fraction compensates partly the influence of dry periods on mortality in our forest model. In this study, we have developed a regionalization method that quantifies the spatial variation of mortality via a geostatistical approach. A logical next step would be to integrate a soil water module into the forest model. Simulating at monthly time steps might detect potential stress induced mortality events during dry seasons. This could be an essential step for potential studies on exploring the impact of climate change scenarios. However, the parameterization of a root zone soil water module for the entire Amazon is challenging and requires further intensive studies.

3.5.2 *Obtained distribution of AGB in the Amazon rainforest*

The simulated AGB patterns across the Amazon rainforest (Fig. 3.3) are mainly driven by two aspects: (1) the variation of forest dynamics due to regionally variable mortality rates and (2) the variation in forest states defined by the canopy height map. The stem-based mortality rates influence local forest dynamics by including small-scale disturbances due to tree fall. Hence, different mortality rates cause different tree species compositions which result in a larger spatial variation of biomass throughout the Amazon rainforest (Fig. 3.2). Simulated mean AGB in climax stage varies between 140 and 366 t ha^{-1} ('undisturbed scenario', Fig. 3.4). This range is similar to old-growth inventories summarized by Malhi et al. [2006]. Our simulation result of potential biomass (Appendix Fig. B14) shows similar patterns in the east and south as in Malhi et al. [2006]. However, the forest model produces higher values in the north-western regions due to high mean precipitation resulting in low mortality rates (Appendix Fig. B13).

Large-scale disturbances are reflected in the canopy height map of Simard et al. [2011]. Canopy heights are lower in flooded regions along the Amazon river compared to old-growth terra firme stands. Pioneer trees prevail in flooded regions [Martinez and Letoan, 2007]. Deforested and secondary forest stands also occur along the 'Arc of deforestation' [Nogueira et al., 2007, 2008]. Such regions are represented by an earlier successional stage in our forest model and thereby have smaller aboveground biomass in our biomass map.

The distribution of AGB in our map resembles in some aspects the distribution of previous AGB maps that are derived from remote sensing data [Saatchi et al., 2011; Avitabile et al., 2016, ; Fig. B6]. Differences result from the variation of mortality rates in our forest model that cause differences in forest dynamics. For values above 200 t ha^{-1}, AGB values are a bit lower than in the previous maps. In the Western Amazon where precipitation and clay content is high, our simulations produce higher values. The AGB frequency distributions show the same patterns for values below 200 t ha^{-1}.

Johnson et al. [2016] tested several DVGMs to derive AGB maps of the Amazon. The AGB maps of four DGVMs all differ in its patterns and values. Other than these DGVMs that traditionally capture undisturbed states of mature forests, forest gap models allow for simulating through all successional states. Thus, the here presented map does not only include mature states, but also considers early to mid-successional states by combining the simulation with additional information from remote sensing.

Our simulated map may resemble a map of kriged observations better than the maps produced with the four DGVMs. With our approach, we obtain high simulated AGB values in the north east and lower simulated values towards the south west. The reason for an AGB gradient in our map lies in the nature of simulating forest structures on the individual tree level with stem-based mortality rates. Higher mortality rates in the south west cause stronger dynamics and thereby lower biomass values (Fig. 3.2). We hope to get deeper insights into processes in future studies. In addition, the modeling approach enables the consideration of natural and anthropogenic disturbances by linking simulations to remote sensing data.

3.5.3 *Limitations of the approach*

Limitations of the forest model. Like every model, forest models include model structure uncertainties due to limitations in the knowledge on functional relations and due to simplifications (e.g., the PFT concept). The comparison of the basal area map (Fig. B7) with field data shows an overestimation by 11% while biomass is slightly underestimated (15%). Partly, this mismatch is ascribable to the assumption of just 3 PFTs for the entire Amazon for which tree geometry (dbh-height relation) parameters are held constant. Additionally, biomass calculations based on allometric relations of field inventories [Feldpausch et al., 2012] might differ from the one used in our simulation [based on allometries commonly used in forestry including a form factor, Pretzsch, 2010]. The trend, however, between basal area and biomass is similar in inventory data and simulated data (Fig. B8). This explains why the pattern of the basal area map resembles the one of Malhi et al. [2006] regarding high values at the Guiana Shield, at the Amazon river close to the Atlantic ocean, at the Ecuadorian boarder and in the south-west (~71°W,12°S). Also, note that for the comparison of biomass (Fig. 3.5), we include more inventory data

(secondary and mature forests) than for the comparison of basal area [mature forests in Mitchard et al., 2014].

Limitations due to climatological and soil data. Additional limitations arise from input data. Meteorological data (PFFD and precipitation) come from an independent modeling approach at a resolution of 0.5° [Weedon et al., 2014]. The clay fraction map arises from an interpolation at 8 km resolution [Wieder et al., 2014]. It is difficult to quantify the influence of its spatial resolution on our AGB map. We assume however that input data are reliable to an extent that uncertainties that arise from the input data should be smaller than structural and methodological uncertainties.

The assumption of canopy height as a proxy for successional states and disturbed forests. This assumption is inspired by a pioneering study that linked canopy height and a forest model to derive biomass for local forests sites in Costa Rica [Hurtt et al., 2004]. Taking the large-scale canopy height map as a proxy for successional states has several limitations. First, the proxy is not explicit since canopy height can be associated to different stem size distributions. The canopy height map does not provide information on the forest history, so a forest could be in a state of regrowth after anthropogenic degradation or in a maturing state after a natural disturbance event. Second, we are aware of the fact that the canopy height map only provides a proxy at a resolution of $1km^2$ and does not capture the full spatial height heterogeneity. The canopy height map is a product of discrete recordings by LIDAR that are transferred into a continuous map via a modeling approach [Simard et al., 2011]. We here rely on those modeled values and assume that they are representative. It is the best information we have at the moment to identify large-scale successional stages within the Amazon.

It would be interesting to integrate also other satellite products into our approach, for example the NDVI [normalized difference vegetation index, Running et al., 2004]. In future studies, they could improve estimates of disturbed regions with lower biomass values and lower tree densities since it is available at high resolution and could be taken as a proxy for leaf area index. However, in dense mature forests, it is known that the NDVI saturates and thus has limited capability to identify spatial variation [Myneni et al., 2001; Hall et al., 2011].

Uncertainties in field inventory data. Forest inventories can include measurement errors, coordinate uncertainties and unrepresentative sample plots [Saatchi et al., 2015]. In addition, inventory data often come from small plots (~1ha). At such small scales, biomass can vary strongly [Chambers et al., 2013b]. The validation of the AGB map (Fig. 3.5) has shown that samples with a sample size $\geqslant$ 4 ha [critical sample size in Réjou-Méchain et al., 2014] match the 1:1 line better than samples of smaller sizes (normalized RMSE of 0.12 vs. 0.15). In total, mean simulated AGB is 15% lower than mean observed AGB. One reason for this underestimation of inventory values might be the 'bias towards ma-

jestic forest stands' for field inventories [Malhi et al., 2002], a bias that results from selecting old-growth, gap-free inventory sites.

3.5.4 *Benefits from linking remote sensing and forest models*

Saatchi et al. [2015] listed the following main challenges when estimating AGB in tropical forests: (1) considering diversity in structure, wood density and dynamics and the complexity of allometries; (2) including natural and anthropogenic disturbances; and (3) weak relationships between environmental conditions and biomass. The authors conclude that ground and remote sensing observations need to be linked to estimate biomass at the large scale. In this study, we additionally integrated an individual-based forest model to estimate the AGB of the Amazon. Forest gap models, in particular FORMIND, are developed to simulate forest structures of highly diverse tropical forests, thus addressing challenge (1) and (2). Calculating forest dynamics at the individual tree level allows for considering complex height structure and enables the analysis of forest structures of disturbed and undisturbed sites [Köhler and Huth, 1998]. In this aspect, forest gap models differ from several dynamic global vegetation models which handle forest stands as an average individual and are often insufficient to capture detailed structures of tropical forests [Johnson et al., 2016]. We tackled challenge (3) by analyzing the influence of local environmental conditions on tree mortality rate.

Bridging the gap between different spatial scales of ground-based observations and remote sensing products with the help of an individual-based forest gap model can provide a better understanding of heterogeneous forest structures. Since forest gap models capture the dynamics and states at the individual tree level, maps of various forest attributes (Fig. 3.6, tree density for different tree sizes in Fig. B12) at different spatial resolutions can be derived ($\geqslant$ 0.16 ha for AGB in Fig. 3.3).

The approach presented here sets a foundation for further structural, large-scale analyses on disturbances [e.g., Huth et al., 2004], secondary forest regrowth [e.g., Poorter et al., 2016], fragmentation [e.g., Pütz et al., 2014] or with an extended model version on future climate scenarios [e.g., Rammig et al., 2010].

3.6 CONCLUSION

Individual-based forest gap models simulate forest dynamics throughout all successional states. By capturing forest structures at small scales, these types of forest models are able to fill a gap between large-scale vegetation modeling (such as DGVMs), remote sensing products and ground observations. With our approach, we see a chance to complement the linkage between ground and remote-sensing observations [Saatchi et al., 2011]. The

individual-based forest gap model delivers a tool with spatially explicit information on forest structures and dynamics. The validation with field inventories has shown that forest structure, in terms of species composition and forest height, has a strong influence on the spatial variation of biomass in the Amazon rainforest. The approach opens new doors to analyze highly diverse, large-scale forest structures of the Amazon rainforest concerning carbon fluxes, disturbances and climate change scenarios. In combination with products of future remote sensing missions [e.g., ESA Biomass, GEDI or proposed Tandem-L Moreira et al., 2015], better insights into large-scale structures and dynamics of tropical forests will be feasible.

ACKNOWLEDGEMENTS

This study was supported by the Helmholtz-Alliance Remote Sensing and Earth System Dynamics. ER was kindly supported by the Helmholtz Impulse and Networking Fund through the Helmholtz Interdisciplinary Graduate School for Environmental Research (HIGRADE). We thank Rico Fischer, Franziska Taubert, Sebastian Paulick, Matthias Zink and Juliane Mai for helpful discussions and technical support.

4 THE IMPORTANCE OF FOREST STRUCTURE FOR THE ESTIMATION OF CARBON FLUXES IN THE AMAZON RAINFOREST

This chapter is based on a manuscript (in prep.):
Rödig, E., Cuntz, M., Rammig, A., Fischer, R., Heinke, J., Taubert F., Huth, A.: The importance of forest structure for the estimation of carbon fluxes in the Amazon rainforest

4.1 ABSTRACT

Understanding the interactions of forest productivity, biomass and structure are essential for the analysis of ecosystem's response to climatic and anthropogenic changes. However, finding explicit relations between fluxes and stocks for the Amazon rainforest is particularly challenging since forests are highly dynamic. We here applied an individual-based forest model on a large-scale, the Amazon rainforest. The simulation results were then combined with remotely-sensed data (forest height map). This linkage enabled to detect different forest states and structures caused by small-scale to large-scale natural and anthropogenic disturbances. Carbon fluxes of the Amazon rainforest were analyzed at a spatial resolution of 0.16 ha (40 m x 40 m).

We found that under current conditions, the Amazon rainforest is a carbon sink, gaining 0.59 Gt C per year. This carbon sink is driven by an estimated mean gross primary production (GPP) of 25.1 tC ha^{-1} a^{-1}, mean woody aboveground biomass (wANPP) of 4.2 tC ha^{-1} a^{-1}, and mean annual net ecosystem productivity (NEP) of 0.8 tC ha^{-1} a^{-1}. We further investigated the relations between productivity and biomass and found that successional states under spatial heterogenic environmental conditions play an important role. Our results show that forests in intermediate successional states are the most productive and that forests have different carbon use efficiencies resulting in a non-linear relation between GPP and wANPP.

We can conclude that forest structure has a substantial impact on productivity and biomass. It is an essential factor that should be taken into account when estimating current carbon budgets or analyzing climate change scenarios for the Amazon rainforest.

4.2 INTRODUCTION

Current estimates on carbon storage and fluxes in the Amazon rainforest diverge [Baccini et al., 2012; Saatchi et al., 2013; Mitchard et al., 2014; Avitabile et al., 2016] and take a great share in the uncertainties of the global carbon cycle [Cox et al., 2013; Le Quéré et al., 2016]. One reason for the diverging estimates is that the Amazon rainforest is constantly exposed to disturbances such as wind blow-downs [Fisher et al., 2008; Chambers et al., 2013b], droughts [Phillips et al., 2009; Gatti et al., 2014], and deforestation [van der Werf et al., 2009; Pütz et al., 2014; Poorter et al., 2016]. Such disturbances shift forests into earlier successional states which differ in species composition and forest structure. This fact is often neglected in large-scale estimates of the carbon budget [Houghton, 2005]. In addition, at the small scale, the successional state of a forest is constantly changing due to natural tree mortality and gap building [Chambers et al., 2013b]. It has been observed in field studies that these dynamics have a strong

influence on biomass, productivity [Chave et al., 2004; Malhi et al., 2015], and forest structure [Dubayah et al., 2010; Feldpausch et al., 2011], however, causalities are poorly understood.

Recent field inventory studies deliver valuable analyses on potential drivers for the spatial variation of biomass and productivity within the Amazon rainforest. It was found that forest dynamics and hence biomass and productivity might be related to seasonality [Chave et al., 2006; Malhi et al., 2015] and soil properties [Quesada et al., 2012]. However, one challenge of field-studies on large regions is that they are limited by their number and by the size of field plots [Marvin et al., 2014]. Analyses on the relation between biomass stocks and climatic conditions are based on ca. 300 1-ha plots [e.g., Malhi et al., 2006], and on biomass increments on even less [ca. 200, Brienen et al., 2015b,a]. A more detailed analysis on carbon partitioning into gross and net primary production, for example, is based on ten field plots [Malhi et al., 2015]. An additional limitation lies in the fact that field studies do not account for the full range of successional states, forest structure, and species compositions. Anyhow, such field studies deliver indispensable information that vegetation modeling and remote sensing research can built up on.

In this study, we see a chance to include different successional states in the analysis on carbon dynamics in the Amazon rainforest. We used an approach that links a canopy height map with an Amazon-wide forest gap model (chapter 3). Forest gap models simulate forest succession at the individual tree level. This brings along two key advantages: First, it allows for considering stem-based mortality rates that vary throughout the Amazon. It was found that individual tree death which can be interpreted as small-scale disturbances, have a strong effect on forest carbon stocks [Espírito-Santo et al., 2014]. Second, forest models simulate forest structure and species compositions throughout all successional states. The approach presented here takes advantage of this characteristic by linking simulated forest structure with remotely sensed canopy height [here a canopy height map, Simard et al., 2011]. One can then derive the current state of the forest at a specific location, considering disturbances at different spatial scales and with spatially heterogenic environmental conditions.

The approach presented here makes it possible to explore the relations between above-ground biomass (AGB), carbon fluxes, and successional states at high continuous spatial resolution ($\geqslant$0.16 ha). This allows for presenting maps of simulated carbon fluxes such as gross primary production (GPP), above-ground woody net primary production (wANPP), and net ecosystem productivity (NEP) for the Amazon rainforest at different spatial scales. Simulation results were compared to previous simulated global maps [MODIS GPP and NPP, Running et al., 2004; Zhao and Running, 2010], estimates of forest inventories [Brienen et al., 2015a; Malhi et al., 2015], and eddy-flux measurements (FLUXNET, GF-Guy, BR-Sa3).

The following research questions will guide us through the present study:
(1) How do successional states influence the carbon dynamics of the Amazon?
(2) How do carbon storage and carbon fluxes vary spatially across the Amazon region?
(3) Is the spatial variability of GPP and NPP in the Amazon rainforest mainly driven by its spatial variability of biomass?

4.3 METHODS

4.3.1 *An Amazon-wide individual-based forest gap model*

4.3.1.1 *Basic concept of the forest model*

The herein presented analyses are based on a regionalized version (chapter 3) of the forest gap model FORMIND [Fischer et al., 2016]. The forest gap model simulates forest dynamics at the individual tree level. In this study, these dynamics are driven by constant mean climatic conditions (mean over years 2003-2012). The following main processes are calculated on a yearly time step: tree growth, competition, establishment, and mortality. Growth of an individual tree depends on its location within the forest community where trees compete for light and space. Hence, tall trees receive more light than smaller ones. A gain in tree biomass results from the difference between photosynthesis and respiration losses. The gross primary production of a tree (GPP_{tree}) is calculated using a light-response function at the leaf level which is then scaled up to the crown of the tree [Thornley and Johnson, 1990; Huth and Ditzer, 2000; Fischer et al., 2016]:

$$GPP_{tree}(I_{ind}) = \frac{p_{max}}{k} \cdot \ln \left\{ \frac{\alpha k I_{ind} + p_{max}[1-m]}{\alpha k I_{ind} e^{-kLAI} + p_{max}[1-m]} \right\} A_c \psi \qquad (4.1)$$

in μmol(CO2) m^{-2} s^{-1}, where I_{ind} [μmol(photons) m^{-2} s^{-1}] is the light that reaches the top of the individual tree, p_{max} [μmol(CO2) m^{-2} s^{-1}] is the maximum leaf photosynthetic rate of the tree species, α is the initial slope of the light-response curve [μmol(CO2) μmol(photons)$^{-1}$], k is the light extinction factor, and m is the transmission coefficient of the leaves. A_c [m^2] is the crown area, and ψ [s a^{-1}] the photosynthetically active period [see Fischer et al., 2016, for a full description of the model; Tab. C1 and Tab. B2 for parameter values].

A seedling can establish if light intensity on the forest floor is sufficient. A tree can die for several reasons. Mortality increases when tree crowns are limited in space (crowding). In addition, every tree underlies a basic mortality rate which is stochastically determined within every model time step. Falling of large trees can damage surrounding trees (gap building) and causes conditional mortality events. Dead biomass is transferred to a dead wood carbon pool from which carbon is constantly transferred to a soil carbon pool (decomposition) or respired to the atmosphere.

The exchange of carbon between the forest and the atmosphere (net ecosystem productivity NEP [tC ha^{-1} a^{-1}]) is described as follows [Paulick et al., 2017; Sato et al., 2007]:

$$NEP = \sum_{tree} (GPP_{tree} - R_{tree}) + t_{DA} S_{dead} + t_{SA} S_{fast} + t_{FA} S_{fast} \quad (4.2)$$

The sum over all tress of gross primary production (GPP_{tree} [tC ha^{-1} a^{-1}]) minus autotrophic respiration (R_{tree} [tC ha^{-1} a^{-1}]) equals the woody above-ground NPP (wANPP) of the forest site ([tC ha^{-1} a^{-1}]). Autotrophic respiration R_{tree} is calculated as the sum of maintenance and growth respiration which also includes root respiration (assumed to be directly emitted to the atmosphere, Fig. C1). Its annual rate is calculated in order to fit observed above-ground biomass growth of a tree. We assume that wANPP is a constant fraction of NPP [NPP = 2.72wANPP, derived from pan-tropical aggregated data for mature forests in Anderson-Teixeira et al., 2015] to convert annual wANPP to annual NPP. S_{dead} is the dead wood pool, S_{slow} the slow decomposing soil carbon pool and S_{fast} the fast decomposing soil carbon pool (all [tC ha^{-1}]) with its respiration rates to the atmosphere (t_{DA}: S_{dead} to atmosphere, t_{SA}: S_{slow} to atmosphere, t_{FA}: S_{fast} to atmosphere).

The advantage of simulating each tree individually is that change in forest structure is captured throughout all different successional states: from bare ground to climax stage including natural tree death. A detailed description of the forest model can be found in Fischer et al. [2016].

4.3.1.2 *The regionalized forest model*

The regionalized version of FORMIND has been introduced and evaluated chapter 3. In the regionalized version, spatially variable precipitation (mean over years 2003-2012) and the clay fraction in soil are used as a proxy for stem-based mortality rates. The variation of mortality rates induce different species compositions which is represented by three plant functional types (PFTs) in the model: early successional, mid successional and late successional tree types that differ mainly in productivity, needed light at establishment and mortality rates (Tab. C1).

Technically, the individual-based model could simulate tree growth for every tree in the Amazon rainforest. However, the computational effort can be reduced for areas with similar environmental conditions. Each 1 km^2 of the Amazon rainforest was therefore categorized into regions of similar model input of annual mean precipitation, annual mean photosynthetic photon flux density (PPFD), and clay content (1040 regions in total). We calculated the growths of every tree within each 1 km^2 on 625 x 0.16 ha plots. In total, we simulated 1040 km^2 of forest including more than 50 Mio individual trees over a simulation time of 1000 years (example for carbon fluxes in Fig. C2) on a high-performance Unix cluster.

4.3.2 *Identifying the current state of the Amazon rainforest*

The successional state of each forest within the Amazon is identified via a canopy height map [Simard et al., 2011] as in chapter 3. For each location in the Amazon rainforest (1 km^2), we selected the time step of the simulation to which the simulated canopy height equals the canopy height of the canopy height map (identified successional state of the forest). We could then identify also the forest's current, simulated carbon stock and its associated carbon fluxes.

4.3.3 *Input data*

The forest model was driven by mean annual photosynthetic photon flux density (PPFD), precipitation [for both mean values over years 2003-1012, WFDEI, Weedon et al., 2014], and clay fraction of soil [Wieder et al., 2014]. The data was re-gridded to the resolution of the forest canopy height map [1 km^2, Simard et al., 2011] with the climate data operators [CDO, 2015].

The study region covers forests in South America that are categorized as rainforest or moist deciduous rainforest (according to the FAO definition), have an annual mean temperature above 18°C, are located at an elevation below 1000 m, and have an AGB > 20 t ha^{-1} (chapter 3).

4.3.4 *Validation*

We compared our simulation results against observed NPP and GPP values from ten inventory sites in the lowland Amazon rainforest [Malhi et al., 2015], measured woody above-ground net primary production (wANPP) from 193 sites [Brienen et al., 2015b,a], and GPP and NEP from two eddy covariance sites [GF-Guy, FLUXNET, Bonal et al., 2008, BR-Sa3, FLUXNET]. Please, note that the eddy covariance method observes the entire net ecosystem exchange (NEE) and we assumed here –NEE=NEP [Chapin et al., 2006]. Global mean GPP and NPP estimates from MODIS at 1 km^2 resolution for the years 2000-2010 [Running et al., 2004; Zhao and Running, 2010] were compared against our simulation results. Both products were re-gridded to the resolution of the canopy height map (1 km^2) using climate data operators [CDO, 2015, nearest neighbor].

4.4 RESULTS

4.4.1 *Dynamics of forests in different successional states*

We use basal area fraction of late successional trees as an index for the successional state of a forest. AGB, GPP, wANPP, and NEP are then analyzed by classifying the forest into different successional states (at 0.16 ha resolution, Fig. 4.1, Fig. C3). AGB increases throughout the successional state of a forest while GPP and wANPP values peak at early/mid-successional state (fraction of late successional trees = 0.25-0.5). NEP is highest in early successional states while the carbon budget of forests in later successional states is around 0.

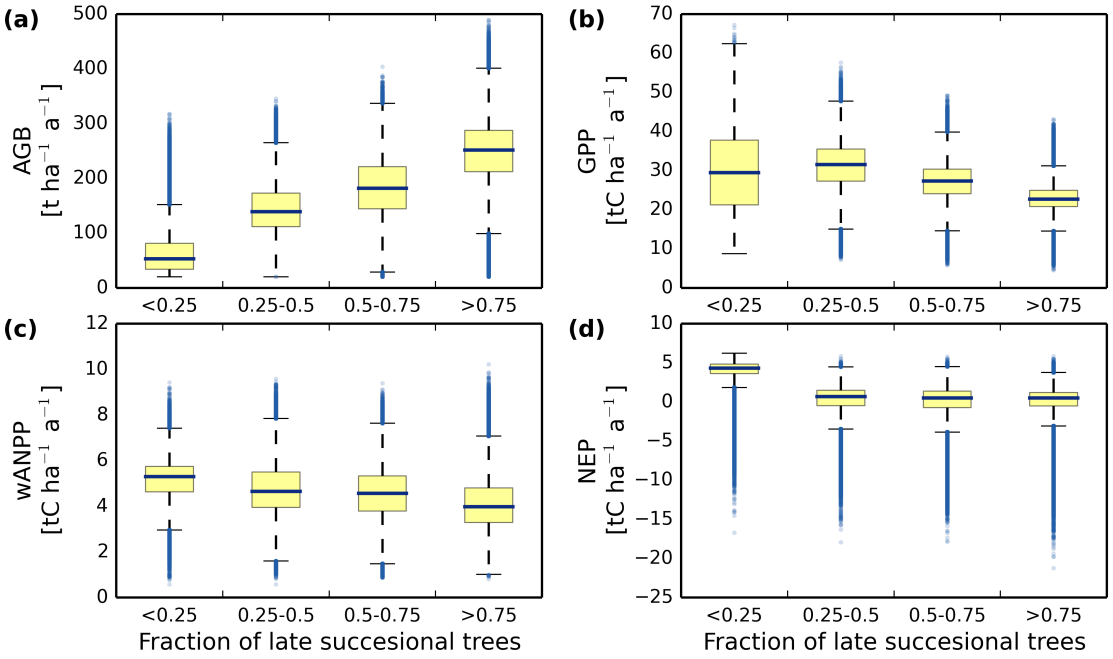

Figure 4.1: Estimated (a) above-ground biomass (AGB), (b) gross primary production (GPP), (c) woody aboveground net primary production (wANPP), (d) net ecosystem productivity (NEP) for forests in the Amazon, analyzed for different successional states (spatial resolution 0.16 ha, 4.8 billion forest plots). The fraction of basal area of late successional trees is used to classify the forest into different successional states. Median is shown as a blue horizontal line and outliers (outside whiskers) as blue dots.

4.4.2 *Spatial distribution of GPP, wANPP and NEP at different spatial scales*

Across the Amazon basin, we obtain a mean forest GPP of 25.1 tC ha^{-1} a^{-1} (Fig. 4.2, Tab. 4.1). We find that GPP values are higher along the Amazon river and in the southern Amazon rainforest (Fig. 4.2 (a)). The pattern of woody aboveground production (wANPP , Fig. 4.2 (b)) across the Amazon rainforest resembles the one of GPP with higher values along the rivers and in southern Amazon. Mean wANPP is 4.2 tC ha^{-1} a^{-1}. In some parts of the Amazon (e.g., the Guiana Shield) GPP values are higher than the mean while wANPP values are lower than the mean. The NEP varies around zero (Fig. 4.2 (c)) with a mean NEP value of 0.8 tC ha^{-1} a^{-1}. Only along the south-east and north-west, NEP values of up to 5 tC ha^{-1} a^{-1} are reached.

The variation of GPP, wANPP, and NEP values at small scales (0.16 ha resolution) is higher than the variation at 1 km^2 resolution (frequency distributions in Fig. 4.2). For example, the analysis of NEP at 0.16 ha resolution shows that forests can release up to 20 tC ha^{-1} a^{-1} to the atmosphere (Fig. 4.1 (d)), while its maximum release at 1 km^2 is 0.23 tC ha^{-1} a^{-1}. These very low NEP values have a strong influence on the mean value over the entire Amazon (frequency distributions at both resolutions in Fig. 4.2 (c)). Within an area of 7.8 Mio km^2, the Amazon rainforest takes up 0.59 PgC per year.

Table 4.1: Mean ± standard deviation (at 1 km^2 resolution) of gross primary production (GPP), woody above-ground net primary production (wANPP), net ecosystem productivity (NEP), and above-ground biomass (AGB, chapter 3) over 7.8 Mio km^2 for four regions [according to Feldpausch et al., 2011] across the Amazon region.

	Mean GPP ± std [tC ha^{-1} a^{-1}]	Mean wANPP ± std [tC ha^{-1} a^{-1}]	Mean NEP ± std [tC ha^{-1} a^{-1}]	Mean AGB ± std [t ha^{-1} a^{-1}]
Western Amazon	24.7±3.0	3.9±1.1	0.7±1.3	208±120
Brazilian Shield	25.7±3.9	4.6±1.0	1.3±1.8	123±112
East Central Amazon	24.7±2.8	4.3±0.9	0.5±1.2	218±86
Guiana Shield	25.0±2.2	3.9±1.0	0.3±0.8	255±93
Amazon region	25.1±3.2	4.2±1.0	0.8±1.4	188±120

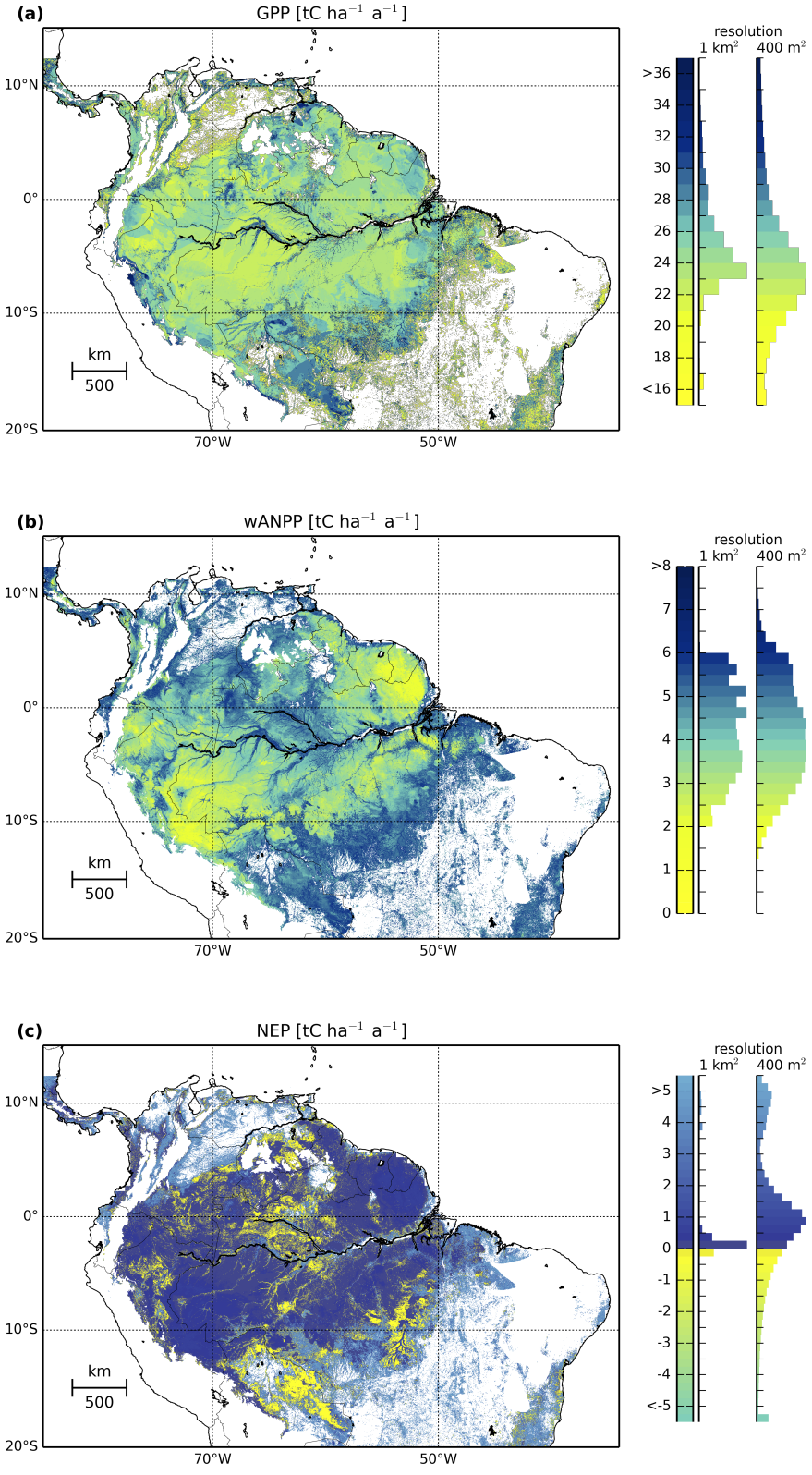

Figure 4.2: Maps and frequency distributions under mean climate conditions of (a) gross primary production (GPP), (b) woody above-ground net primary production (wANPP), and (c) net ecosystem productivity (positive values indicate a sink of atmospheric carbon), estimated with FORMIND. The maps and the left histograms have a resolution of 1 km^2. The right histograms have a resolution of 0.16 ha.

4.4.3 *Comparison of simulation results with other flux estimates*

We compare our obtained values at 1 km^2 resolution (Fig. 4.3) with estimates derived from MODIS [1 km^2 resolution, Running et al., 2004; Zhao and Running, 2010], inventory data [ca. 1 ha plots, Brienen et al., 2015a; Malhi et al., 2015] and eddy-covariance measurements (< 1 km^2 footprint, FLUXNET stations GF-Guy and BR-Sa3).

Gross primary production: The distribution of simulated GPP resembles closely the one derived from MODIS (Fig. 4.3 (a)). GPP derived from inventory data [24-42 tC ha^{-1} a^{-1}, Malhi et al., 2015] and from eddy flux measurements at GF-Guy [32-40 tC ha^{-1} a^{-1},

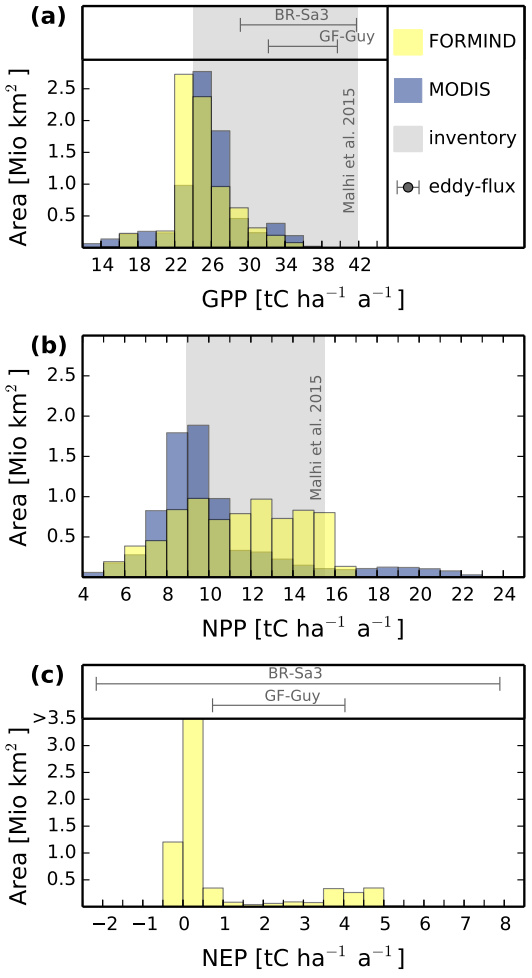

Figure 4.3: Frequency distributions of FORMIND estimates for (a) gross primary production (GPP), (b) net primary production (NPP), and (c) net ecosystem productivity (NEP) for forests in the Amazon at 1 km^2 resolution in comparison to: estimates from remote sensing [1 km^2 resolution, MODIS, Running et al., 2004], inventory data [$\leqslant$ 1 ha resolution, 10 plots with recorded GPP and NPP, Malhi et al., 2015], and eddy covariance measurements (GF-Guy and BR-Sa3). The ranges of estimated values from field inventories are marked in grey. Eddy-flux measurements at two sites are shown for the full range of annual sums. Note that positive values of NEP indicate a sink of atmospheric carbon.

Bonal et al., 2008] and BR-Sa3 eddy flux station (29-42 tC ha^{-1} a^{-1}) fall into the upper ranges of our simulated GPP.

Net primary production: MODIS NPP shows a similar pattern as its related GPP distribution and has a clearly defined peak at 9-10 tC ha^{-1} a^{-1} (Fig. 4.3 (b)). FORMIND simulated NPP, on the other hand, displays a wide plateau of 8 to 16 tC ha^{-1} a^{-1}. NPP values derived from forest inventory range from 9-16 tC ha^{-1} a^{-1} [Malhi et al., 2015]. Estimated wANPP from field inventories [Brienen et al., 2015a] range from 1.1 to 4.7 tC ha^{-1} a^{-1}, while FORMIND reaches high wANPP values of up to 6 tC ha^{-1} a^{-1} (Fig. C4). Note that the field inventories are limited to a few measurements (193 sites) mainly taken in old-grown forests.

Net ecosystem productivity: Simulated NEP values under mean climate conditions fall into the range of recordings at the GF-Guy eddy flux station (0.5-3.5 tC ha^{-1} a^{-1}) and the BR-Sa3 station (-2.2-7.0 tC ha^{-1} a^{-1}).

4.4.4 *Relation between analyzed carbon stocks, dynamics and species compositions*

Fig. 4.4 shows the obtained relations between carbon fluxes and stocks according to the successional state of a forest plot. Forests of early successional state (yellowish) reach AGB values of 100-150 t ha^{-1}. Forests of the mid-successional state (light-bluish) reach values up to 300 t ha^{-1}. Late successional forests (dark- bluish) occur for higher AGB greater than 250 t ha^{-1}. wANPP and AGB stock show a bell-shaped relation (Fig. 4.4 (a)). GPP values and AGB values form a triangle (Fig. 4.4 (b)). Forests in early successional states reach higher GPP values than late successional forests (with the same AGB). Comparing both figures ((a) and (b)) in late successional state (dark- bluish dots), it can be noticed that wANPP decreases with increasing AGB while GPP increases with AGB. The relation between GPP and wANPP displays the woody above-ground carbon use efficiency which varies for different successional states (Fig. 4.4 (c)). Low GPP values are reached for all successional states with a broad range of wANPP values. NEP is always positive for early successional forests. NEP values of late successional forests show a high variation (Fig. 4.4 (d)).

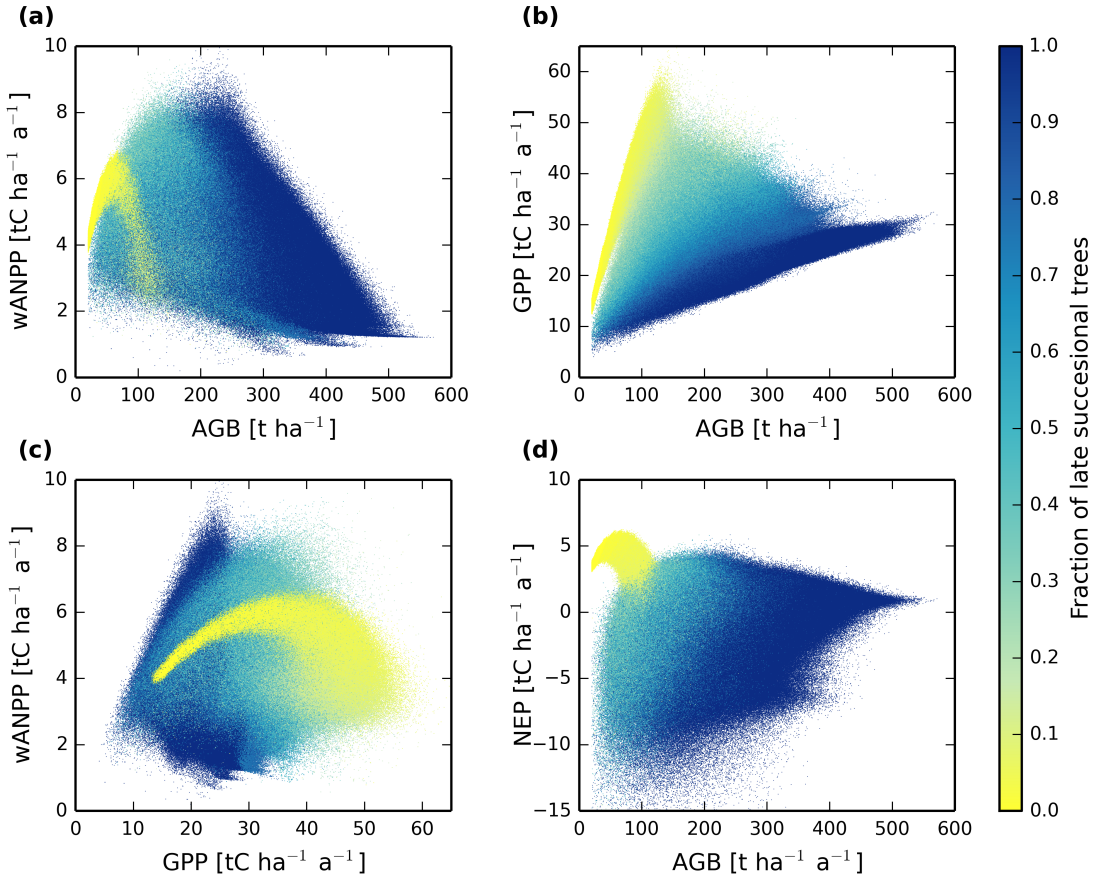

Figure 4.4: Relation between simulated carbon fluxes and successional states within the Amazon rainforest at a resolution of 0.16 ha (Fig. C5 for 1 ha resolution). Successional states are represented by the basal area fraction of late successional trees within each 0.16 ha plot (yellow for early successional state to dark blue for late successional states). (a) Aboveground biomass (AGB) vs. AGB, (b) gross primary production (GPP) vs. AGB, (c) GPP vs. wANPP, and (d) GPP vs. net ecosystem productivity (NEP). GPP, NEP, and wANPP are in tons carbon per hectare per year (tC ha^{-1} a^{-1}); AGB values are in tons dry mass per hectare per year (t ha^{-1} a^{-1}).

4.5 DISCUSSION

In this study, we show that our individual-based simulation allows for assessing the Amazon rainforest under different forest structure and species compositions. The approach aims for extending our knowledge on carbon dynamics in the Amazon including various successional states.

4.5.1 *Carbon fluxes and stocks at different successional states*

Our analysis shows that the successional state of a forest has a strong influence on carbon stocks and fluxes as some selected examples show in the following. It is noticeable that GPP, wANPP, and NEP are highest for forests in early to mid-successional states (Fig. 4.1). Such forests of high productivity can be found in our maps (Fig. 4.2), for example, along the 'Arc of deforestation' in the south-east [Nogueira et al., 2007, 2008] where forests are influenced by human activities. The successional state of a forest is not only determined by such disturbances at the large scale, but also influenced by individual tree death. This means that, even undisturbed, large forests in mature state, consist of different successional states at the small scale (e.g., 0.16 ha, Fig. C2) and, hence, can show strong fluctuations in its carbon dynamics. Chambers et al. [2013b] found, for example, that cumulative biomass of a mature forest is stable over time only for sample plots greater than 10 ha. For that reason, flux values at 0.16 ha resolution show larger variability than at 1 km^2 resolution (frequency distributions in Fig. 4.2).

The strength of our approach is that it allows for analyzing relations between forest states, and fluxes at different spatial resolutions. Analyses of field studies can be expanded by evaluating simulation results. For example, we can confirm (Fig. 4.4 (a) at 0.16 ha resolution, Fig. C5 (a) at 1 ha resolution) the assumption that highly productive forests may limit AGB values due to a dominance of species with low wood density [Keeling and Phillips, 2007]. Productivity seems to follow the intermediate disturbance hypothesis where productivity is highest at intermediate successional state (Fig. 4.1 (c)). This finding differs from simulation results of 4 DGVMs at 1° resolution for the Amazon region presented in Johnson et al. [2016]. In their study, three DGVMs simulate increasing productivity with increasing AGB. Only one DGVM shows a slight reduction of productivity at high AGB values. They conclude that stem based mortality need to be included in order to capture the relation as observed in the field [Johnson et al., 2016]. Here, we consider stem based mortality and forest structure at the individual tree level. This is particularly important for the Amazon, where carbon stocks and dynamics are driven by a variation of stem based mortality [Baker et al., 2004; Phillips et al., 2004; Quesada et al., 2012; Galbraith et al., 2013; Malhi et al., 2015].

The relation between AGB and NEP shows that most carbon is lost from forests in intermediate to late successional states (Fig. 4.4 (d)). This finding supports the finding of Espírito-Santo et al. [2014] that internal gap-formations of mature forests cause greatest carbon losses, whereas large-scale disturbances can be compensated by forest growth. This is pronounced particularly at 0.16 ha resolution where individual tree death has a strong impact on carbon estimates as compared to at coarser resolution (Fig. C5 (d), where the forest is closer to steady-state condition).

4.5.2 *Comparison with field data and remote sensing measurements*

Testing the representativeness of our simulated carbon flux maps relies on the comparison with another map derived from remote sensing and simulation [MODIS, Running et al., 2004; Zhao and Running, 2010] since direct carbon flux field measurements in the Amazon rainforest are rare. The number of field inventories in the Amazon is increasing, but still cover only a small fraction of the Amazon and plot sizes are relatively small [e.g., ca. 200 1 ha plots in Brienen et al., 2015b]. Hence, its representativeness for the entire Amazon and accuracy remains an open question [e.g., Réjou-Méchain et al., 2014]. Also, eddy-covariance measurements are only partly suitable for large-scale estimates. Keep in mind that NEE are measured half-hourly and come with measurement errors. Hence, annual NEE values are based on gap-filling procedures which makes them less representative than values at small temporal scales [Moffat et al., 2007]. However, inventory and eddy-flux measurements give valuable evidence on dimensions and ranges of carbon fluxes that occur in the Amazon rainforest regardless all their limitations.

GPP: The GPP frequency distribution is here shown at the highest resolution of the MODIS product (1 km^2). The MODIS GPP pattern [Running et al., 2004; Zhao and Running, 2010] resembles our simulated GPP pattern (Fig. 4.3 (a)) although both maps are derived from different remote sensing techniques (NDVI vs. LIDAR). This resemblance strengthens the general representativeness of our GPP map. Observed GPP values (field and eddy flux measurements) show partly higher values than simulated GPP values at 1 km^2 resolution. Note, however, that our simulation reaches the observed values at 1 ha resolution (resolution of field inventories, Fig. C5).

NPP: The NPP histograms (Fig. 3.3 (b)) show that the approach used here displays more areas of high NPP values (>12 tC ha^{-1} a^{-1}) than the MODIS product. We can draw the following two conclusions from this comparison: First, the NPP pattern of the MODIS product seems to correlate strongly with the GPP pattern. In our approach, NPP depend on two factors: spatially variable forest dynamics, and the canopy height map. This results in a broad relation between the two fluxes (carbon use efficiency is not constant, Fig. 4.4 (c)). Other than the MODIS approach, our forest model approach allows for considering different species compositions and successional states across the Amazon

which leads to higher NPP values. These higher NPP values can also be observed in field inventories. Second, the MODIS product is limited by the fact that it is derived from NDVI values which tend to saturate in dense mature forests and, thus, have limited capability to identify spatial variations, such as in the Amazon [Myneni et al., 2001; Hall et al., 2011]. The approach presented here uses a canopy height map [Simard et al., 2011] that is derived from LIDAR measurements (active traces). Such active remote sensing tracers have the advantage that they identify forest structure better than passive tracers as used with MODIS [Lefsky et al., 2002]. This allows for capturing more spatial heterogeneity.

NEP: It was found that the Amazon forest gains, on average, 0.59 Pg of carbon per year. Our estimate compensates approximately the amount of carbon currently emitted due to deforestation and land-use change in South America [Baccini et al., 2012]. In particular forests in earlier successional states, contribute to an uptake of atmospheric carbon (Fig. 4.1 (d)). NEP measurements at eddy flux station BR-Sa3 show a broader range than at GF-Guy. This may result from the fact that BR-Sa3 is a logged forest site which includes different species compositions and forest structures, while GF-Guy is assumed to be an undisturbed site. In our approach, a logged forest is represented by an earlier successional state which is characterized by a higher uptake of atmospheric carbon. The NEP values can only be compared to a few sites. Anyhow, this analysis helps to get a better insight into the relation between forest structure, biomass, and carbon fluxes.

4.5.3 *Limitations of our approach*

The current approach is based on linking a regionalized forest model with a canopy height map. The present study focuses on spatial differences in carbon dynamics due to forest structural and environmental differences under current climatic conditions. Consequently, results capture fluxes at one point in time. The study design does not yet consider the effects of inter- or intra-annual variations of temperature or atmospheric CO2 on forest structure. It is anticipated to integrate such effects into a future analysis. Though, it remains a challenge how to predict the quantity of large-scale disturbances.

We here extended an approach that was developed to derive a biomass map of the Amazon rainforest (Chaper 3). The approach brings along structural uncertainties like the assumption that NPP is a constant fraction of wANPP, and limitations due to the resolution of input data like climatological data and the canopy height map [Simard et al., 2011]. The canopy height map is based on discrete LIDAR shots and provides estimates for maximum canopy height at a resolution of 1 km^2. Nevertheless, it remains a challenge how to fill missing information between shots (Chaper 3). In future work, it is desirable to integrate LIDAR shots into the analyses by directly comparing LIDAR profiles with forest simulations.

Carbon fluxes and budgets of mature forests are in steady-state with a NEP around 0 tC ha^{-1} a^{-1}, and stable dead wood and carbon soil pools. In disturbed forests, on the other hand, dead wood and soil fluxes may depend on its disturbance history (fire event, logging, etc.) which cannot be reconstructed from the canopy height map. Thus, our study is based on the assumption that the forest either regenerates after deforestation (simulation from bare ground with initialized dead wood and soil pools, Tab. C1), or is influenced by natural tree fall and its surrounding damage (gap-dynamics).

4.6 CONCLUSION

We show here that forest productivity of Amazon rainforests is strongly determined by the stored biomass, species compositions, and forest structure. In previous studies, these relations were analyzed based on forest inventories and remote sensing data but could not be fully resolved. Linking both, inventory and remote sensing data, with vegetation modeling at the tree scale enables to examine the Amazon rainforest at different successional states. With our approach, dynamics of forests can be examined at different spatial resolutions (individual to Amazon-wide scale). Derived values can thereby be compared to any desired spatial scale of observations. This allows also for considering strong spatial variability in carbon fluxes caused by small- (gap-building) to large-scale (e.g., deforestation) disturbances. The successional state, and hence the forest structure and species composition, have a strong effect on NPP and NEP estimates. Spatial variability of AGB alone cannot explain spatial differences in productivity across the Amazon. Our analyses highlight the importance of forest structure for carbon dynamics, which is often a neglected aspect in dynamic vegetation modeling.

ACKNOWLEDGEMENTS

ER, RF, AR, JH, and AH were supported by the Helmholtz-Alliance Remote Sensing and Earth System Dynamics. We thank Damien Bonal for providing eddy covariance data.

5 CONCLUSION AND OUTLOOK

5.1 MAIN RESULTS, LIMITATIONS AND POTENTIALS

Ecological processes act across spatial and temporal scales and these scales define the extent of variability in such ecological processes [Levin, 1992; Chave, 2013]. This thesis explores the potentials and limitations of simulating carbon fluxes of forest ecosystems. The main tool used in this thesis is a forest gap model. It calculates forest dynamics at the individual tree level and therefore allows for looking at processes at different spatial and temporal scales. The forest model was linked with inventory, remote sensing, and eddy covariance data to analyze the influence of climatic variability and forest structure on carbon dynamics in forest ecosystems.

5.1.1 *Applying a local forest gap model at the regional scale*

Forest gap models such as FORMIND [Fischer et al., 2016], JEBOWA [Botkin et al., 1972], or ForClim [Bugmann et al., 2000] are well established tools to analyze forest dynamics throughout successional states under different environmental conditions. They have proven to describe processes of forest ecosystems better than pure statistical approaches [Bugmann, 2001]. However, they are traditionally applied at local scales. One possibility to transfer processes from the local to regional scale are up-scaling approaches. These involve averaging processes and thereby loose information at the individual tree level as in the models MOSAIC [Acevedo et al., 1995], LANDCLIM [Schumacher et al., 2004], GAPPARD [Scherstjanoi et al., 2013], or a modification of FORMIND [Tietjen and Huth, 2006]. Additionally, up-scaling underlies several challenges such as considering feedback processes across scales, nonlinear ecological processes, and spatial heterogeneity of forest ecosystems [Bugmann et al., 2000]. Nowadays, computational power provides new possibilities and allows for directly applying individual-based forest models for larger regions.

In this thesis, we took advantage of modern high-performance computers and applied the forest model FORMIND at the continental scale, the Amazon rainforest. It was the first large-scale application of this forest model (chapter 3) and involved two major steps: (1) the technical implementation and (2) the regionalization approach.

The technical implementation: Other than previous up-scaling approaches, we here implemented the forest model processes at the individual tree level [as in iLAND, Seidl

et al., 2012]. Thereby, the approach avoids process-averaging issues and overcomes some limitations that arise from traditional up-scaling approaches (as listed above). In this framework, the FORMIND model was adapted to Unix systems in order to be applied on a high-performance computer. Algorithms were developed to run forest sites parallel under spatially variable input. This allowed for simulating 1000 years of forest succession of more than 100,000 ha within a few minutes.

The advantages of simulating individual trees have already been recognized in previous studies. The basic idea of the forest gap approach was implemented to dynamic global vegetation models (DGVM) like LPJml-FIT [Sakschewski et al., 2015], or the Ecosystem Demography (ED) model [Moorcroft et al., 2001]. However, such approaches are often limited by computational capacity (e.g., simulating only 4 ha plots representatively for each 0.5° cell in LPJml-FIT) or model structure (e.g., a size- and age-structured approximation in ED). Our approach differs from these previous models by its implementation strategy. In DGVMs, processes of the gap approach were implemented top-down into their global model setup [Hickler et al., 2004], while in our approach the model was developed for a specific site before it was applied for larger regions (bottom-up). This bottom-up approach has the advantage that it takes species diversity and forest succession along. In our study, this means that species compositions were characterized by three plant functional types (early, mid and late successional trees). Spatially different model input results in spatially different species compositions. Hence, the major challenge was to identify model characteristics that cause such spatial differences in species compositions and forest dynamics (regionalization approach).

The regionalization approach: Applying a forest model at the regional scale involved the regional adaptation of model parameters for which a process-based description is normally missing (e.g., stem-based mortality rates). At the local scale, these parameters are derived from inventory data directly which rely on a time-consuming model parameterization [Fischer et al., 2016]. Due to this parameterization process, forest gap models are often accused to be 'data-hungry' [Guisan and Thuiller, 2005; Jeltsch et al., 2008]. In order to identify regional differences of these parameters across the Amazon, we developed a regionalization scheme that was inspired by regionalization methods used in hydrology [Blöschl and Sivapalan, 1995; Samaniego et al., 2010]. The idea is that the parameter is identified at locations where inventory data are available (Fig. 5.1). Parameter values are related to environmental conditions via functional relations. These relations are then used to assign a parameter value to areas where no inventory data are available.

Based on this regionalization approach, we have identified mean annual precipitation and clay content of the soil as a proxy for the mortality rate of late successional trees for the Amazon rainforest (chapter 3). This relation is based on the assumption that tree mortality is influenced by environmental conditions [Malhi et al., 2015] and soil properties [Quesada et al., 2012]. The novelty and strength of the regionalized mortality

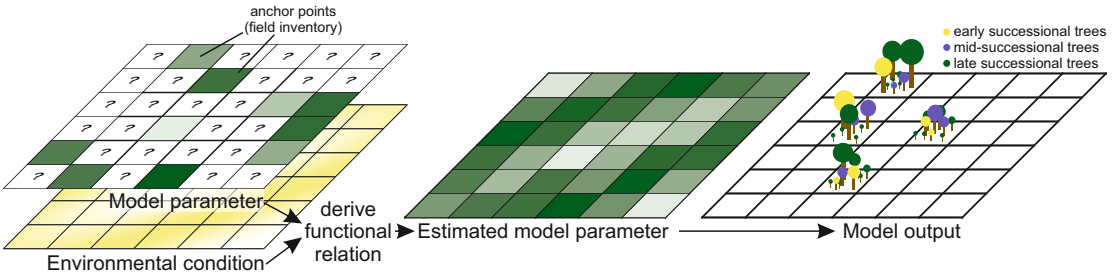

Figure 5.1: Regionalization scheme developed for this thesis (chapter 3). First, parameters (here: mortality rate) are identified for anchor points where inventory data are available (left). In a second step, environmental conditions (left) are functionally related to anchor points. In a third step, the functional relation is used to fill the gaps where no inventory data are available (middle). Different model parameters result in different forest dynamics and species compositions (right).

rates is that it allows for simulating forest dynamics at the individual tree level resulting in spatial variable biomass stocks across the Amazon.

The approach, however, brings along several limitations. Due to simplification, only the mortality rate of late successional trees was spatially adapted. One could think about spatially varying tree geometries in future since it has been monitored that diameter-tree height allometries can be related to biomass differences [Nogueira et al., 2008; Feldpausch et al., 2012]. Another limitation is that mortality is regression-based instead of using process-based formulations. In the LPJ-GUESS model, mortality rate is related to growth-efficiency which is effected by water stress [Smith et al., 2008]. However, this process-based implementation and parameterization is rather ad hoc (personal communication). What seems like a limitation of our approach at first sight, highlights its potential at second sight. Our method can overcome such ad hoc parameterizations and sets a basis for fundamental process-based analyses. We suggest integrating processes step-by-step-wise from a regression-based to a process-based description.

A next possible step is to develop an approach that simulates water stress across the Amazon since our study (chapter 3) has shown that mortality is related to plant available water. One possibility is to activate the water module of the forest model [Bohn et al., 2014; Fischer et al., 2014]. However, the parameterization for such a large region is challenging, especially the parameterization of the rooting depth and soil attributes. A more promising and simpler approach is a parsimonious process-based description of the soil water pool where the plant available water is solely estimated from the plant available water capacity [determined by field capacity and permanent wilting point, Cassel and Nielsen, 1986] and actual available water from precipitation. It will also allow for integrating monthly time steps in order to consider seasonality. Once we have a better understanding on the relation between mortality and water availability, mortality can be linked to stress induced limitations of growth or productivity.

5.1.2 *Linking eddy covariance data and a forest gap model*

The analysis at two spruce forest sites (chapter 2) showed that, in general, forest gap models are capable of simulating GPP, respiration, and NEE of forest ecosystems at high temporal resolution. We adapted the forest model to simulate carbon dynamics at daily time steps. Simulation results were than compared with measurements of the eddy covariance method [Grünwald and Bernhofer, 2007; Rebmann et al., 2010]. The performance of the forest model is satisfying considering the fact that it calculates photosynthesis based on a Michaelis-Menton function. This function describes potential photosynthesis as a direct response to light at the leaf level [Thornley and Johnson, 1990; Fischer et al., 2016]. Limitations due to water and temperature stress are included by multiplying the potential photosynthesis with a limiting factor [Bohn et al., 2014]. The light-response function is a more simple interpretation of photosynthesis than the photosynthesis model of Farquhar [1989], often used in DGVMS (e.g., LPJ). The Farquhar model describes the responses of carbon exchange by leaves under CO_2 and oxygen concentration, temperature, and light. The simplified photosynthesis model in FORMIND has the advantage that model calculations are faster by at least factor 100 compared to the Farquhar [1989] model (personal communication with LPJ users). Despite this simplification, the analysis has shown that the results at the spruce forests Wetzstein and Tharandt was comparable to those of a LPJ-GUESS application to another European monocultural forest [Vermeulen et al., 2015].

The analysis additionally allowed for examining limitations of photosynthesis and respiration due to water and temperature stress that are commonly used in vegetation modeling. We have developed a filtering method that allows for extracting a model parameterization that cannot be detected with a numerical parameter calibration alone [Lehmann and Huth, 2015]. The analysis exposed a new function for photosynthetic reduction due to temperature stress with only two parameter values instead of four in the previous function.

In an ongoing study, we extract our findings and methods on the spruce forest and transfer them to a tropical forest site in French Guyana (master thesis by Anne Piechulla, in prep.). Eddy covariance data [Bonal et al., 2008] are compared to simulation results of the Amazon-wide forest model (parameterization of chapter 3) at the local scale. Other than previous studies which analyzed limiting factors in dynamic global vegetation models for mature forests [Baker et al., 2008; Poulter et al., 2009; Verbeeck et al., 2011], we here detect limitations under consideration of different forest structure and species compositions. Both forest attributes have been identified to be an important factor in forest ecosystem carbon fluxes (chapter 4) and an essential aspect in the simulation of forest dynamics under climate change [Huntingford et al., 2008; Sakschewski et al., 2016]. This ongoing study is a first preliminary step towards a new model version that will also be able to perform drought-stress analyses.

5.1.3 *Linking remote sensing data and a forest gap model*

Modern computational power enables to apply individual-based forest models at the large scale and link simulated forest dynamics with those observed by remote sensing [Shugart et al., 2015]. We developed a novel framework for the Amazon rainforest which uses a forest gap model and a canopy height map derived from LIDAR measurements [Simard et al., 2011]. This canopy height was used as a proxy to identify the current successional state within our forest simulations (chapter 3). This approach resulted in high-resolution (0.16 ha spatially implicitly within spatially explicit mean values over 1 km^2) maps of biomass, productivity, and net ecosystem productivity. We also found that forest structure and species compositions influence carbon stocks and fluxes differently resulting in spatial heterogeneity across the Amazon (chapter 4). It was shown that this novel approach may identify more spatial heterogeneity of productivity than a previous approach that derives productivity from MODIS data [Running et al., 2004; Zhao et al., 2005].

Active remote sensors (LIDAR and RADAR) have proven to be valuable observers of forest structure [Lefsky et al., 2005]. Forest structural attributes like maximum and mean canopy heights are indicators for the successional state of a forest [Dubayah et al., 2010] from which estimates on biomass, tree growth, and leaf distribution can be derived [Lefsky et al., 2002; Nasset and Gobakken, 2005]. Field inventories have shown that canopy height alone is not sufficient to identify carbon stocks and dynamics correctly since they are additionally influenced by environmental conditions [Clark and Clark, 2000; Quesada et al., 2012; Mitchard et al., 2014; Malhi et al., 2015]. Forest models have the potential to complement inventory and remotely sensed data in order to include environmental conditions in the analysis of carbon stocks and dynamics [as in a study on local forest sites in Costa Rica, Hurtt et al., 2004; Dubayah et al., 2010]. In this thesis, this idea has been demonstrated at the large scale, the entire Amazon rainforest (chapter 3 and 4).

Spatial variations due to environmental conditions were confronted with the regionalization approach which resulted in an Amazon-wide individual-based forest model. The linkage of the forest gap model with a remote sensing product was performed with the canopy height map of Simard et al. [2011]. The 1 km^2 resolution canopy height map is a product of LIDAR data from Geoscience Laser Altimeter System (GLAS) onboard Ice, Cloud and land Elevation Satellite (ICESat). Using this wall-to-wall canopy height map has the advantage that gaps between GLAS shots were already filled via a correlation model. It is limited by the fact that it describes a mean value at a resolution of 1 km where forest structure may be highly heterogenic. The major challenge of our approach was to specify the corresponding tree height of our highly dynamic simulation results. The satisfying validation showed that it served well as a framework to link remote sensing data and a forest gap model at such a large scale.

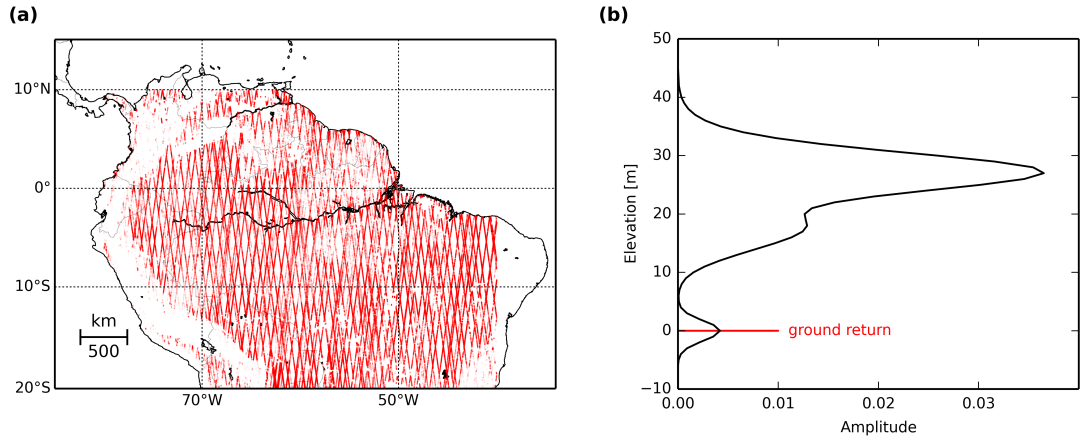

Figure 5.2: (a) GLAS shots (red) in South America. Cloudy shots or shots with slope effects (> 10°, e.g. in Andes) were eliminated. (b) Example for one laser signal described with 6 Gaussian fits. As the shot often covers rough terrain, the signal was shifted that the peak of the ground return meets 0 [both figures were plotted based on data of Los et al., 2012; Tang and Dubayah, 2017]

In a next step, we are planning on directly comparing leaf profiles of the GLAS shots (Fig. 5.2 (b)) with those of our simulation results. With the help of the SIDAR module (SImulated liDAR module) of the forest model FORMIND (Knapp et al., in review), we will be able to derive height metrics for the simulated Amazon rainforest. These allow for a direct comparison with processed GLAS data [Los et al., 2012; Tang and Dubayah, 2017, Fig. 5.2 (b)]. One counts up to 2 Mio shots for the Amazon rainforest when eliminating cloudy shots or shots affected by slope effects [>10°, Los et al., 2012, Fig. 5.2 (a)]. NDVI observations [Huete et al., 2002] and land cover maps [Hansen et al., 2013] may supply additional information to produce wall-to-wall maps of the Amazon. Our study has shown that NDVI alone may not be able to detect all spatial heterogeneity of NPP (chapter 4). However, it may be a potential proxy for leaf area index which might help to fill gaps between discrete GLAS shots.

Several planned and proposed satellite remote sensing missions promise better insights into large-scale structures and dynamics of forests. The ESA Biomass mission will be ready to be launched in 2021 for a 5-years RADAR mission [ESA, 2016]. The satellite will carry a P-Band polarimetric synthetic aperture radar (SAR) with a 100-200 m spatial resolution and 25-45 days revisiting time [Le Toan et al., 2011]. For 2018-2024, the NASA is planning on starting the Global Ecosystems Dynamics Investigation Lidar (GEDI) mission. Three laser transmitters will produce 14 ground tracks spaced 500 m across-track and 60 m along-track with 25 m footprints [NASA, 2017]. The proposed Tandem-L mission with a L-band SAR could observe forest structures with a spatial resolution of 10 meters (horizontal) with a two weeks revisiting time [Moreira et al., 2015]. In combination with individual-based models, such remote sensing missions are promising to improve and complement our understanding on forest dynamics.

5.2 SYNTHESIS AND OUTLOOK

5.2.1 *The Amazon across temporal and spatial scales: the journey continues*

The Amazon rainforest is constantly exposed to climatic and anthropogenic changes which all need to be considered when simulating forest dynamics. The three approaches that were discussed above (regionalization of, linking eddy data with, and linking remote sensing data with a forest model), could jointly contribute to a better understanding of forest dynamics in the Amazon rainforest. The approach might have the potential of complement previous methods like kridging [Malhi et al., 2006], machine learning [Saatchi et al., 2011], or geostatistical diagnostic models [Beer et al., 2010]. The here presented bottom-up approach has the possibility to integrate, interpret, and extrapolate discrete field and remotely-sensed data at different spatial and temporal scales.

The studies presented here provide a basis for interesting additional analyses. Once the driver of spatial variability of mortality within the Amazon is identified process-based via the regionalization approach (chapter 5.1.1), we can project our knowledge from space to time. This means that we can use our newly gained knowledge on how spatial variability of precipitation effects tree mortality, to run the forest model under temporal variable climate. In combination with our improved knowledge on limiting factors of photosynthesis and respiration derived from the comparison with eddy covariance data (chapter 5.1.2), we will be able to improve analyses on drought [Phillips et al., 2009; Gatti et al., 2014] and the Amazon 'dieback' [Huntingford et al., 2008; Rammig et al., 2010]. These steps set a basis for the simulation of climate change scenarios in the Amazon rainforest. This approach differentiates from previous projections with DGVMs by its consideration of forest structure and species compositions. Taking additionally the current condition of the Amazon regarding anthropogenic disturbance via remote sensing data into account (chapter 5.1.3), will advance knowledge on secondary forests [Poorter et al., 2016] and consequences of deforestation [Pütz et al., 2014; Brinck et al., 2017]. A forest gap model provides the opportunity to investigate microclimatic changes in forest fragments [Laurance, 1997] and its follow-up feedback mechanisms, as well as additional influences due to climatic changes. Applying this knowledge on the entire Amazon will potentially reduce substantial uncertainties of the global carbon cycle.

5.2.2 *Large-scale simulations of other biomes*

The thesis shows how forest models (here FORMIND) can be technically set up to simulate forest dynamics at the individual tree level for large regions. This technical implementation can be used to address country- or continent wide research questions on forest ecosystems.

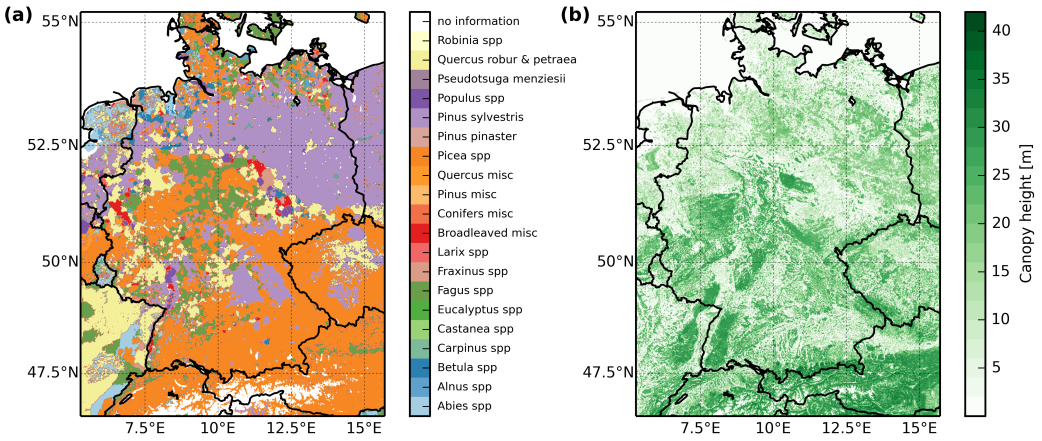

Figure 5.3: (a) Dominant tree species in Germany [modified from Brus et al., 2012]; (b) Canopy height map of Germany derived from lidar remote sensing data [modified from Simard et al., 2011].

The approach, that links the forest model and the canopy height map, can be applied to every region were a basic parameterization is available. Considering the fact that the forest model FORMIND has been applied at various forest sites in the tropics [Huth et al., 2004; Dislich and Huth, 2012; Fischer et al., 2014; Kazmierczak et al., 2014], a logical next step is to derive pan-tropical maps on above-ground biomass, basal area, productivity, and net ecosystem productivity.

Also, a large-scale analysis on forest ecosystems in Germany should be easily feasible. Bohn et al. [2014] have developed a FORMIND parameterization for all major tree species in Germany. A map of proportional tree species [Brus et al., 2012, Fig. 5.3 (a)] could be used as basis for initializing the forest model. The canopy height map [Simard et al., 2011, Fig. 5.3 (b)] can be used to identify forested areas and their successional states. Non-forested areas can be complemented by simulations of the grassland model GRASSMIND [Taubert, 2014]. This approach is fundamental to derive Germany-wide maps of biomass and productivity and analyze the influence of climate variability on forest and grassland dynamics.

This thesis demonstrates that large-scale analyses of forest ecosystems are highly promising when using different methods jointly. Field inventories set the fundamental basis for understanding structure and species compositions of forests. Eddy covariance data help interpreting the influence of variable climate on forest dynamics. Remote sensing data provide large-scale information on spatial variability in forest structure which can be then interpreted and extrapolated with forest modeling. Consequently, this thesis sets a base for future simulations of large regions using individual-based forest models.

APPENDICES

A APPENDIX OF CHAPTER 2

A1 *Functional relationships*

GPP vs. soil water content. GPP data were filtered and normalized for optimal temperature conditions and sunny days in order to analyze the relationship between GPP of the ecosystem and soil water content (Fig. A1 (a)). We compare the filtered data with the three model versions. The literature-based permanent wilting point (19.7%) for clay loam [Maidment, 1993] is too high. Therefore, we assume a lower permanent wilting point (9.5%) and field capacity (20.7%) as for sandy loam for the filter-based parameterization. The numerical calibration estimated an intermediate permanent wilting point. The filtered EC-data does not show any clear limitation of photosynthesis for several potential reasons. Measuring soil water content is challenging and the available data may not be representative. There are only short periods in this temperate forest in which soil water limits photosynthesis, even in the severe drought year of 2003. This makes annual GPP very insensitive to the parameters of the water reduction function. Also, the event in 2003 came with a heat wave [Ciais et al., 2005] which makes it extremely difficult to separate potential limitations. Therefore, water limitation factors are the most uncertain values in the calibrated parameterization. The permanent wilting point for clay loam of the literature-based parameterization was obviously too high. The impact of water stress on photosynthesis has long been a topic of discussion amongst soil scientists and plant physiologists [Slatyer, 1957; Gardner and Nieman, 1964; Hsiao, 1973; Sperry et al., 2002; Chaves, 2002]. In the forest model, the wilting point was set for a specific soil type [Maidment, 1993] rather than for a specific plant type. The limitation due to water stress is not distinguishable from the filtered data. However, note that the permanent wilting point needed to be reduced for the filter-based parameterization.

GPP vs. PPFD. Measured GPP data were filtered to restrain the relation between GPP of the ecosystem and PPFD (Fig. A1 (b)). The data were filtered for optimal soil water conditions and optimal temperature conditions in order to exclude limitations by soil water and temperature (Eq. 2.2. In the model, the potential photosynthesis of the ecosystem equals the sum of GPP of all trees without soil water or temperature limitations. Potential GPP of a tree is described with a light-response function at the leaf level that is integrated over the entire canopy (Eq. 2.1). It is a function of not only PPFD, but also depends on the forest structure. In order to fit the model process through the filtered data, the model

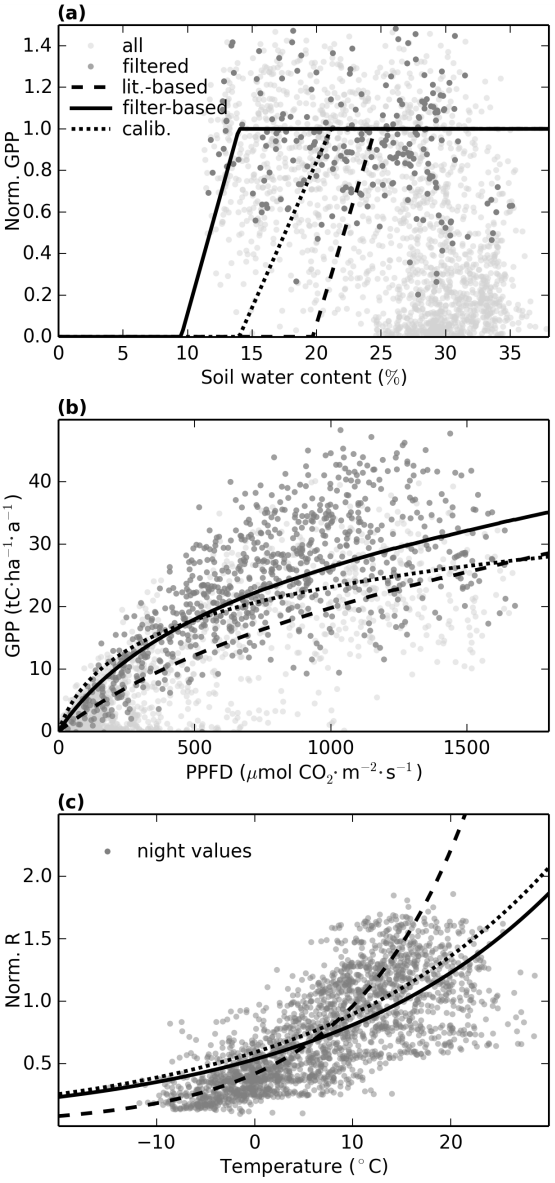

Figure A1: (a) Limitation of photosynthesis by soil water content (Eq. 2.5). Observed data of the Wetzstein site are filtered for optimal temperature conditions and sunny days. (b) PPFD vs. GPP and the forest model's functional relation (sum over Eq. 2.1). Observed data were filtered for optimal temperature and water conditions. (c) Normalized, filtered ecosystem respiration vs. temperature and the models' functional relation (Eq. 2.7). Data were filtered for night time values. The normalized respiration of the ecosystem approximately equals the normalized maintenance respiration.

was calibrated specifically for days with optimal soil water and temperature conditions (filtered EC-data). The new parameter values for the filter-based (and calibrated) parameterization are: slope of the light response curve α = 0.08 μmol(photons) m^{-2} s^{-1} (0.15) and maximum rate of photosynthesis p_{max} =10.981 μmol(CO_2) m^{-2} s^{-1} (5.670). The literature-based and calibrated parameterizations do not reach high GPP values as observed with the EC-method. This finding is reflected in filtered data (Fig. A1) and in the comparison of daily simulated values to observed values (Fig. 2.1). The literature-based parameterization for potential photosynthesis is derived from measurements on the leaf level [Sonntag, 1998]. Physiological attributes of leaves, however, vary according to climatic conditions and their positions within the canopy. Even if the parameter values were consistent on the leaf scale, it is not assured that they are also accurate at the forest scale. Due to model simplicity, FORMIND assumes that the photosynthetic capacity of leaves is the same throughout the canopy (Eq. 2.1). In the frame of this study, we have also tested the assumption of a vertical decrease of nitrogen within the canopy [e.g. Meir et al., 2002] and therefore a decrease of the maximum photosynthetic capacity [Sellers et al., 1992]. The integration of the modified light-response function leads to a Gaussian hypergeometric function with an additional parameter (A3 Nitrogen decrease in canopy). The resulting function looks very similar to our original curve but with different parameter values. Instead of adapting the forest model to a more complex functional relation, which assumes a nitrogen decrease throughout the canopy, we stayed with the less complex original function. We here present two options to derive suitable parameter values: fitting the functional relation through filtered data or via a parameter numerical calibration. However, the comparison to filtered EC-data shows that such a calibration needs to be handled with care. Although, in total, the calibrated parameterization showed the best performance (Tab. 2.3), it clearly underestimated GPP at high PPFD values.

Maintenance respiration vs. temperature. The observed respiration was filtered for nighttime values in order to exclude day-time growth respiration (Fig. A1 (c)). In the forest model, growth respiration is directly dependent on photosynthesis. Since autotrophic and heterotrophic respiration have a similar temperature dependency [Reichstein et al., 2005], the normalized respiration of the ecosystem approximately equals the normalized maintenance respiration. The fit through filtered data resulted in Q_{10} = 1.52 with a reference temperature of T_{ref} = 15.06°C. The numerical calibration resulted in Q_{10} = 1.52 with a reference temperature of T_{ref} = 12.61°C. The temperature reduction curve (Eq. 2.3) of the literature-based parameterization with Q_{10} = 2.3 [Piao et al., 2010; Bohn et al., 2014] was too high. A lower Q_{10} value of the fitted parameterization is consistent with values observed, ranging between 1.5 and 2.2 for old black spruce at different stands [Lavigne and Ryan, 1997]. Due to the variations between stands Lavigne and Ryan [1997] advise the use of stand-specific values instead of generic parameter values. In general, values of Q_{10} range in the literature from 1.4 to 3.0 [Ryan, 1991]. More recent studies even show that Q_{10} values are not constant but acclimate with

temperature [Tjoelker et al., 2001; Atkin and Tjoelker, 2003]. But the Q_{10} formulation confounds diverse ecosystem processes such as substrate availability [Kirschbaum, 2006] or soil moisture and temperature gradients [Graf et al., 2011]. Here we stay with the Q_{10} acknowledging its simplicity. The approach is strengthened by the facts that the fit through filtered data and the numerical calibration resulted in the same value and they improved the simulations on the daily (Fig. 2.2) and yearly (Fig. 2.3) scale.

A2 *The numerical calibration*

We calibrate the listed parameters (Tab. 2.2) against measured NEE, GPP and respiration with a dynamically dimensioned search [dds, Lehmann and Huth, 2015]. The objective function Q is the root mean square error of the individual fluxes and built as follows:

$$Q = \sqrt{\frac{\sum_n (NEE_{obs} - NEE_{sim})^2}{n}} + \sqrt{\frac{\sum_n (GPP_{obs} - GPP_{sim})^2}{n}} + \sqrt{\frac{\sum_n (R_{obs} - R_{sim})^2}{n}}$$

where n is the number of simulated days, obs is the indices for observational data and sim the one for simulated data.

A3 *Nitrogen decrease in canopy*

Photosynthesis on the leaf level P_L of leaf L_i is described by a Michaelis-Menton function [Thornley and Johnson, 1990]:

$$P_L(L_i) = \frac{\alpha I_L p_{max}}{\alpha I_L + p_{max}}$$

where p_{max} (μmol(CO_2) m^{-2} s^{-1}) is the maximum photosynthetic rate of the tree type, α is the initial slope of the light-response curve (μmol(CO_2) μmol(photons)$^{-1}$) and I_L is the photosynthetic active radiation that reaches the leaf. The integration over the canopy of one tree then equals [Huth and Ditzer, 2000]:

$$P_{ind}(I_{ind}) = \frac{p_{max}}{k} ln(\frac{\alpha k I_{ind}(PPFD) + p_{max}[1-m]}{\alpha k I_{ind}(PPFD) e^{-kL_T} + p_{max}[1-m]})$$

where I_{ind} is the light that reaches the canopy of an individual tree, PPFD the incoming light above the forest, k the light extinction factor, L_T the leaf area index of the tree [m^2 m^{-2}] and m the transmission coefficient of leafs.
If we now assume an exponential decrease with u of p_{max_o} (above canopy) due to decreasing nitrogen concentration in leaves (with cumulative leaf area index l) within the canopy [Sellers et al., 1992]:

$$p_{max} = p_{max_0} e^{-ul}$$

The integration of the modified Michaelis-Menton function over the canopy leads to:

$$P_T(I_{ind}, u) = \alpha \frac{k}{1-m} (\frac{{}_2F_1[1, \frac{k}{k-u}, \frac{2k-u}{k-u}, \frac{-\alpha k I_{ind}}{(1-m)p_{max_0}}]}{k p_{max_0}} - \frac{{}_2F_1[1, \frac{k}{k-u}, \frac{2k-u}{k-u}, \frac{-\alpha k I_{ind} e^{(-k+u)L_T}}{(1-m)p_{max_0}}]}{k p_{max_0}})$$

where ${}_2F_1$ is the hypergeometric function:

$$ {}_2F_1[a,b,c,z] = \sum_{k=0}^{\infty} \frac{(a)_k (b)_k}{(c)_k} \frac{z^k}{k!} $$

and

$$ (a)_k = \prod_{l=1}^{k} a(a+(l-1)), (b)_k = \prod_{l=1}^{k} b(b+(l-1)), (c)_k = \prod_{l=1}^{k} c(c+(l-1)) $$

with a = 1, b= $\frac{k}{(k-u)}$ and c= $\frac{2k-u}{k-u}$.

A4 *Calculation of the maintenance respiration*

That base respiration R_b (Eq. 2.6) is defined as follows:

$$ R_b = G\check{P}P - \Delta B(1-r_g) $$

where ΔB is the biomass increment of the tree and r_g is the growth respiration factor. The base respiration is back calculated from a potential gross primary production $G\check{P}P$. This potential GPP is based on a mean climate of the first half of the 20th century [Bohn et al., 2014].

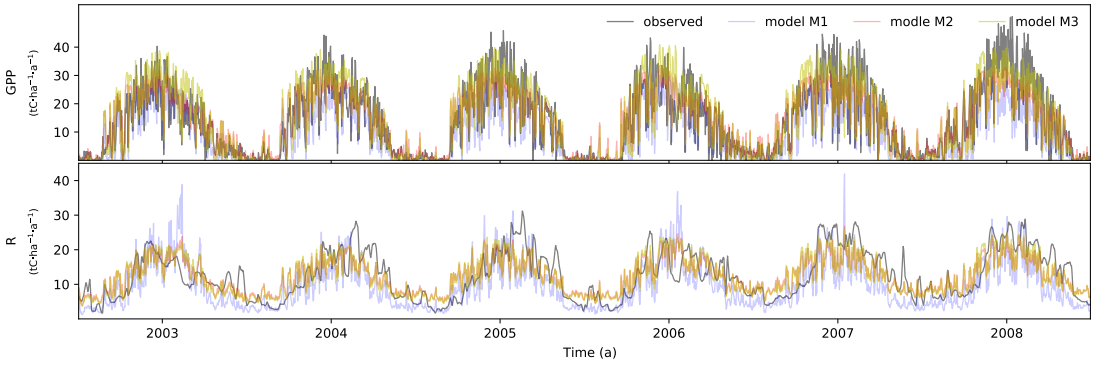

Figure A2: Simulated and observed gross primary production (GPP) and respiration (R) at Wetzstein for the year 2003.

B APPENDIX OF CHAPTER 3

B1 *Parameterization and regionalization of FORMIND*

B1.1 *The general concept*

FORMIND is an individual-based, spatially explicit and process-based model designed to simulate species-rich forests [Fischer et al., 2016]. It has been applied to various local forest sites in Malaysia, Madagascar, Ecuador, Venezuela, Mexico, Panama, Brazil and French Guyana [Köhler and Huth, 1998; Kammesheidt et al., 2001; Huth et al., 2004; Pütz et al., 2014; Fischer et al., 2016]. Vegetation is simulated on an area which is divided into regularly ordered, quadratic plots of 20 x 20 m^2 (Fig. B4).

Individual trees grow within the plots but do not have spatially explicit positions within a plot [gap model approach, Shugart, 1984]. The trees change their size during the simulation according to a set of eco-physiological (recruitment and establishment, growth, mortality) and morphological (allometries) parameters.

B1.2 *Parameterization of the forest gap model*

In this study, we set up a forest model for the central Amazon basin. We used inventory data in order to classify trees into plant functional types and to parameterize allometric functions. Parameters of functions that were not directly derived from forest inventories were calibrated numerically (locations listed in Tab. B3).

Plant functional types. Species were assigned to one of the plant functional types (PFT): fast growing, early successional trees (PFT 1), semi-fast growing trees, mid successional trees (PFT 2) and slow-growing, late successional trees (PFT3). A species was assigned to a PFT according to its mean dry wood density [Chave et al., 2006] as wood density is related to forest dynamics. Slow-growing trees tend to have higher wood densities than fast-growing trees [Malhi et al., 2006]. Species with a mean wood density of below 0.45 t m-3 (organic dry matter) were assigned to PFT1, between 0.45 and 0.55 t m-3 to PFT2 and above 0.55 t m-3 to the slow-growing PFT3 so that slow-growing trees are rather associated to PFT3 and fast-growing to PFT1 [Kazmierczak et al., 2014].

B1.3 *Calibration, fine tuning and validation*

We used tree records (dbh $<$ 10 cm) of the Large Scale Biosphere-Atmosphere Experiment in Amazonia (LBA), [Brondizio and Moran, 2009; Chambers et al., 2009, 2013a; Jirka et al., 2010]. We gathered all available species, stem diameter, height and maximum growth rate of each tree to derive parameters for allometric functions

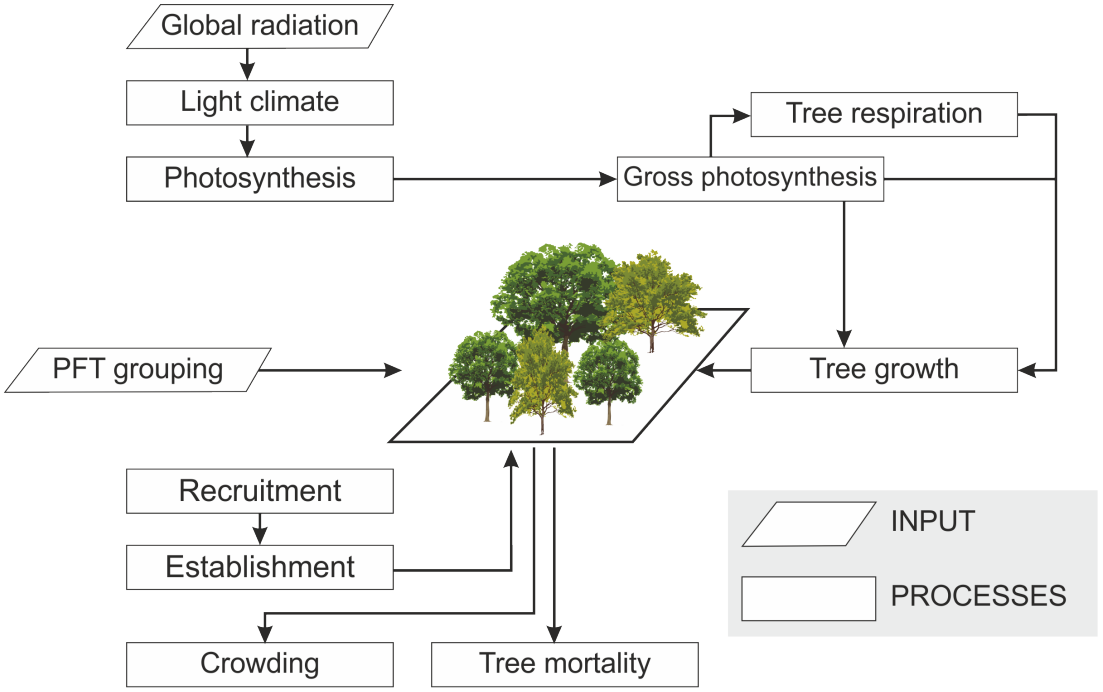

Figure B1: The basic concept of the forest model FORMIND. The forest model is mainly driven by light (photosynthetic photon flux density (PPFD)). Every year, establishment, competition for light, growth and mortality are simulated. The light that reaches a seed determines whether it can establish. Each tree competes under individual conditions for space and light. Growth of an individual results from photosynthetic production and respiratory losses. Mortality is determined stochastically. Specific functions that are used for this study are listed in Tab. B1 and its parameters in Tab. B2. A full model description has been published in Fischer et al. [2016] and is also available on www.formind.org.

(Tab. B2). Common tree names were assigned to species according to Grandtner and Chevrette [2013].

The parameters that describe mortality (m_0,m_1), photosynthesis (p_{max} and α) and minimum light availability (I_{min}) for establishment play a crucial role in forests' succession and species composition. They were numerically calibrated or 'fine tuned' [dynamically dimensioned search (DDS) as in Lehmann and Huth, 2015] against inventories of forests in different successional stages so that modeled biomass and tree diameter distributions match those observed. The Manaus forest site (MA) represents a forest in climax state [4 x 1 ha subplots, Kunert et al., 2015]. At the other locations (YA, BR, PP, Tab. B3), forest inventory data was available for different successional stages [10 x 0.4-1 ha subplots, 5-100 years old tree populations Brondizio and Moran, 2009].

The calibration has been performed including all sites (MA, YA, BR, PP) regarding their specific environmental condition (here light). The calibration method DDS ran with 5000 iterations. The objective function was built as follows:

$$Q = \sum_{l} \left(\sum_{p} \left(\frac{1}{c_B(p)} \left(\frac{B_o(l) - B_m(l)}{B_o(l)\sigma(l)} \right)^2 + \frac{1}{c_{N_s}(p)} \left(\frac{N_{s_o}(l) - N_{s_m}(l)}{N_{s_o}(l)\sigma(l)} \right)^2 + \frac{1}{c_{N_l}(p)} \left(\frac{N_{l_o}(l) - N_{l_m}(l)}{N_{l_o}(l)\sigma(l)} \right)^2 \right) \right) \tag{B1}$$

with: index represents l different locations and different successional stages, p PFTs, observed biomass B_o , observed number of small trees (dbh $<$ 50 cm) N_{s_o}, observed number of large trees (dbh $\geqslant$ 50 cm) N_{l_o}, modeled biomass B_m , modeled number of small trees (dbh $<$ 50 cm) N_{s_m} and modeled number of large trees (dbh $\geqslant$ 50 cm) N_{l_m}. σ is the variability in biomass in the tropics based on the area of sample plot [Réjou-Méchain et al., 2014]: the bigger the inventory, the less its variability/uncertainty. c_B is the maximum biomass, c_{N_l} the maximum number of large trees and c_{N_s} the maximum number of small trees over all inventories per PFT. These weights were needed to relate biomass and tree size distributions:

c_B(PFT1,PFT2,PFT3)=(40,73,234);
c_{N_s}(PFT1,PFT2,PFT3)=(184,190,547);
c_{N_l}(PFT1,PFT2,PFT3)=(5,5,24).

Ranges for the parameters are:

p_{max}(PFT1)$\in$[11,18], p_{max}(PFT2)$\in$[8,11], p_{max}(PFT3)$\in$[5,7.5];
α(PFT1,PFT2,PFT3)$\in$[0.05,0.3] and α(PFT3)$>$ α(PFT2)$>$ α(PFT1);
I_{min}(PFT1)$\in$[0.09,0.18], I_{min}(PFT2)$\in$[0.03,0.09], I_{min}(PFT3)$\in$[0.005,0.03];
m_0(PFT1)$\in$[0.07,0.1], m_0(PFT2)$\in$[0.035,0.07], m_0(PFT3)$\in$[0.001,0.35];
m_1(PFT1)$\in$[0.3,0.6], m_1(PFT2)$\in$[0.5,0.7], m_1(PFT3)$\in$[0.6,0.9]
and m_1(PFT3)$>$ m_1(PFT2) $>$ m_1(PFT1).

The ranges are set according to preliminary knowledge from previous studies [e.g., Dislich et al., 2009; Fischer et al., 2014, 2016; Kazmierczak et al., 2014]. Note that none of the calibrated parameters reach the upper or lower limits (Tab. B2).

Taking 3 PFTs at 14 plots results in 14 (independent sites) x 9 (summary statistics of the objective function: biomass, stem number of small tress, stem number of large trees per PFT) = 126 field measurements the model is calibrated against. Extensive preliminary testing of objective functions showed that the chosen summary statistics (summing up values for large (dbh $\geqslant$ 50 cm) and small (dbh $<$ 50 cm) trees instead of fitting against all diameter classes) were the most effective within this study.

The fine tuning resulted in one generic set of model parameters. The derived parameter set reproduced biomass and stem size distributions well (Fig. B3), considering the fact, that the inventory sites represent different successional states, they have different environmental conditions and that tropical forests are highly diverse. The forest model was validated with independent measurement: Kunert et al. [2015] report a mean leaf area index (LAI) of 5.09 for the forest stand in Manaus while FORMIND simulates a

mean leaf area index of 4.63 in climax stage (mean over 100 ha during simulation years 500-1000).

Table B1: Specific functional relations used in this study with dbh: diameter at breast height; h: tree height, cd: crown diameter; f: form factor; cl: crown length; lai: leaf area index; g: stem diameter increment; m: stem based mortality rate. Further basic functions are listed in Fischer et al. [2016].

Description	Function
height - dbh	$h = h_0 dbh^{h_1}$
crown diameter - dbh	$cd = cd_0 dbh$
form factor - dbh	$f = f_0 dbh^{f_1}$
crown length - height	$cl = cl_0 h$
LAI - dbh	$lai = l_0 dbh^{l_1}$
growth curve	$g = g_0 dbh^{g_1} e^{g_2 dbh}$
mortality	$m = m_0 e^{-m_1 dbh}$

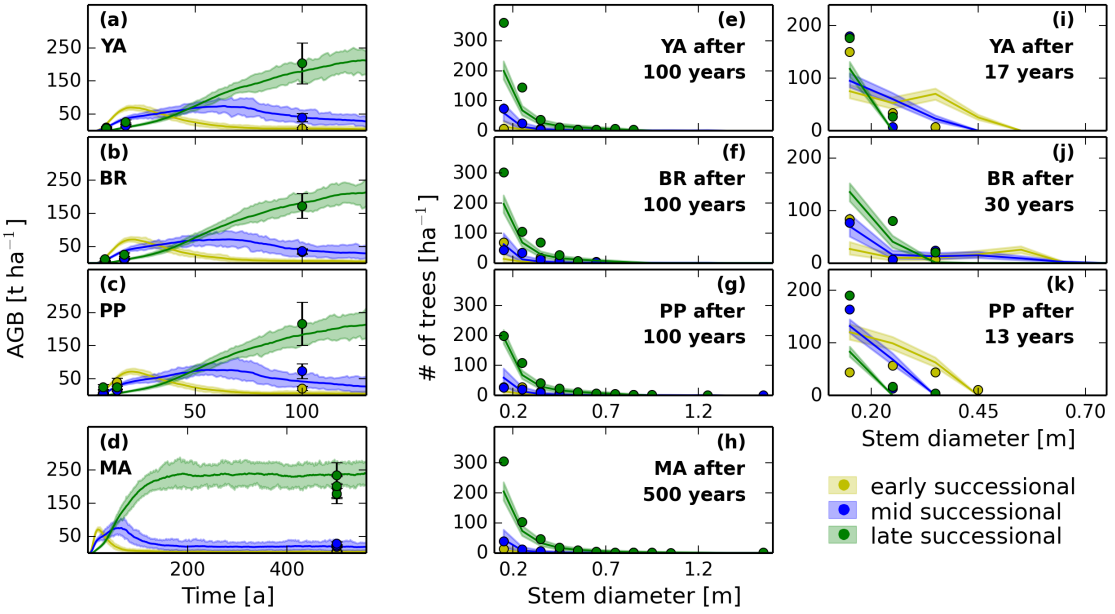

Figure B2: (a-d) Simulation of forest succession at different sites (locations listed in Tab. B3) for three different plant functional types (early, mid and late successional trees) using the best fit parameters (Tab. B2). The simulation envelope shows the variation of simulated biomass at the scale of 1 ha (95% quantile for 100 simulations). Comparison with field data (dots) in different successional stages (different ages of forest stands at YA, BR and PP recorded in Brondizio and Moran [2009], at Manaus (MA) we assume an old-growth forest in climax stage). (e-k) Simulated tree size distributions compared to field data in different successional stages. The simulation envelopes show the variations at the scale of 1 ha (95% quantile for 100 simulations).

Table B2: PFT-specific parameter values of the forest model. *Brondizio and Moran [2009]; Chambers et al. [2009, 2013a]; Jirka et al. [2010]

Parameter	Description	Unit	PFT1	PFT2	PFT3	Reference
Light and Establishment						
k	light extinction factor	-	0.6	0.6	0.6	Larcher [2001]; Dislich et al. [2009]
N_{seeds}	number of global seeds	ha^{-1}	100	60	40	estimated
I_{min}	min. light intensity to establish	%	0.13	0.07	0.01	calibrated
Geometry						
H_{max}	max. height	m	30	40	65	derived from inventory data*
h_0	height-dbh relation	-	38.305	35.975	36.544	derived from inventory data*
h_1			0.552	0.518	0.522	
cd_0	crown diameter- dbh relation	-	19	19	19	Dislich et al. [2009]
cl_0	crown length- height relation	-	0.4	0.4	0.4	Fischer et al. [2014]
l_0	LAI-dbh relation	-	4	4	4	estimated
l_1			-0.1	-0.1	-0.1	
f_0	form factor-dbh relation	-	0.3361	0.3361	0.3361	Fischer et al. [2014]
f_1			-0.18	-0.18	-0.18	
Biomass and Productivity						
ρ	wood density	tm^{-3}	0.374	0. 512	0.712	Chave et al. [calcualted from 2006]
m	transmission coefficient of leaves	-	0.1	0.1	0.1	Larcher [2001]
p_{max}	max. assimilation rate	$\mu molCO_2\ s^{-1}\ m^{-2}$	13.42	7.93	3.39	calibrated, ranges from Reich et al. [1997]
α	slope of light response curve	$\mu mol(CO_2)\ \mu mol(photons)^{-1}$	0.268	0.201	0.125	calibrated
g_0	growth curve	-	33.965	4.382	3.494	derived from inventory data*
g_1			0.898	0.356	0.502	
g_2			-5.428	-1.141	-1.885	
σ	ratio total aboveground- stem biomass	-	0.7	0.7	0.7	Fischer et al. [2014]
Mortality						
m_0	max. mortality at establishment	-	0.075	0.061	0.016	calibrated
m_1	slope of mortality	-	0.31	0.54	0.83	calibrated

Table B3: Inventory sites used for the calibration of the local forest model in central Amazon rainforest.

Location	Region	Reference
53.80°W, 1.00°S	Bragantina (BR)	Brondizio and Moran [2009]
60.16°W, 2.64°S	Manaus (MA)	Kunert et al. [2015]
48.86°W, 1.36°S	Ponta de Pedras (PP)	Brondizio and Moran [2009]
70.00 °W, 2.00°S	Yapu (YA)	Brondizio and Moran [2009]

B1.4 *Regionalization of the forest gap model*

Expanding the forest model from the local scale (stand level) to the regional scale (entire Amazon rainforest) implied some model adaptations. The mortality at establishment parameter (m_0) for PFT3 was calibrated against inventory data. We used a database [Lopez-Gonzalez et al., 2011; Mitchard et al., 2014] in which mean biomass, basal area and specific wood density of 413 sites have been documented (dbh $>$ 10 cm). 372 sites fall into our study area of which we pick 186 randomly for model calibration (the rest is taken for validation; we sort out observed mature forests where google maps shows heavy deforestation). The calibration method (dynamically dimensioned search algorithm, DDS) ran with 1000 reiterations [Lehmann and Huth, 2015]. For calibration, we used the following observed data (dbh $>$ 10 cm): mean total biomass of the plot $\overline{B}_o$, mean basal area $\overline{BA}_o$ and mean wood specific gravity $\overline{\rho}_{s_o}$ ([g cm^{-3}]) weighted per stem number and $\overline{\rho}_{BA_o}$ weighted per basal area. The objective function is built as follows:

$$Q = \frac{1}{4}\Big((\frac{\overline{B}_o - \overline{B}_m}{\overline{B}_o \sigma})^2 + (\frac{\overline{BA}_o - \overline{BA}_m}{\overline{BA}_o \sigma})^2 + (\frac{\overline{\rho}_{S_o} - \overline{\rho}_{S_m}}{\overline{\rho}_{S_o} \sigma})^2 + (\frac{\overline{\rho}_{BA_o} - \overline{\rho}_{BA_m}}{\overline{\rho}_{BA_o} \sigma})^2 \Big), \qquad \text{(B2)}$$

where m indicates the simulated and o the observed values. σ is the variability in biomass in the tropics (see above).

We performed a linear regression between the calibrated parameter values and environmental conditions which were available as Amazon-wide maps (Tab. B4). In addition, we applied a multivariate regression (all combinations of two environmental conditions). The correlations between the fit and calibrated parameters were best for a combination of water related (precipitation, length of dry season, climatic water deficit) and soil type and structure related (clay, silt, gravel) conditions. These correlations are listed in Tab. B5. We chose precipitation (mm a^{-1}) and subsoil clay fraction ([0,1]) as a proxy for mortality at establishment of PFT3 since it showed the smallest standard error with a relatively high R^2. The fit function is describes as follows:

$$m_f = 0.080417 - 37.093213e-03 \cdot \mathit{clayfraction} - 1.724374e-05 \cdot \mathit{precipitation} \qquad \text{(B3)}$$

Mortality of PFT3 varies for each simulated hectare plot within (randomly picked for each ha):

$$m_0(\text{PFT3}) = m_f \pm std, \tag{B4}$$

while m_0(PFT3)$\in$[0.004,0.055] and standard error (std) = 0.08.

In general, mortality is age-dependent and decreases with stem diameter. The change in the parameter m_0 with precipitation and clay fraction scales the age-dependent mortality curve (see equation in Tab. B1) vertically.

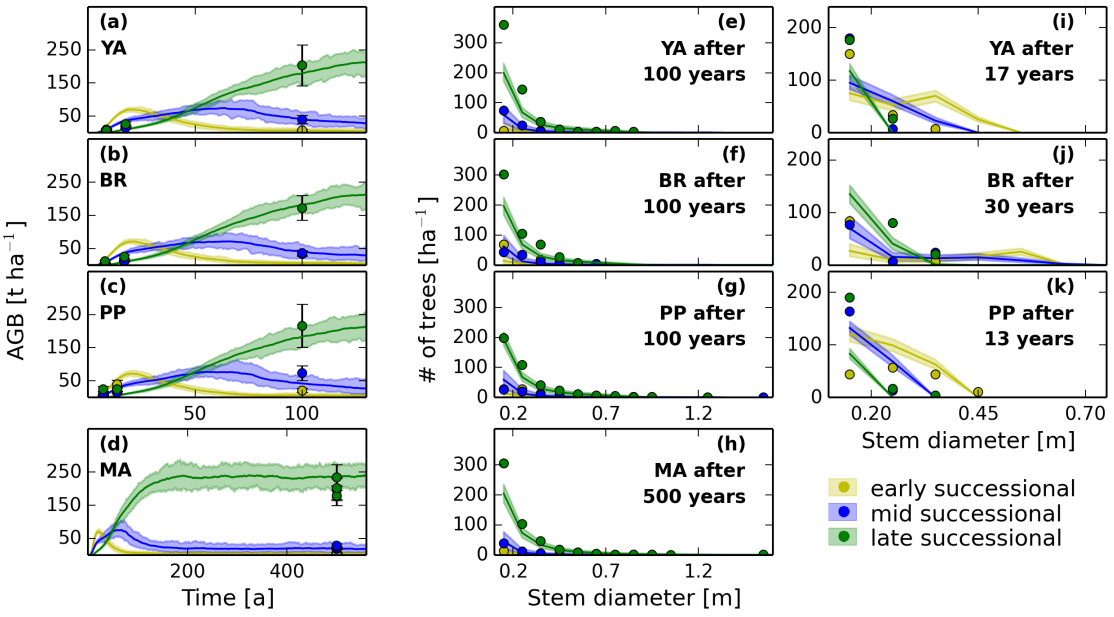

Figure B3: (a-d) Simulation of forest succession at different sites (locations listed in Tab. B3) for three different plant functional types (early, mid and late successional trees) using the best fit parameters (Tab. B2). The simulation envelope shows the variation of simulated biomass at the scale of 1 ha (95% quantile for 100 simulations). Comparison with field data (dots) in different successional stages (different ages of forest stands at YA, BR and PP recorded in Brondizio and Moran [2009], at Manaus (MA) we assume an old-growth forest in climax stage). (e-k) Simulated tree size distributions compared to field data in different successional stages. The simulation envelopes show the variations at the scale of 1 ha (95% quantile for 100 simulations).

B2 *Linking model and canopy height map*

We assumed that the observed canopy height [Simard et al., 2011] reflects the current successional state of each 1km^2 patch in the Amazon rainforest. The smallest resolution of FORMIND is 20 m x 20 m where trees grow individually. The challenge lies in linking information at two different spatial scales (Fig. B4). Therefore, we needed to clarify two

Table B4: Coefficient of determination (R^2) between local climatic (annual mean) or soil conditions and calibrated mortality parameter, standard error (stdErr) and p values. Local conditions are derived from [1]Weedon et al. [2014], [2]GLOBE Task Team et al. [1999]; [3]climatic water deficit, Chave et al. [2014], [4]Wieder et al. [2014].

Local condition	R^2	stdErr	p value	Local condition	R^2	stdErr	p value
length of dry season[1]	0.162	0.157	<0.001	topsoil silt fraction[4]	0.081	0.174	<0.001
elevation a. s. l.[2]	0.012	0.606	0.184	subsoil gravel fraction[4]	0.11	0.212	<0.001
temperature[1]	0.001	0.322	0.741	topsoil gravel fraction[4]	0.086	0.22	<0.001
temperature range[1]	0.09	0.191	<0.001	subsoil bulk density[4]	0.003	>>1	0.511
precipitation[1]	0.132	0.188	<0.001	topsoil bulk density[4]	0.006	0.867	0.369
cwd[3]	0.125	0.198	<0.001	subsoil organic carbon[4]	0.03	0.516	0.038
subsoil clay fraction[4]	0.109	0.161	<0.001	topsoil organic carbon[4]	0.001	>1	0.731
topsoil clay fraction[4]	0.024	0.299	0.062	subsoil carbon[4]	0.029	0.368	0.04
subsoil sand fraction[4]	0.001	>1	0.668	topsoil carbon[4]	0.003	0.67	0.491
topsoil sand fraction[4]	0.031	0.334	0.034	topsoil ph of H_2O[4]	0.07	0.29	0.001
subsoil silt fraction[4]	0.076	0.213	0.001	subsoil ph of H_2O[4]	0.002	>1	0.584

Table B5: Coefficient of determination (R^2) between fit (multivariate regression driven by two local conditions) and calibrated mortality parameters, standard error (stdErr) and p value. We chose precipitation and subsoil clay fraction as a proxy for mortality since it showed the lowest standard error with an R^2>0.22.

Local condition	R^2	stdErr	p value	Local condition	R^2	stdErr	p value
length of dry season, topsoil silt fraction	0.042	0.291	0.013	precipitation, subsoil clay fraction	0.224	0.08	<0.001
length of dry season, subsoil silt fraction	0.257	0.14	<0.001	precipitation, topsoil gravel fraction	0.201	0.148	<0.001
length of dry season, topsoil clay fraction	0.185	0.116	<0.001	precipitation, subsoil gravel fraction	0.211	0.123	<0.001
length of dry season, subsoil clay fraction	0.25	0.099	<0.001	cwd, topsoil silt fraction	0.225	0.132	<0.001
length of dry season, topsoil gravel fraction	0.209	0.125	<0.001	cwd, subsoil silt fraction	0.203	0.121	<0.001
length of dry season, subsoil gravel fraction	0.221	0.121	<0.001	cwd, topsoil clay fraction	0.132	0.145	<0.001
precipitation, topsoil silt fraction	0.218	0.105	<0.001	cwd, subsoil clay fraction	0.208	0.121	<0.001
precipitation, subsoil silt fraction	0.153	0.09	<0.001	cwd, topsoil gravel fraction	0.186	0.146	<0.001
precipitation, topsoil clay fraction	0.163	0.14	<0.001	cwd, subsoil gravel fraction	0.213	0.132	<0.001

Table B6: Datasets used for analyses and localization of the Amazon region. All data are regridded to the grid of the canopy height map with the climate data operators [CDO, 2015].

Variable	Dataset	Year	Resolution	Reference
Topography [m]	Global Land One-km Base Elevation Project	-	1 km	GLOBE Task Team et al. [1999]
Precipitation [mm a^{-1}]	WFDEI Forcing Data	2003-2012	0.5°	Weedon et al. [2014]
Temperature [°C]	WFDEI Forcing Data	2003-2012	0.5°	Weedon et al. [2014]
PPFD [µmol m^{-2} s^{-1}]	WFDEI Forcing Data	2003-2012	0.5°	Weedon et al. [2014]
Soil data	Harmonized World Soil Database	-	8 km	Wieder et al. [2014]
Max. canopy height [m]	canopy height map	-	1 km	Simard et al. [2011]

aspects: (1) the interpretation of the values in the canopy height map and (2) the time step in the forest simulation that matches the conditions of the canopy height map.

Aspect (1): The canopy height map was validated with the 3 tallest trees within a 20 m radius [Simard et al., 2011]. This area is comparable to the size of a GLAS footprint where the LIDAR signal is the strongest. The canopy height of the map is therefore compared to the simulation on 40 m x 40 m patches within the simulated 1km^2 (marked in red by example for three 40 m x 40 m patches in Fig. B4).

Aspect (2): In order to identify the successional state (simulation time steps) to which the observation can be compared to, we searched for all time steps when the observed canopy height ($\pm$1 m) fits to simulated forest heights on a 40 m x 40 m patch. In total, we select at least 625 40 m x 40 m patches (= 100 ha = 1km^2). These patches have no spatially explicit position within the 1 km^2. Biomass, stem number or basal area values can only be plotted spatially explicitly at 1 km^2 resolution (mean over 625 40 m x 40 m patches).

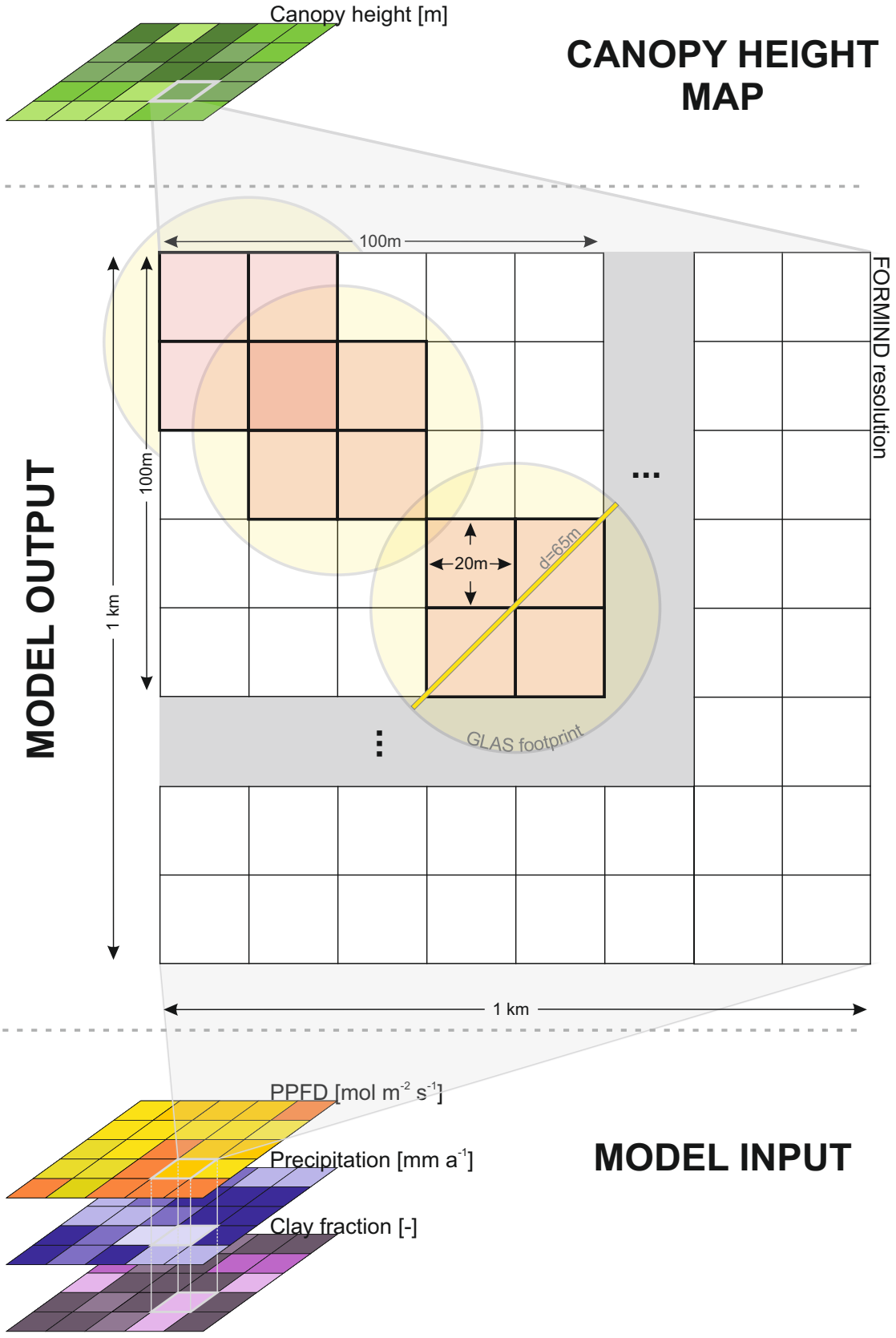

Figure B4: GLAS (LIDAR satellite) resolution versus FORMIND resolution. The yellow circles indicate the GLAS footprint. The squared grids indicate the resolution of the forest model (20m x 20m plots in 100 ha = 1km^2). The height derived from LIDAR is compared to the simulated maximum height within an area of 40m x 40m (red box).

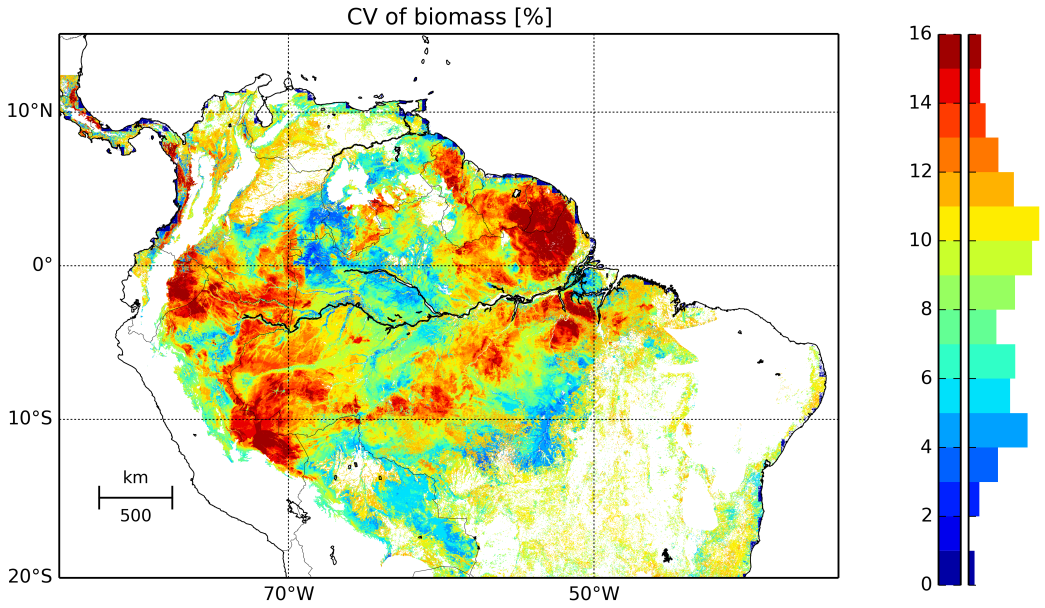

Figure B5: Coefficient of variation (CV) of biomass that results from different biomass values that are assigned to a specific canopy height.

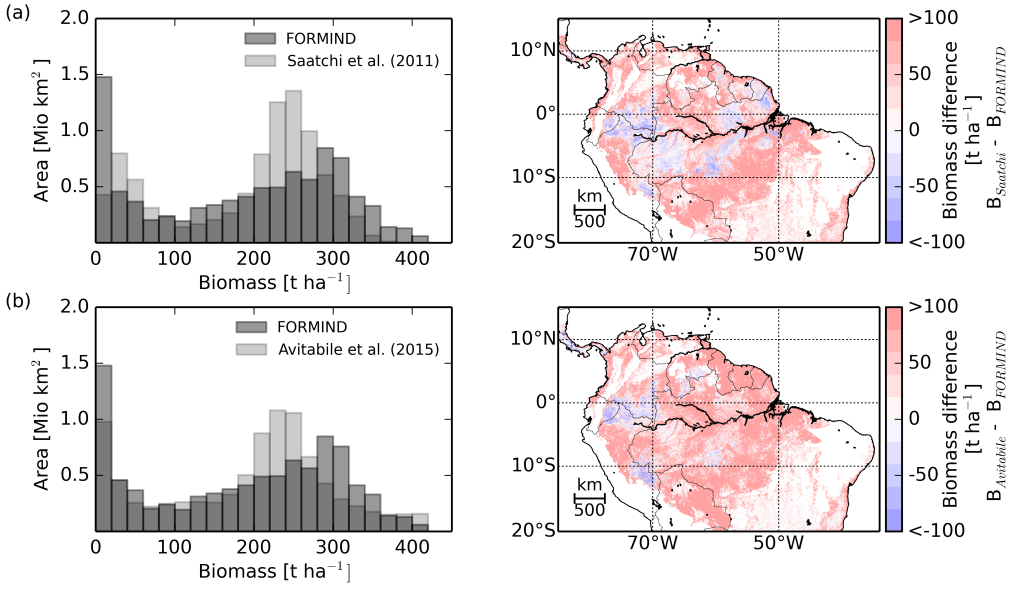

Figure B6: Simulation results vs. maps of (a) Saatchi et al. [2011] and (b) Avitabile et al. [2016].

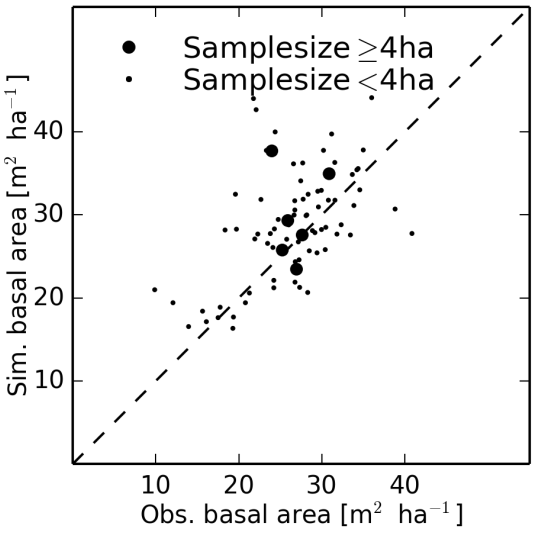

Figure B7: Comparison of simulated basal area (closest location to inventory in basal area map, Fig. 6a) and observed basal area at 80 field inventories [Lopez-Gonzalez et al., 2011; Mitchard et al., 2014]. The dashed line is the 1:1 line. R^2 = 0.26, RMSE = 6.6 m^2 ha^{-1}, normalized RMSE = 0.21.

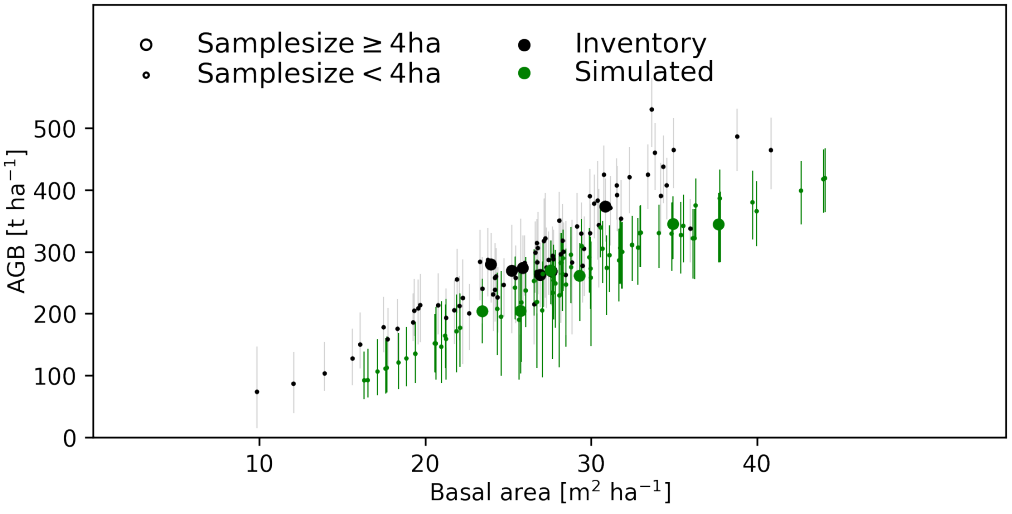

Figure B8: Comparison of simulated basal area (closest location to inventory in basal area map, Fig. 6a) and observed basal area at 80 field inventories [Lopez-Gonzalez et al., 2011; Mitchard et al., 2014]. The dashed line is the 1:1 line. R^2 = 0.26, RMSE = 6.6 m^2 ha^{-1}, normalized RMSE = 0.21.

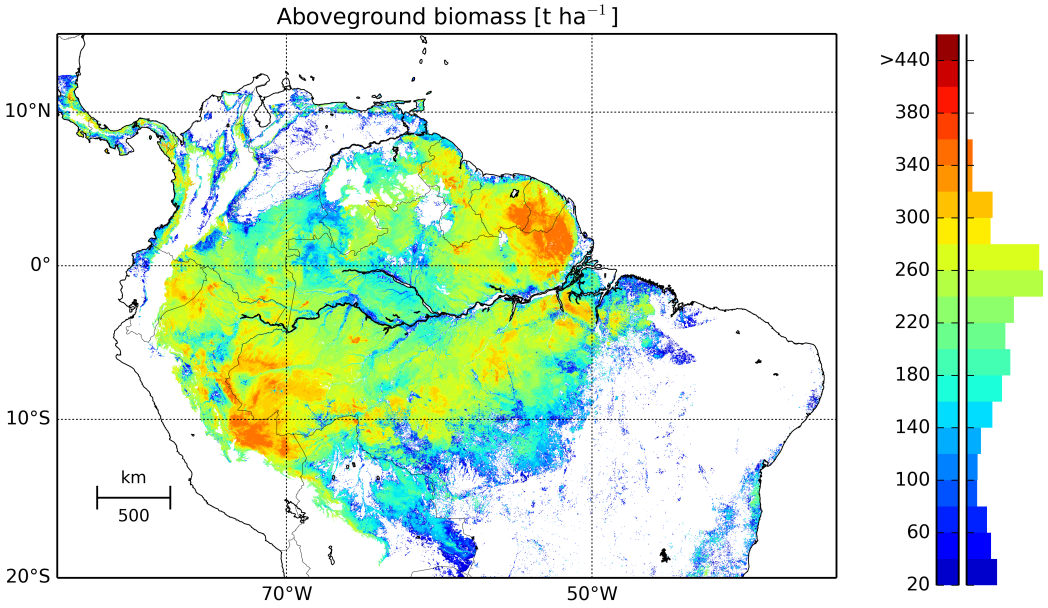

Figure B9: Simulation results with constant mortality rates. Map of aboveground biomass (stem diameter $>$ 10 cm) in the Amazon rainforest (South American rainforest with elevation $<$ 1000 m) and frequency distributions (right) simulated with an individual-based forest model. Successional stages within the simulation were identified via a canopy height map. Mean AGB = 199$\pm$82 t ha^{-1} with Western Amazon 216$\pm$83 t ha^{-1}, Brazilian Shield 161$\pm$88 t ha^{-1}, East Central Amazon 201$\pm$63 t ha^{-1} and Guiana Shield 228$\pm$65 t ha^{-1}.

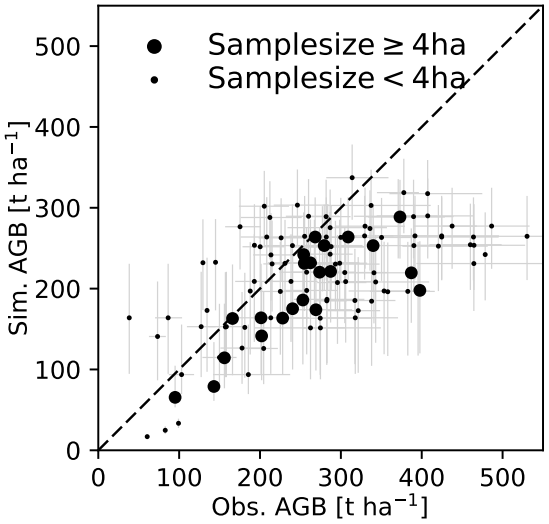

Figure B10: Comparison of simulated above-ground biomass AGB (closest location to inventory in AGB map, Fig. B9) and observed AGB at 114 field inventories [Houghton et al., 2001; Lopez-Gonzalez et al., 2011; Mitchard et al., 2014; Poorter et al., 2015]. Mortality rates are constant throughout the entire Amazon rainforest. The range of observed AGB (horizontal grey error bars) comes from different allometries used in Mitchard et al. [2014]. The error bars for the simulated biomass (vertical grey error bars) result from different time steps at which the observed canopy height matches the simulated canopy height. The dashed line is the 1:1 line. R^2 = 0.37, RMSE = 83.8 t ha^{-1}, nRMSE=0.17.

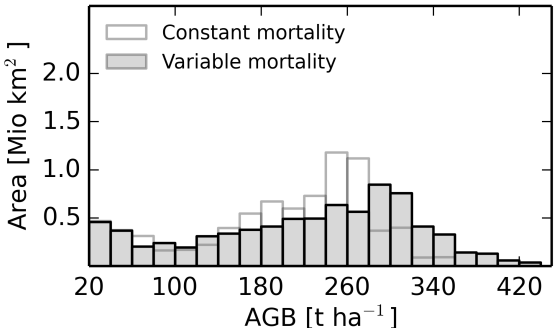

Figure B11: Frequency distribution of simulated aboveground biomass with constant mortality rates and variable mortality rates.

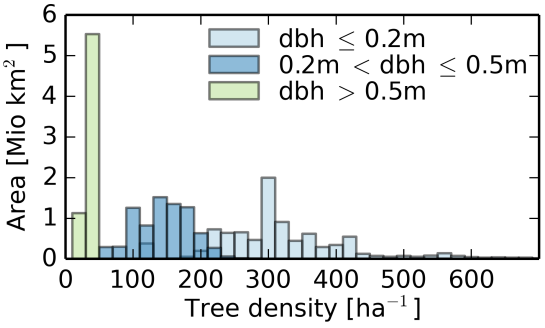

Figure B12: Tree density distribution for small, intermediate and large trees derived from simulation approach (dbh – diameter at breast height).

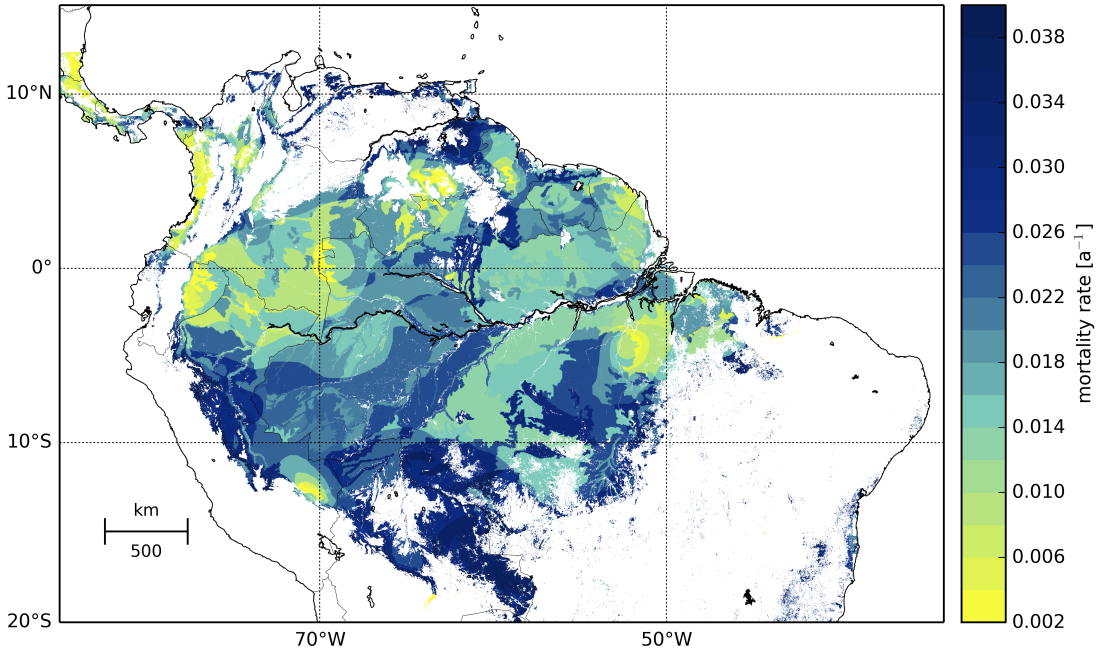

Figure B13: Mortality response units for mature trees (diameter at breast height = 0.5 m).

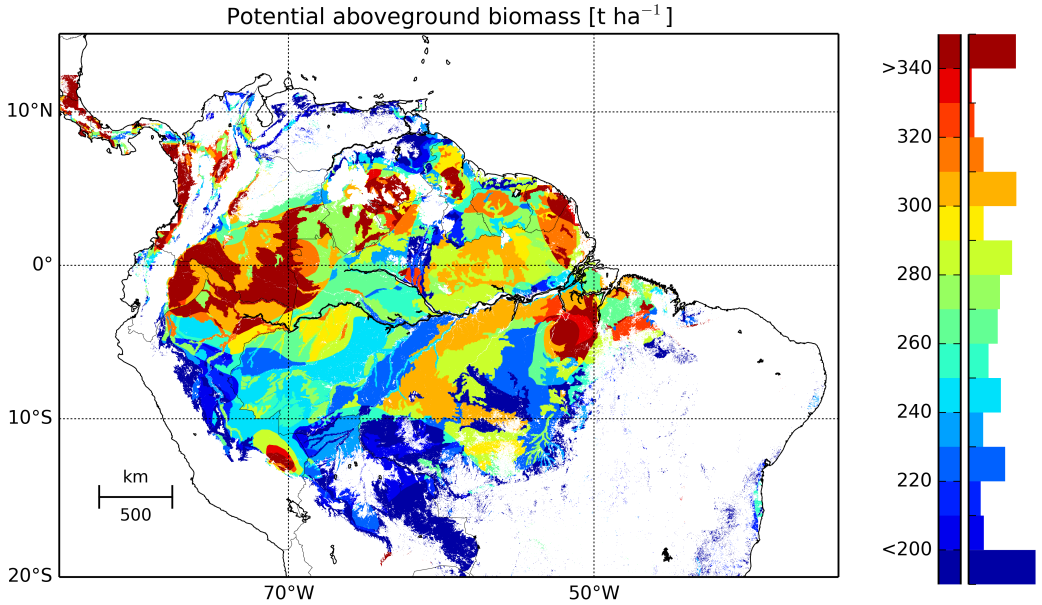

Figure B14: Simulation results with spatially variable mortality rates (Fig. B13). Map of potential aboveground biomass (stem diameter > 10 cm, mean over simulation years 500-1000) in the Amazon rainforest and frequency distributions (right) simulated with an individual-based forest model.

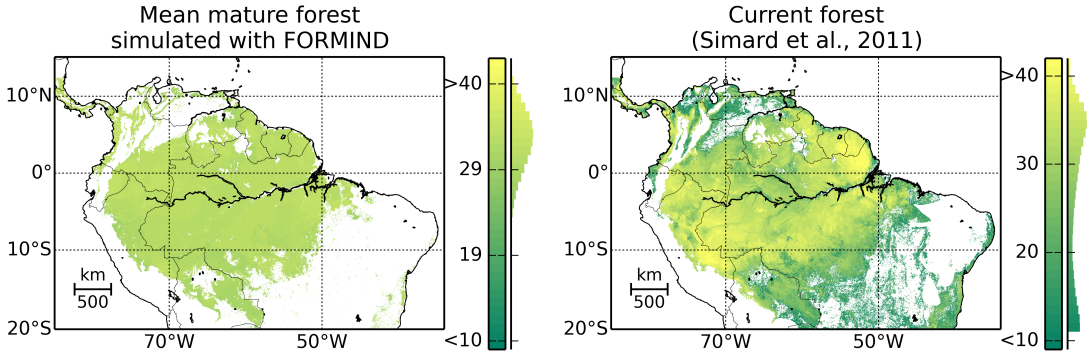

Figure B15: Maps of mean maximum canopy height at 1 km^2 resolution: (a) for a mature forest simulated with FORMIND and its normalized frequency distribution at 0.04 ha resolution (right); (b) canopy height map of Simard et al. [2011] and normalized frequency distribution (right).

C APPENDIX OF CHAPTER 4

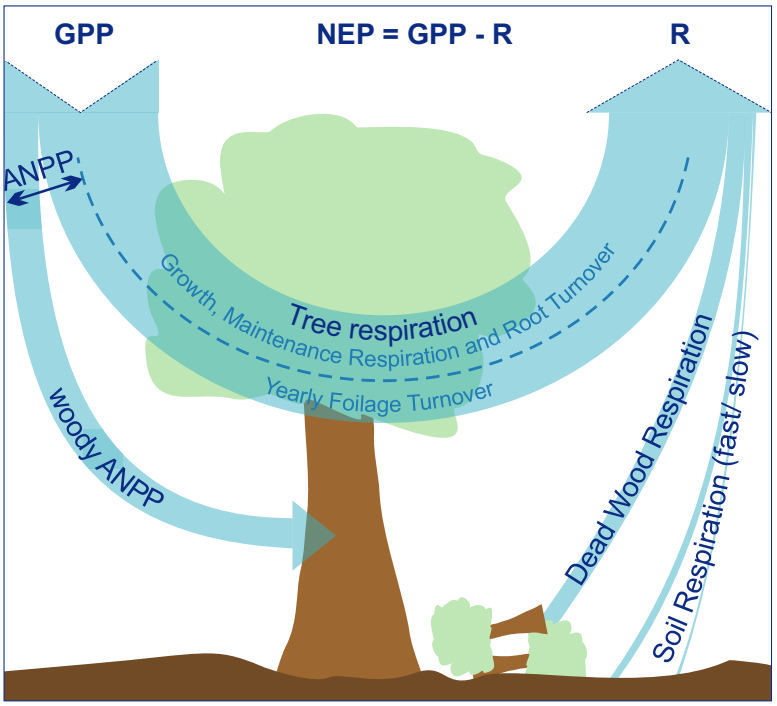

Figure C1: Carbon fluxes as simulated in the forest model FORMND. Gross primary production (GPP) is divided into wANPP and tree respiration. Since the model calculates on yearly time steps, foliage turnover is included in the trees' respiration. The sum of foliage turnover and wANPP is the above-ground net primary production (ANPP). Roots are not included in the model. Long-term root turnover is part of the trees' respiration. The fast and slow soil carbon pools built up from decomposing dead trees. The net ecosystem productivity (NEP) than equals the difference between GPP and respiration (R).

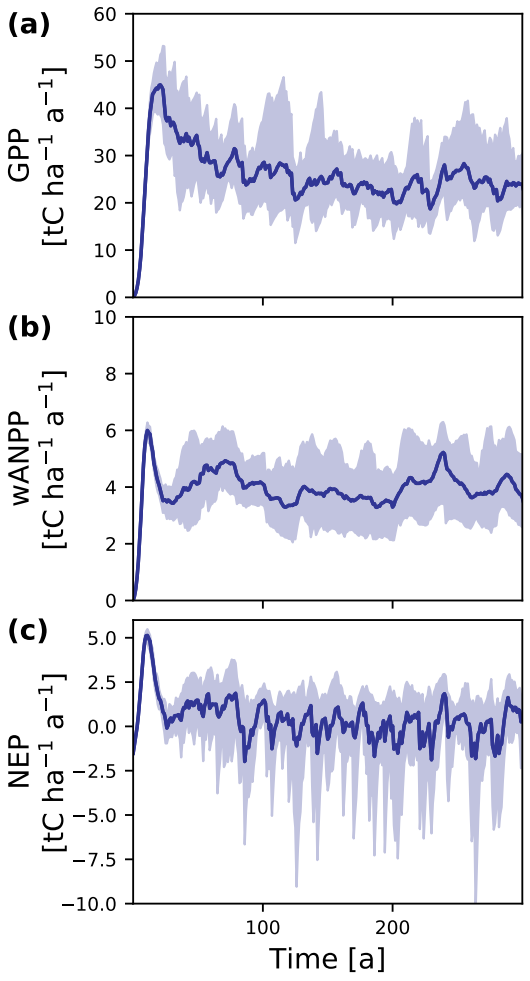

Figure C2: Simulated (a) gross primary production (GPP), (b) woody above-ground primary production (wANPP), and (c) net ecosystem productivity (NEP) from bare ground to steady-state, exemplary for a randomly picked 1 ha plot in the Amazon. The range around the mean indicates the variability of 0.16 ha within 1 ha.

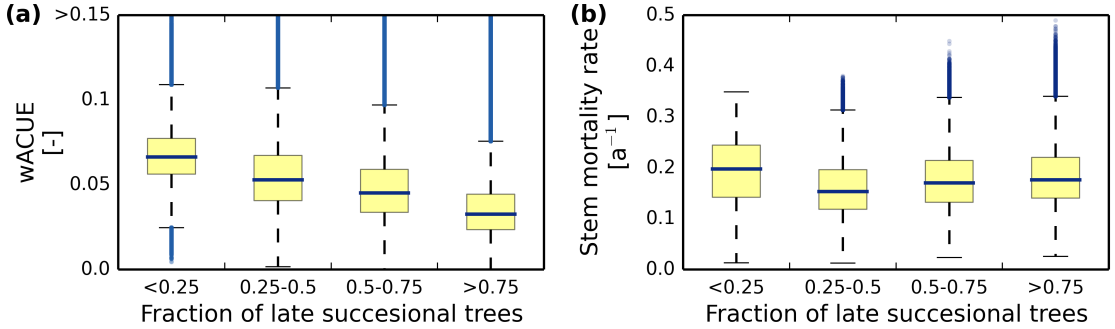

Figure C3: Fluxes at different successional states of the forest at 0.16 ha resolution. The successional state is indicated by the fraction of basal area of late successional trees within a patch. Boxplots with median (blue horizontal line) and outliers (blue dots) for (a) woody above-ground carbon use efficiency (wACUE), (b) stem mortality rate.

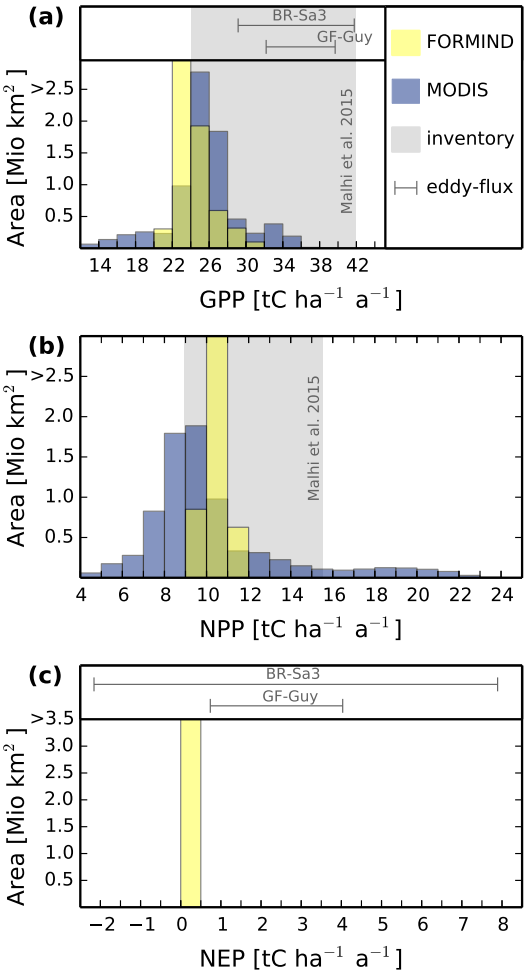

Figure C4: Frequency distributions of FORMIND estimates for potential (in climax state, average over simulation years 500-1000) (a) gross primary production (GPP), (b) net primary production (NPP), and (c) net ecosystem productivity (NEP) for forests in the Amazon at 1 km^2 resolution in comparison to: estimates from remote sensing [1 km^2 resolution, MODIS, Running et al., 2004], inventory data [<1ha resolution, 10 plots with recorded GPP and NPP, Malhi et al., 2015], and eddy covariance measurements (at GF-Guy and BR-Sa3). The ranges of estimated values from field inventories are marked in grey. Eddy-flux measurements at two sites are shown for the full range of annual sums. Note that positive values of NEP indicate a sink of atmospheric carbon.

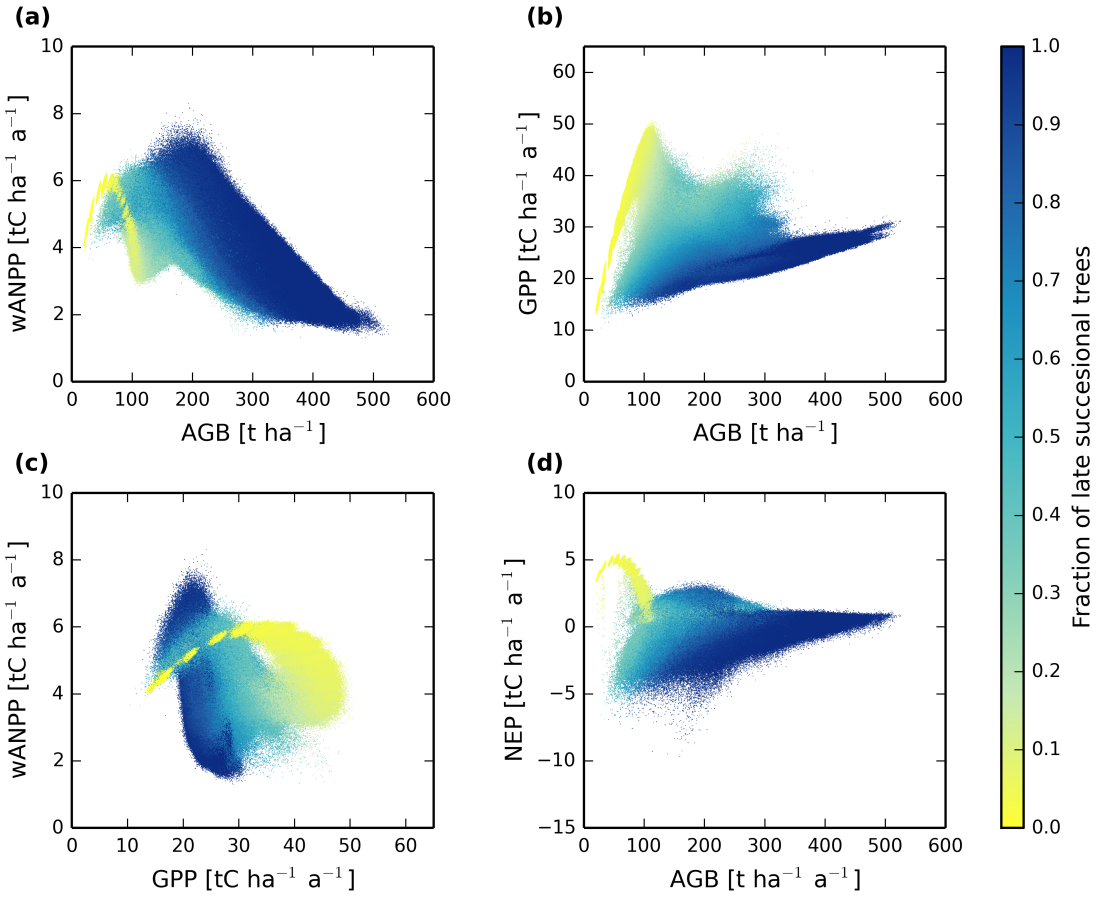

Figure C5: Relation between simulated carbon fluxes and successional states within the Amazon rainforest at a resolution of 1 ha. Successional states are represented by the basal area fraction of late successional trees within each 1 ha plot (yellow for early successional state to dark blue for late successional states). (a) Aboveground biomass (AGB) vs. AGB, (b) gross primary production (GPP) vs. AGB, (c) GPP vs. wANPP, and (d) GPP vs. net ecosystem productivity (NEP). GPP, NEP and wANPP are in tons carbon per hectare per year (tC ha^{-1} a^{-1}); AGB values are in tons dry mass per hectare per year (t ha^{-1} a^{-1}).

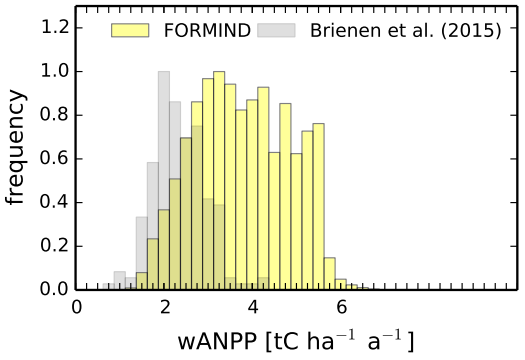

Figure C6: Relative frequency distribution of observed woody above-ground net primary production (wANPP) of mature forest sites [Brienen et al., 2015b] and of simulates wANPP across the entire Amazon at different successional states at 1 ha resolution.

Table C1: Parameter values of the forest model.

Parameter	Description	Unit	PFT1	PFT2	PFT3	Reference
Mortality						
m_0	max. mortality at establishment	-	0.075	0.061	[0.004,0.055]	B2
m_1	slope of mortality	-	0.31	0.54	0.83	B2
Soil polls						
S_{dead}	initial dead wood pool	tC ha^{-1}		5.5		randomly picked from long-term simulation
S_{slow}	initial slow decomposing soil carbon pool	tC ha^{-1}		10.5		randomly picked from long-term simulation
S_{fast}	initial fast decomposing soil carbon pool	tC ha^{-1}		12.5		randomly picked from long-term simulation
t_{DA}	respiration rate S_{dead} to the atmosphere	a^{-1}		0.168		Paulick et al. [2017]
t_{SA}	respiration rate S_{slow} to the atmosphere	a^{-1}		1/750		Paulick et al. [2017]
t_{FA}	respiration rate S_{fast} to the atmosphere	a^{-1}		1/15		Paulick et al. [2017]

LIST OF FIGURES

LIST OF TABLES

LIST OF ABBREVIATIONS

Abbreviation	Long name
EC	eddy covariance
GPP	gross primary production
LAI	leaf area index
LIDAR	light detection and ranging
NDVI	normalized difference vegetation index
NEE	net ecosystem exchange
NEP	net ecosystem productivity
NPP	net primary production
odm	organic dry matter
PPFD	photosynthetic photon flux density
R	ecosystem respiration
RADAR	radio detection and ranging
RMSE	root mean square error
wANPP	woody above-ground net primary production

BIBLIOGRAPHY

Acevedo, M. F., Urban, D. L., and Ablan, M. Transition and Gap Models of Forest Dynamics. *Ecological Applications*, 5(4):1040, 1995. doi: 10.2307/2269353.

Ainsworth, E. A. and Long, S. P. What have we learned from 15 years of free air CO2 enrichment (FACE)? A meta-analytic review of the response of photosynthesis, canopy properties and plant production to rising CO2. *New Phytol.*, 179(2):5, 2005. doi: 10.1111/j.1469-8137.2004.01224.x.

Anderson-Teixeira, K. J., Davies, S. J., Bennett, A. C., Gonzalez-Akre, E. B., Muller-Landau, H. C., Joseph Wright, S., Abu Salim, K., Almeyda Zambrano, A. M., Alonso, A., Baltzer, J. L., Basset, Y., Bourg, N. A., Broadbent, E. N., Brockelman, W. Y., Bunyavejchewin, S., Burslem, D. F. R. P., Butt, N., Cao, M., Cardenas, D., Chuyong, G. B., Clay, K., Cordell, S., Dattaraja, H. S., Deng, X., Detto, M., Du, X., Duque, A., Erikson, D. L., Ewango, C. E., Fischer, G. A., Fletcher, C., Foster, R. B., Giardina, C. P., Gilbert, G. S., Gunatilleke, N., Gunatilleke, S., Hao, Z., Hargrove, W. W., Hart, T. B., Hau, B. C., He, F., Hoffman, F. M., Howe, R. W., Hubbell, S. P., Inman-Narahari, F. M., Jansen, P. A., Jiang, M., Johnson, D. J., Kanzaki, M., Kassim, A. R., Kenfack, D., Kibet, S., Kinnaird, M. F., Korte, L., Kral, K., Kumar, J., Larson, A. J., Li, Y., Li, X., Liu, S., Lum, S. K., Lutz, J. A., Ma, K., Maddalena, D. M., Makana, J.-R., Malhi, Y., Marthews, T., Mat Serudin, R., McMahon, S. M., McShea, W. J., Memiaghe, H. R., Mi, X., Mizuno, T., Morecroft, M., Myers, J. A., Novotny, V., de Oliveira, A. A., Ong, P. S., Orwig, D. A., Ostertag, R., den Ouden, J., Parker, G. G., Phillips, R. P., Sack, L., Sainge, M. N., Sang, W., Sri-ngernyuang, K., Sukumar, R., Sun, I.-F., Sungpalee, W., Suresh, H. S., Tan, S., Thomas, S. C., Thomas, D. W., Thompson, J., Turner, B. L., Uriarte, M., Valencia, R., Vallejo, M. I., Vicentini, A., Vrška, T., Wang, X., Wang, X., Weiblen, G., Wolf, A., Xu, H., Yap, S., and Zimmerman, J. CTFS-ForestGEO: a worldwide network monitoring forests in an era of global change. *Global Change Biology*, 21(2):528–549, 2015. doi: 10.1111/gcb.12712.

Asner, G. P., Knapp, D. E., Broadbent, E. N., Oliveira, P. J. C., Keller, M., and Silva, J. N. Selective Logging in the Brazilian Amazon. 2:19–22, 2002. doi: 10.1126/science.1118051.

Asner, G. P. and Mascaro, J. Mapping tropical forest carbon: Calibrating plot estimates to a simple LiDAR metric. *Remote Sensing of Environment*, 140:614–624, 2014. doi: 10.1016/j.rse.2013.09.023.

Asner, G. P., Powell, G. V. N., Mascaro, J., Knapp, D. E., Clark, J. K., Jacobson, J., Kennedy-Bowdoin, T., Balaji, A., Paez-Acosta, G., Victoria, E., Secada, L., Valqui, M., and Hughes, R. F. High-resolution forest carbon stocks and emissions in the Amazon. *Proceedings of the National Academy of Sciences of the United States of America*, 107(38):16738–42, 2010. doi: 10.1073/pnas.1004875107.

Atkin, O. K. and Tjoelker, M. G. Thermal acclimation and the dynamic response of plant respiration to temperature. *Trends in plant science*, 8(7):343–51, 2003. doi: 10.1016/S1360-1385(03)00136-5.

Aubinet, M., Grelle, A., Ibrom, A., Rannik, Ü., Moncrieff, J., Foken, T., Kowalski, A., Martin, P., Berbigier, P., Bernhofer, C., Clement, R., Elbers, J., Granier, A., Grünwald, T., Morgenstern, K., Pilegaard, K., Rebmann, C., Snijders, W., Valentini, R., and Vesala, T. Estimates of the Annual Net Carbon and Water Exchange of Forests: The EUROFLUX Methodology. volume 30, pp. 113–175. Advances in Ecological Research, 1999. doi: https://doi.org/10.1016/S0065-2504(08)60018-5.

Avitabile, V., Herold, M., Heuvelink, G. B. M., Lewis, S. L., Phillips, O. L., Asner, G. P., Armston, J., Ashton, P. S., Banin, L., Bayol, N., Berry, N. J., Boeckx, P., de Jong, B. H. J., DeVries, B., Girardin, C. A. J., Kearsley, E., Lindsell, J. a., Lopez-Gonzalez, G., Lucas, R., Malhi, Y., Morel, A., Mitchard, E. T. A., Nagy, L., Qie, L., Quinones, M. J., Ryan, C. M., Ferry, S. J. W., Sunderland, T., Laurin, G. V., Gatti, R. C., Valentini, R., Verbeeck, H., Wijaya, A., and Willcock, S. An integrated pan-tropical biomass map using multiple reference datasets. *Global Change Biology*, 22(4):1406–1420, 2016. doi: 10.1111/gcb.13139.

Baccini, A., Goetz, S. J., Walker, W. S., Laporte, N. T., Sun, M., Sulla-Menashe, D., Hackler, J., Beck, P. S. a., Dubayah, R., Friedl, M. a., Samanta, S., and Houghton, R. a. Estimated carbon dioxide emissions from tropical deforestation improved by carbon-density maps. *Nature Climate Change*, 2(3):182–185, 2012. doi: 10.1038/nclimate1354.

Baker, I. T., Prihodko, L., Denning, A. S., Goulden, M., Miller, S., and da Rocha, H. R. Seasonal drought stress in the Amazon: Reconciling models and observations. *Journal of Geophysical Research: Biogeosciences*, 113(G1):n/a–n/a, 2008. doi: 10.1029/2007JG000644.

Baker, T. R., Phillips, O. L., Malhi, Y., Almeida, S., Arroyo, L., Di Fiore, A., Erwin, T., Killeen, T. J., Laurance, S. G., Laurance, W. F., Lewis, S. L., Lloyd, J., Monteagudo, A., Neill, D. A., Patiño, S., Pitman, N. C. A., M. Silva, J. N., and Vásquez Martínez, R. Variation in wood density determines spatial patterns in Amazonian forest biomass. *Global Change Biology*, 10:545–562, 2004. doi: 10.1111/j.1365-2486.2004.00751.

Bala, G., Caldeira, K., Wickett, M., Phillips, T. J., Lobell, D. B., Delire, C., and Mirin, A. Combined climate and carbon-cycle effects of large-scale deforestation. *Proceedings*

of the National Academy of Sciences, 104(16):6550–6555, 2007. doi: 10.1073/pnas.0608998104.

Baldocchi, D. Measuring fluxes of trace gases and energy between ecosystems and the atmosphere - the state and future of the eddy covariance method. *Global Change Biology*, 20(12):3600–9, 2014. doi: 10.1111/gcb.12649.

Baldocchi, D., Valentini, R., Running, S., Oechel, W., and Dahlman, R. Strategies for measuring and modelling carbon dioxide and water vapour fluxes over terrestrial ecosystems. *Global Change Biology*, 2(3):159–168, 1996. doi: 10.1111/j.1365-2486.1996.tb00069.x.

Baldocchi, D. D., Hincks, B. B., and Meyers, T. P. Measuring Biosphere-Atmosphere Exchanges of Biologically Related Gases with Micrometeorological Methods. *Ecology*, 69(5):1331–1340, 1988. doi: 10.2307/1941631.

Bauer, J. E., Cai, W.-J., Raymond, P. a., Bianchi, T. S., Hopkinson, C. S., and Regnier, P. a. G. The changing carbon cycle of the coastal ocean. *Nature*, 504(7478):61–70, 2013. doi: 10.1038/nature12857.

Beer, C., Reichstein, M., Tomelleri, E., Ciais, P., Jung, M., Carvalhais, N., Rödenbeck, C., Arain, M. A., Baldocchi, D., Bonan, G. B., Bondeau, A., Cescatti, A., Lasslop, G., Lindroth, A., Lomas, M., Luyssaert, S., Margolis, H., Oleson, K. W., Roupsard, O., Veenendaal, E., Viovy, N., Williams, C., Woodward, F. I., and Papale, D. Terrestrial gross carbon dioxide uptake: global distribution and covariation with climate. *Science (New York, N.Y.)*, 329(5993):834–8, 2010. doi: 10.1126/science.1184984.

Berner, R. a. Fuels and Atmospheric Composition. *Nature*, 426(November):323–326, 2003. doi: 10.1038/nature02131.

Blöschl, G. and Sivapalan, M. Scale issues in hydrological modelling: A review. *Hydrological Processes*, 9(3-4):251–290, 1995. doi: 10.1002/hyp.3360090305.

Bohn, F. J., Frank, K., and Huth, A. Of climate and its resulting tree growth: Simulating the productivity of temperate forests. *Ecological Modelling*, 278:9–17, 2014. doi: 10.1016/j.ecolmodel.2014.01.021.

Bonal, D., Bosc, A., Ponton, S., Goret, J. Y., Burban, B. T., Gross, P., Bonnefond, J. M., Elbers, J., Longdoz, B., Epron, D., Guehl, J. M., and Granier, A. Impact of severe dry season on net ecosystem exchange in the Neotropical rainforest of French Guiana. *Global Change Biology*, 14(8):1917–1933, 2008. doi: 10.1111/j.1365-2486.2008.01610.x.

Bondeau, A., Smith, P. C., Zaehle, S., Schaphoff, S., Lucht, W., Cramer, W., Gerten, D., Lotze-campen, H., Müller, C., Reichstein, M., and Smith, B. Modelling the role of agriculture for the 20th century global terrestrial carbon balance. *Global Change Biology*, 13(3):679–706, 2007. doi: 10.1111/j.1365-2486.2006.01305.x.

Botkin, D. B., Janak, J. F., and Wallis, J. R. Some Ecological Consequences of a Computer Model of Forest Growth. *The Journal of Ecology*, 60(3):849, 1972. doi: 10.2307/2258570.

Brienen, R., Phillips, O., Feldpausch, T., Gloor, E., Baker, T., Lloyd, J., Lopez-Gonzalez, G., Monteagudo-Mendoza, A., Malhi, Y., Lewis, S., Martinez, R. V., Alexiades, M., Dávila, E. Á., Alvarez-Loayza, P., Andrade, A., Aragão, L., Araujo, A., and Zagt, R. Plot Data from: "Long-term decline of the Amazon carbon sink". ForestPlots.NET. 2015a. doi: 10.5521/ForestPlots.net/2014_4.

Brienen, R. J. W., Phillips, O. L., Feldpausch, T. R., Gloor, E., Baker, T. R., Lloyd, J., Lopez-Gonzalez, G., Monteagudo-Mendoza, a., Malhi, Y., Lewis, S. L., Vásquez Martinez, R., Alexiades, M., Álvarez Dávila, E., Alvarez-Loayza, P., Andrade, a., Aragão, L. E. O. C., Araujo-Murakami, a., Arets, E. J. M. M., Arroyo, L., Aymard C, G. a., Bánki, O. S., Baraloto, C., Barroso, J., Bonal, D., Boot, R. G. a., Camargo, J. L. C., Castilho, C. V., Chama, V., Chao, K. J., Chave, J., Comiskey, J. a., Cornejo Valverde, F., da Costa, L., de Oliveira, E. a., Di Fiore, a., Erwin, T. L., Fauset, S., Forsthofer, M., Galbraith, D. R., Grahame, E. S., Groot, N., Hérault, B., Higuchi, N., Honorio Coronado, E. N., Keeling, H., Killeen, T. J., Laurance, W. F., Laurance, S., Licona, J., Magnussen, W. E., Marimon, B. S., Marimon-Junior, B. H., Mendoza, C., Neill, D. a., Nogueira, E. M., Núñez, P., Pallqui Camacho, N. C., Parada, a., Pardo-Molina, G., Peacock, J., Peña-Claros, M., Pickavance, G. C., Pitman, N. C. a., Poorter, L., Prieto, a., Quesada, C. a., Ramírez, F., Ramírez-Angulo, H., Restrepo, Z., Roopsind, a., Rudas, a., Salomão, R. P., Schwarz, M., Silva, N., Silva-Espejo, J. E., Silveira, M., Stropp, J., Talbot, J., ter Steege, H., Teran-Aguilar, J., Terborgh, J., Thomas-Caesar, R., Toledo, M., Torello-Raventos, M., Umetsu, R. K., van der Heijden, G. M. F., van der Hout, P., Guimarães Vieira, I. C., Vieira, S. a., Vilanova, E., Vos, V. a., and Zagt, R. J. Long-term decline of the Amazon carbon sink. *Nature*, 519(7543):344–8, 2015b. doi: 10.1038/nature14283.

Brinck, K., Fischer, R., Groeneveld, J., Lehmann, S., Dantas De Paula, M., Pütz, S., Sexton, J. O., Song, D., and Huth, A. High resolution analysis of tropical forest fragmentation and its impact on the global carbon cycle. *Nature Communications*, 8:14855, 2017. doi: 10.1038/ncomms14855.

Brondizio, E. and Moran, E. LBA-ECO LC-09 Vegetation Composition and Structure in the Brazilian Amazon: 1992-1995. Data set. Available on-line [http://daac.ornl.gov] from Oak Ridge National Laboratory Distributed Active Archive Center, Oak Ridge, Tennessee, U.S.A. 2009. doi: 10.3334/ORNLDAAC/939.

Brus, D. J., Hengeveld, G. M., Walvoort, D. J. J., Goedhart, P. W., Heidema, A. H., Nabuurs, G. J., and Gunia, K. Statistical mapping of tree species over Europe. *European Journal of Forest Research*, 131(1):145–157, 2012. doi: 10.1007/s10342-011-0513-5.

Bugmann, H. A Review of Forest Gap Models. *Climatic Change*, 51(3-4):259–305, 2001.

Bugmann, H., Lindner, M., Lasch, P., Flechsig, M., Ebert, B., and Cramer, W. Scaling Issues in Forest Succession Modelling. *Climatic Change*, 44(3):265–289, 2000.

Bugmann, H. K. M. and Solomon, A. M. The Use of a European Forest Model in North America: A Study of Ecosystem Response to Climate Gradients. *Journal of Biogeography*, 22(2/3):477, 1995. doi: 10.2307/2845944.

Carvalhais, N., Forkel, M., Khomik, M., Bellarby, J., Jung, M., Migliavacca, M., Mu, M., Saatchi, S., Santoro, M., Thurner, M., Weber, U., Ahrens, B., Beer, C., Cescatti, A., Randerson, J. T., and Reichstein, M. Global covariation of carbon turnover times with climate in terrestrial ecosystems. *Nature*, 514(7521):213–217, 2014. doi: 10.1038/nature13731.

Cassel, D. K. and Nielsen, D. R. Field capacity and available water capacity. In *Methods of Soil Analysis: Part 1. Physical and Mineralogical Methods*, pp. 901–926. American Society of Agronomy and Soil Science Society of America, Madison, Wis., 1986.

Castanho, A. D. A., Coe, M. T., Costa, M. H., Malhi, Y., Galbraith, D., and Quesada, C. A. Improving simulated Amazon forest biomass and productivity by including spatial variation in biophysical parameters. *Biogeosciences*, 10(4):2255–2272, 2013. doi: 10.5194/bg-10-2255-2013.

de Castilho, C. V., Magnusson, W. E., de Araújo, R. N. O., Luizão, R. C. C., Luizão, F. J., Lima, A. P., and Higuchi, N. Variation in aboveground tree live biomass in a central Amazonian Forest: Effects of soil and topography. *Forest Ecology and Management*, 234(1-3):85–96, 2006. doi: 10.1016/j.foreco.2006.06.024.

CDO. CDO 2015: Climate Data Operators. 2015.

Chambers, J., dos Santos, J., Ribeiro, R., and Higuchi, N. LBA-ECO CD-08 Tree Inventory Data, Ducke Reserve, Manaus, Brazil: 1999. Data set. Available on-line [http:/ daac.ornl.gov] from Oak Ridge National Laboratory Distributed Active Archive Center, Oak Ridge, Tennessee, U.S.A. 2009. doi: doi:10.3334/ORNLDAAC/910.

Chambers, J., da Silva, R., Tribuzy, E. S., dos Santos, J., and Higuchi, N. LBA-ECO CD-08 Tree Diameter Measurements, Jacaranda Plots, Manaus, Brazil: 1999-2001. Data set. Available on-line [http://daac.ornl.gov] from Oak Ridge National Laboratory Distributed Active Archive Center, Oak Ridge, Tennessee, USA. 2013a. doi: http://dx.doi.org/10.3334/ORNLDAAC/1194.

Chambers, J. Q., Negron-Juarez, R. I., Marra, D. M., Di Vittorio, A., Tews, J., Roberts, D., Ribeiro, G. H. P. M., Trumbore, S. E., and Higuchi, N. The steady-state mosaic of disturbance and succession across an old-growth Central Amazon forest landscape. *Proceedings of the National Academy of Sciences*, 110(10):3949–3954, 2013b. doi: 10.1073/pnas.1202894110.

Chapin, F. S., Woodwell, G. M., Randerson, J. T., Rastetter, E. B., Lovett, G. M., Baldocchi, D. D., Clark, D. A., Harmon, M. E., Schimel, D. S., Valentini, R., Wirth, C., Aber, J. D., Cole, J. J., Goulden, M. L., Harden, J. W., Heimann, M., Howarth, R. W., Matson, P. A., McGuire, A. D., Melillo, J. M., Mooney, H. A., Neff, J. C., Houghton, R. A., Pace, M. L., Ryan, M. G., Running, S. W., Sala, O. E., Schlesinger, W. H., and Schulze, E.-D. Reconciling Carbon-cycle Concepts, Terminology, and Methods. *Ecosystems*, 9(7):1041–1050, 2006. doi: 10.1007/s10021-005-0105-7.

Chave, J. The problem of pattern and scale in ecology: what have we learned in 20 years? *Ecology Letters*, 16(SUPPL.1):4–16, 2013. doi: 10.1111/ele.12048.

Chave, J., Muller-Landau, H. C., Baker, T. R., Easdale, T. A., ter Steege, H., and Webb, C. O. Regional and phylogenetic variation of wood density across 2456 Neotropical tree species. *Ecological Applications*, 16(6):2356–2367, 2006. doi: 10.1890/1051-0761(2006)016[2356:RAPVOW]2.0.CO;2.

Chave, J., Réjou-Méchain, M., Búrquez, A., Chidumayo, E., Colgan, M. S., Delitti, W. B., Duque, A., Eid, T., Fearnside, P. M., Goodman, R. C., Henry, M., Martínez-Yrízar, A., Mugasha, W. a., Muller-Landau, H. C., Mencuccini, M., Nelson, B. W., Ngomanda, A., Nogueira, E. M., Ortiz-Malavassi, E., Pélissier, R., Ploton, P., Ryan, C. M., Saldarriaga, J. G., and Vieilledent, G. Improved allometric models to estimate the aboveground biomass of tropical trees. *Global Change Biology*, 20(10):3177–3190, 2014. doi: 10.1111/gcb.12629.

Chave, J. J. J., Condit, R., Aguilar, S., Hernandez, A., Lao, S., and Perez, R. Error propagation and scaling for tropical forest biomass estimates. *Philosophical Transactions of the Royal Society of London. Series B: Biological Sciences*, 359(1443):409–420, 2004. doi: 10.1098/rstb.2003.1425.

Chaves, M. M. How Plants Cope with Water Stress in the Field? Photosynthesis and Growth. *Annals of Botany*, 89(7):907–916, 2002. doi: 10.1093/aob/mcf105.

Ciais, P., Reichstein, M., Viovy, N., Granier, A., Ogée, J., Allard, V., Aubinet, M., Buchmann, N., Bernhofer, C., Carrara, A., Chevallier, F., De Noblet, N., Friend, a. D., Friedlingstein, P., Grünwald, T., Heinesch, B., Keronen, P., Knohl, A., Krinner, G., Loustau, D., Manca, G., Matteucci, G., Miglietta, F., Ourcival, J. M., Papale, D., Pilegaard, K., Rambal, S., Seufert, G., Soussana, J. F., Sanz, M. J., Schulze, E. D., Vesala, T., and Valentini, R. Europe-wide reduction in primary productivity caused by the heat and drought in 2003. *Nature*, 437(7058):529–33, 2005. doi: 10.1038/nature03972.

Clark, D. and Clark, D. Landscape-scale variation in forest structure and biomass in a tropical rain forest. *Forest Ecology and Management*, 137(1-3):185–198, 2000. doi: 10.1016/S0378-1127(99)00327-8.

Clark, D. A., Brown, S., Kicklighter, D. W., Chambers, J. Q., Thomlinson, J. R., Ni, J., Holland, E. A., Thomlinson, J. R., Ni, S. J., and Holland, E. A. Net Primary Production in Tropical Forests : An Evaluation and Synthesis of Existing Field Data Published by : Wiley Stable URL : http://www.jstor.org/stable/3060895. 11(2):371–384, 2001.

COHEN, W. B. and GOWARD, S. N. Landsat's Role in Ecological Applications of Remote Sensing. *BioScience*, 54(6):535, 2004. doi: 10.1641/0006-3568(2004)054[0535:LRIEAO]2.0.CO;2.

Collatz, G. J., Ball, J. T., Grivet, C., and Berry, J. A. Physiological and Environmental-Regulation of Stomatal Conductance, Photosynthesis and Transpiration - a Model That Includes a Laminar Boundary-Layer. *Agricultural and Forest Meteorology*, 54(2-4):107–136, 1991. doi: 10.1016/0168-1923(91)90002-8.

Cotta, H. *Hülfstafeln für forstwirthe und forsttaxatoren*. Arnold, 1821.

Cox, P. M., Betts, R. a., Jones, C. D., Spall, S. a., and Totterdell, I. J. Acceleration of global warming due to carbon-cycle feedbacks in a couples climate model. *Nature*, 408(6809):184–187, 2000. doi: 10.1038/35041539.

Cox, P. M., Pearson, D., Booth, B. B., Friedlingstein, P., Huntingford, C., Jones, C. D., and Luke, C. M. Sensitivity of tropical carbon to climate change constrained by carbon dioxide variability. *Nature*, 494(7437):341–4, 2013. doi: 10.1038/nature11882.

Cramer, W., Bondeau, A., Woodward, F. I., Prentice, I. C., Betts, R. A., Brovkin, V., Cox, P. M., Fisher, V., Foley, J. A., Friend, A. D., Kucharik, C., Lomas, M. R., Ramankutty, N., Sitch, S., Smith, B., White, A., and Young-Molling, C. Global response of terrestrial ecosystem structure and function to CO 2 and climate change: results from six dynamic global vegetation models. *Global Change Biology*, 7(4):357–373, 2001. doi: 10.1046/j.1365-2486.2001.00383.x.

DeFries, R. S. and Townshend, J. R. G. NDVI-derived land cover classifications at a global scale. *International Journal of Remote Sensing*, 15(17):3567–3586, 1994. doi: 10.1080/01431169408954345.

Delbart, N., Ciais, P., Chave, J., Viovy, N., Malhi, Y., and Le Toan, T. Mortality as a key driver of the spatial distribution of aboveground biomass in Amazonian forest: results from a dynamic vegetation model. *Biogeosciences*, 7(10):3027–3039, 2010. doi: 10.5194/bg-7-3027-2010.

Dislich, C., Günter, S., Homeier, J., Schröder, B., and Huth, A. Simulating forest dynamics of a tropical montane forest in South Ecuador. *Erdkunde*, 63(4):347–364, 2009. doi: 10.3112/erdkunde.2009.04.05.

Dislich, C. and Huth, A. Modelling the impact of shallow landslides on forest structure in tropical montane forests. *Ecological Modelling*, 239:40–53, 2012. doi: 10.1016/j.ecolmodel.2012.04.016.

Doughty, C. E., Metcalfe, D. B., Girardin, C. a. J., Amézquita, F. F., Cabrera, D. G., Huasco, W. H., Silva-Espejo, J. E., Araujo-Murakami, a., da Costa, M. C., Rocha, W., Feldpausch, T. R., Mendoza, a. L. M., da Costa, a. C. L., Meir, P., Phillips, O. L., and Malhi, Y. Drought impact on forest carbon dynamics and fluxes in Amazonia. *Nature*, 519(7541):78–82, 2015. doi: 10.1038/nature14213.

Dubayah, R. O., Sheldon, S. L., Clark, D. B., Hofton, M. A., Blair, J. B., Hurtt, G. C., and Chazdon, R. L. Estimation of tropical forest height and biomass dynamics using lidar remote sensing at la Selva, Costa Rica. *Journal of Geophysical Research: Biogeosciences*, 115(2):1–17, 2010. doi: 10.1029/2009JG000933.

ESA. Ready to build the Biomass Forest Mission. 2016.

Espírito-Santo, F. D. B., Gloor, M., Keller, M., Malhi, Y., Saatchi, S., Nelson, B., Junior, R. C. O., Pereira, C., Lloyd, J., Frolking, S., Palace, M., Shimabukuro, Y. E., Duarte, V., Mendoza, A. M., López-González, G., Baker, T. R., Feldpausch, T. R., Brienen, R. J. W., Asner, G. P., Boyd, D. S., and Phillips, O. L. Size and frequency of natural forest disturbances and the Amazon forest carbon balance. *Nature Communications*, 5:1–6, 2014. doi: 10.1038/ncomms4434.

Falkowski, P. The Global Carbon Cycle: A Test of Our Knowledge of Earth as a System. *Science*, 290(5490):291–296, 2000. doi: 10.1126/science.290.5490.291.

FAO. Global Forest Resources Assessment. 2001.

Farquhar, G. D. Models of Integrated Photosynthesis of Cells and Leaves. *Philosophical Transactions of the Royal Society of London. Series B, Biological Sciences*, 323(1216):357–367, 1989.

Farquhar, G. D. Models of Photosynthesis. *Plant Physiology*, 125(1):42–45, 2001. doi: 10.1104/pp.125.1.42.

Feldpausch, T. R., Banin, L., Phillips, O. L., Baker, T. R., Lewis, S. L., Quesada, C. a., Affum-Baffoe, K., Arets, E. J. M. M., Berry, N. J., Bird, M., Brondizio, E. S., de Camargo, P., Chave, J., Djagbletey, G., Domingues, T. F., Drescher, M., Fearnside, P. M., França, M. B., Fyllas, N. M., Lopez-Gonzalez, G., Hladik, A., Higuchi, N., Hunter, M. O., Iida, Y., Salim, K. a., Kassim, a. R., Keller, M., Kemp, J., King, D. a., Lovett, J. C., Marimon, B. S., Marimon-Junior, B. H., Lenza, E., Marshall, a. R., Metcalfe, D. J., Mitchard, E. T. a., Moran, E. F., Nelson, B. W., Nilus, R., Nogueira, E. M., Palace, M., Patiño, S., Peh, K. S.-H., Raventos, M. T., Reitsma, J. M., Saiz, G., Schrodt, F., Sonké, B., Taedoumg, H. E., Tan, S., White, L., Wöll, H., and Lloyd, J. Height-diameter allometry of tropical forest trees. *Biogeosciences*, 8(5):1081–1106, 2011. doi: 10.5194/bg-8-1081-2011.

Feldpausch, T. R., Lloyd, J., Lewis, S. L., Brienen, R. J. W., Gloor, M., Monteagudo Mendoza, A., Lopez-Gonzalez, G., Banin, L., Abu Salim, K., Affum-Baffoe, K.,

Alexiades, M., Almeida, S., Amaral, I., Andrade, A., Aragão, L. E. O. C., Araujo Murakami, A., Arets, E. J. M., Arroyo, L., Aymard C., G. A., Baker, T. R., Bánki, O. S., Berry, N. J., Cardozo, N., Chave, J., Comiskey, J. A., Alvarez, E., De Oliveira, A., Di Fiore, A., Djagbletey, G., Domingues, T. F., Erwin, T. L., Fearnside, P. M., França, M. B., Freitas, M. A., Higuchi, N., Honorio C., E., Iida, Y., Jiménez, E., Kassim, A. R., Killeen, T. J., Laurance, W. F., Lovett, J. C., Malhi, Y., Marimon, B. S., Marimon-Junior, B. H., Lenza, E., Marshall, A. R., Mendoza, C., Metcalfe, D. J., Mitchard, E. T. A., Neill, D. A., Nelson, B. W., Nilus, R., Nogueira, E. M., Parada, A., S.-H. Peh, K., Pena Cruz, A., Peñuela, M. C., Pitman, N. C. A., Prieto, A., Quesada, C. A., Ramírez, F., Ramírez-Angulo, H., Reitsma, J. M., Rudas, A., Saiz, G., Salomão, R. P., Schwarz, M., Silva, N., Silva-Espejo, J. E., Silveira, M., Sonké, B., Stropp, J., Taedoumg, H. E., Tan, S., Ter Steege, H., Terborgh, J., Torello-Raventos, M., Van Der Heijden, G. M. F., Vásquez, R., Vilanova, E., Vos, V. A., White, L., Willcock, S., Woell, H., and Phillips, O. L. Tree height integrated into pantropical forest biomass estimates. *Biogeosciences*, 9(8):3381–3403, 2012. doi: 10.5194/bg-9-3381-2012.

Fischer, R., Armstrong, A., Shugart, H. H., and Huth, A. Simulating the impacts of reduced rainfall on carbon stocks and net ecosystem exchange in a tropical forest. *Environmental Modelling & Software*, 52:200–206, 2014. doi: 10.1016/j.envsoft.2013.10.026.

Fischer, R., Bohn, F., Dantas de Paula, M., Dislich, C., Groeneveld, J., Gutiérrez, A. G., Kazmierczak, M., Knapp, N., Lehmann, S., Paulick, S., Pütz, S., Rödig, E., Taubert, F., Köhler, P., and Huth, A. Lessons learned from applying a forest gap model to understand ecosystem and carbon dynamics of complex tropical forests. *Ecological Modelling*, 326:124–133, 2016. doi: 10.1016/j.ecolmodel.2015.11.018.

Fisher, J. I., Hurtt, G. C., Thomas, R. Q., and Chambers, J. Q. Clustered disturbances lead to bias in large-scale estimates based on forest sample plots. *Ecology Letters*, 11(6):554–563, 2008. doi: 10.1111/j.1461-0248.2008.01169.x.

Flügel, W.-A. Delineating hydrological response units by geographical information system analyses for regional hydrological modelling using PRMS/MMS in the drainage basin of the River Bröl, Germany. *Hydrological Processes*, 9(3-4):423–436, 1995. doi: 10.1002/hyp.3360090313.

Friedlingstein, P., Cox, P., Betts, R., Bopp, L., Von Bloh, W., Brovkin, V., Cadule, P., Doney, S., Eby, M., Fung, I., Bala, G., John, J., Jones, C., Joos, F., Kato, T., Kawamiya, M., Knorr, W., Lindsay, K., Matthews, H. D., Raddatz, T., Rayner, P., Reick, C., Roeckner, E., Schnitzler, K. G., Schnur, R., Strassmann, K., Weaver, A. J., Yoshikawa, C., and Zeng, N. Climate – Carbon Cycle Feedback Analysis : Results from the C 4 MIP Model Intercomparison. *Journal of Climate*, 19:3337–3353, 2006.

Friend, A. D., Arneth, A., Kiang, N. Y., Lomas, M., Ogée, J., Rödenbeck, C., Running, S. W., Santaren, J.-D., Sitch, S., Viovy, N., Ian Woodward, F., and Zaehle, S. FLUXNET and modelling the global carbon cycle. *Global Change Biology*, 13(3):610–633, 2007. doi: 10.1111/j.1365-2486.2006.01223.x.

Friend, A. D., Lucht, W., Rademacher, T. T., Keribin, R., Betts, R., Cadule, P., Ciais, P., Clark, D. B., Dankers, R., Falloon, P. D., Ito, A., Kahana, R., Kleidon, A., Lomas, M. R., Nishina, K., Ostberg, S., Pavlick, R., Peylin, P., Schaphoff, S., Vuichard, N., Warszawski, L., Wiltshire, A., and Woodward, F. I. Carbon residence time dominates uncertainty in terrestrial vegetation responses to future climate and atmospheric CO2. *Proceedings of the National Academy of Sciences of the United States of America*, 111(9):3280–5, 2014. doi: 10.1073/pnas.1222477110.

Galbraith, D., Malhi, Y., Affum-Baffoe, K., Castanho, A. D., Doughty, C. E., Fisher, R. a., Lewis, S. L., Peh, K. S.-H., Phillips, O. L., Quesada, C. a., Sonké, B., and Lloyd, J. Residence times of woody biomass in tropical forests. *Plant Ecology & Diversity*, 6(1):139–157, 2013. doi: 10.1080/17550874.2013.770578.

Gardner, W. R. and Nieman, R. H. Lower Limit of Water Availability to Plants. *Science*, 143(3613):1460–1462, 1964. doi: 10.1126/science.143.3613.1460.

Gatti, L. V., Gloor, M., Miller, J. B., Doughty, C. E., Malhi, Y., Domingues, L. G., Basso, L. S., Martinewski, a., Correia, C. S. C., Borges, V. F., Freitas, S., Braz, R., Anderson, L. O., Rocha, H., Grace, J., Phillips, O. L., and Lloyd, J. Drought sensitivity of Amazonian carbon balance revealed by atmospheric measurements. *Nature*, 506(7486):76–80, 2014. doi: 10.1038/nature12957.

GLOBE Task Team et al. The Global Land One-kilometer Base Elevation (GLOBE) Digital Elevation Model, Version 1.0. National Oceanic and Atmospheric Administration, National Geophysical Data Center, 325 Broadway, Boulder, Colorado 80305-3328, U.S.A. Digital data base on the World. 1999.

Goward, S. N., Compton, J. T., and Dye, D. G. North American Vegetation Patterns Observed with the NOAA-7 Advanced Very High Resolution Radiometer. *Vegetatio*, 64(1):3–14, 1985. doi: 10.2307/20037229.

Grace, J., Malhi, Y., Lloyd, J., McIntyre, J., Miranda, A., Meir, P., and Miranda, H. The use of eddy covariance to infer the net carbon dioxide uptake of Brazilian rain forest. *Global Change Biology*, 2(3):209–217, 1996. doi: 10.1111/j.1365-2486.1996.tb00073.x.

Graf, A., Weihermuller, L., Huisman, J. A., Herbst, M., and Vereecken, H. Comment on "Global Convergence in the Temperature Sensitivity of Respiration at Ecosystem Level". *Science*, 331(6022):1265–1265, 2011. doi: 10.1126/science.1196948.

Grandtner, M. and Chevrette, J. *Dictionary of Trees, Volume 2: South America: Nomenclature, Taxonomy and Ecology (Elsevier's Dictionary of Trees)*, volume 2. Academic Press, 2013. ISBN 9780123969545.

Granier, A., Bréda, N., Biron, P., and Villette, S. A lumped water balance model to evaluate duration and intensity of drought constraints in forest stands. *Ecological Modelling*, 116(2-3):269–283, 1999. doi: 10.1016/S0304-3800(98)00205-1.

Granier, A., Reichstein, M., Bréda, N., Janssens, I., Falge, E., Ciais, P., Grünwald, T., Aubinet, M., Berbigier, P., Bernhofer, C., Buchmann, N., Facini, O., Grassi, G., Heinesch, B., Ilvesniemi, H., Keronen, P., Knohl, A., Köstner, B., Lagergren, F., Lindroth, A., Longdoz, B., Loustau, D., Mateus, J., Montagnani, L., Nys, C., Moors, E., Papale, D., Peiffer, M., Pilegaard, K., Pita, G., Pumpanen, J., Rambal, S., Rebmann, C., Rodrigues, A., Seufert, G., Tenhunen, J., Vesala, T., and Wang, Q. Evidence for soil water control on carbon and water dynamics in European forests during the extremely dry year: 2003. *Agricultural and Forest Meteorology*, 143(1-2):123–145, 2007. doi: 10.1016/j.agrformet.2006.12.004.

Greco, S. and Baldocchi, D. D. Seasonal variations of CO2 and water vapour exchange rates over a temperate deciduous forest. *Global Change Biology*, 2(3):183–197, 1996. doi: 10.1111/j.1365-2486.1996.tb00071.x.

Grünwald, T. and Bernhofer, C. A decade of carbon, water and energy flux measurements of an old spruce forest at the Anchor Station Tharandt. *Tellus B*, 59(3):387–396, 2007. doi: 10.1111/j.1600-0889.2007.00259.x.

Guisan, A. and Thuiller, W. Predicting species distribution: Offering more than simple habitat models. *Ecology Letters*, 8(9):993–1009, 2005. doi: 10.1111/j.1461-0248.2005.00792.x.

Gutiérrez, A. G., Armesto, J. J., Aravena, J.-C., Carmona, M., Carrasco, N. V., Christie, D. a., Peña, M.-P., Pérez, C., and Huth, A. Structural and environmental characterization of old-growth temperate rainforests of northern Chiloé Island, Chile: Regional and global relevance. *Forest Ecology and Management*, 258(4):376–388, 2009. doi: 10.1016/j.foreco.2009.03.011.

Gutiérrez, A. G., Armesto, J. J., Díaz, M. F., and Huth, A. Sensitivity of North Patagonian temperate rainforests to changes in rainfall regimes: a process-based, dynamic forest model. *Biogeosciences Discussions*, 9(6):6293–6333, 2012. doi: 10.5194/bgd-9-6293-2012.

Hall, F. G., Bergen, K., Blair, J. B., Dubayah, R., Houghton, R., Hurtt, G., Kellndorfer, J., Lefsky, M., Ranson, J., Saatchi, S., Shugart, H. H., and Wickland, D. Characterizing 3D vegetation structure from space: Mission requirements. *Remote Sensing of Environment*, 115(11):2753–2775, 2011. doi: 10.1016/j.rse.2011.01.024.

Hansen, M. C., Defries, R. S., Townshend, J. R. G., and Sohlberg, R. Global land cover classification at 1 km spatial resolution using a classification tree approach. *International Journal of Remote Sensing*, 21(6-7):1331–1364, 2000. doi: 10.1080/014311600210209.

Hansen, M. C., Potapov, P. V., Moore, R., Hancher, M., Turubanova, S. A., Tyukavina, A., Thau, D., Stehman, S. V., Goetz, S. J., Loveland, T. R., Kommareddy, A., Egorov, A., Chini, L., Justice, C. O., and Townshend, J. R. G. High-Resolution Global Maps of 21st-Century Forest Cover Change. *Science*, 342(6160):850–853, 2013. doi: 10.1126/science.1244693.

Hansen, M. C., Stehman, S. V., and Potapov, P. V. Quantification of global gross forest cover loss. *Proceedings of the National Academy of Sciences of the United States of America*, 107(19):8650–5, 2010. doi: 10.1073/pnas.0912668107.

Hartig, F., Dyke, J., Hickler, T., Higgins, S. I., O'Hara, R. B., Scheiter, S., and Huth, A. Connecting dynamic vegetation models to data - an inverse perspective. *Journal of Biogeography*, 39(12):2240–2252, 2012. doi: 10.1111/j.1365-2699.2012.02745.x.

Heiri, C., Bugmann, H., Tinner, W., Heiri, O., and Lischke, H. A model-based reconstruction of Holocene treeline dynamics in the Central Swiss Alps. *Journal of Ecology*, 94(1):206–216, 2006. doi: 10.1111/j.1365-2745.2005.01072.x.

Hickler, T., Smith, B., Sykes, M. T., Davis, M. B., Sugita, S., and Walker, K. Using a generalized vegetation model to simulate vegetation dynamics in northern USA. *Ecology*, 85(2):519–530, 2004. doi: 10.1890/02-0344.

Hoffman, F. M. and Randerson, J. T. Causes and implications of persistent atmospheric carbon. *Journal of Geophysical Research, Biogeosciences*, pp. 1–22, 2013. doi: 10.1002/2013JG002381.Received.

Hofhansl, F., Andersen, K. M., Fleischer, K., Fuchslueger, L., Rammig, A., Schaap, K. J., Valverde-Barrantes, O. J., and Lapola, D. M. Amazon Forest Ecosystem Responses to Elevated Atmospheric CO2 and Alterations in Nutrient Availability: Filling the Gaps with Model-Experiment Integration. *Frontiers in Earth Science*, 4(February):1–9, 2016. doi: 10.3389/feart.2016.00019.

Houghton, R. A. Aboveground forest biomass and the global carbon balance. *Global Change Biology*, 11(6):945–958, 2005. doi: 10.1111/j.1365-2486.2005.00955.x.

Houghton, R. A., House, J. I., Pongratz, J., van der Werf, G. R., DeFries, R. S., Hansen, M. C., Le Quéré, C., and Ramankutty, N. Carbon emissions from land use and land-cover change. *Biogeosciences*, 9(12):5125–5142, 2012. doi: 10.5194/bg-9-5125-2012.

Houghton, R. A., Lawrence, K. T., Hackler, J. L., and Brown, S. The spatial distribution of forest biomass in the Brazilian Amazon: a comparison of estimates. *Global Change Biology*, 7(7):731–746, 2001. doi: 10.1111/j.1365-2486.2001.00426.x.

Hsiao, T. C. Plant Responses to Water Stress. *Annual Review of Plant Physiology*, 24(1):519–570, 1973. doi: 10.1146/annurev.pp.24.060173.002511.

Huete, A., Didan, K., Miura, T., Rodriguez, E., Gao, X., and Ferreira, L. Overview of the radiometric and biophysical performance of the MODIS vegetation indices. *Remote Sensing of Environment*, 83(1-2):195–213, 2002. doi: 10.1016/S0034-4257(02)00096-2.

Huntingford, C., Fisher, R. a., Mercado, L., Booth, B. B. B., Sitch, S., Harris, P. P., Cox, P. M., Jones, C. D., Betts, R. a., Malhi, Y., Harris, G. R., Collins, M., and Moorcroft, P. Towards quantifying uncertainty in predictions of Amazon 'dieback'. *Philosophical transactions of the Royal Society of London. Series B, Biological sciences*, 363(1498):1857–64, 2008. doi: 10.1098/rstb.2007.0028.

Hurtt, G. C., Dubayah, R., Drake, J., Moorcroft, P. R., Pacala, S. W., Blair, J. B., and Fearon, M. G. Beyond potential vegetation: Combining lidar data and a height-structured model for carbon studies. *Ecological Applications*, 14(3):873–883, 2004. doi: 10.1890/02-5317.

Huth, A. and Ditzer, T. Simulation of the growth of a lowland Dipterocarp rain forest with FORMIX3. *Ecological Modelling*, 134(1):1–25, 2000. doi: 10.1016/S0304-3800(00)00328-8.

Huth, A., Drechsler, M., and Koehler, P. Multicriteria evaluation of simulated logging scenarios in a tropical rain forest. *Journal of Environmental Management*, 71(4):321–33, 2004. doi: 10.1016/j.jenvman.2004.03.008.

Huth, A., Drechsler, M., and Koehler, P. Using multicriteria decision analysis and a forest growth model to assess impacts of tree harvesting in Dipterocarp lowland rain forests. *Forest Ecology and Management*, 207(1-2):215–232, 2005. doi: 10.1016/j.foreco.2004.10.028.

IPCC. *Climate Change 2013: The Physical Science Basis. Contribution of Working Group I to the Fifth Assessment Report of the Intergovern - mental Panel on Climate Change [Stocker, T.F., D. Qin, G.-K. Plattner, M. Tignor, S.K. Allen, J. Boschung, A. Nauels, Y. X.* Cambridge University Press, Cambridge, United Kingdom and New York, NY, USA, 2013. ISBN 978-1-107-05799-1.

Jeltsch, F., Moloney, K. A., Schurr, F. M., Köchy, M., and Schwager, M. The state of plant population modelling in light of environmental change. *Perspectives in Plant Ecology, Evolution and Systematics*, 9(3-4):171–189, 2008. doi: 10.1016/j.ppees.2007.11.004.

Jirka, S., Feldpausch, T., and Riha, S. LBA-ECO ND-11 Ecotone Vegetation Survey and Biomass, NW Mato Grosso, Brazil: 2004. Data set. Available on-line [http://daac.ornl.gov] from Oak Ridge National Laboratory Distributed Active Archive Center, Oak Ridge, Tennessee, U.S.A. 2010. doi: 10.3334/ORNLDAAC/964.

Johnson, M. O., Galbraith, D., Gloor, M., De Deurwaerder, H., Guimberteau, M., Rammig, A., Thonicke, K., Verbeeck, H., von Randow, C., Monteagudo, A., Phillips, O. L., Brienen, R. J., Feldpausch, T. R., Lopez Gonzalez, G., Fauset, S., Quesada, C. A., Christoffersen, B., Ciais, P., Sampaio, G., Kruijt, B., Meir, P., Moorcroft, P., Zhang, K., Alvarez-Davila, E., Alves de Oliveira, A., Amaral, I., Andrade, A., Aragao, L. E., Araujo-Murakami, A., Arets, E. J., Arroyo, L., Aymard, G. A., Baraloto, C., Barroso, J., Bonal, D., Boot, R., Camargo, J., Chave, J., Cogollo, A., Cornejo Valverde, F., Lola da Costa, A. C., Di Fiore, A., Ferreira, L., Higuchi, N., Honorio, E. N., Killeen, T. J., Laurance, S. G., Laurance, W. F., Licona, J., Lovejoy, T., Malhi, Y., Marimon, B., Marimon, B. H., Matos, D. C., Mendoza, C., Neill, D. A., Pardo, G., Pena-Claros, M., Pitman, N. C., Poorter, L., Prieto, A., Ramirez-Angulo, H., Roopsind, A., Rudas, A., Salomao, R. P., Silveira, M., Stropp, J., ter Steege, H., Terborgh, J., Thomas, R., Toledo, M., Torres-Lezama, A., van der Heijden, G. M., Vasquez, R., Guimaraes Vieira, I. C., Vilanova, E., Vos, V. A., and Baker, T. R. Variation in stem mortality rates determines patterns of above-ground biomass in Amazonian forests: implications for dynamic global vegetation models. *Global Change Biology*, 22(12):3996–4013, 2016. doi: 10.1111/gcb.13315.

June, T., Evans, J. R., and Farquhar, G. D. A simple new equation for the reversible temperature dependence of photosynthetic electron transport: a study on soybean leaf. *Functional Plant Biology*, 31(3):275 – 283, 2004. doi: 10.1071/FP03250.

Jung, M., Reichstein, M., Margolis, H. A., Cescatti, A., Richardson, A. D., Arain, M. A., Arneth, A., Bernhofer, C., Bonal, D., Chen, J., Gianelle, D., Gobron, N., Kiely, G., Kutsch, W., Lasslop, G., Law, B. E., Lindroth, A., Merbold, L., Montagnani, L., Moors, E. J., Papale, D., Sottocornola, M., Vaccari, F., and Williams, C. Global patterns of land-atmosphere fluxes of carbon dioxide, latent heat, and sensible heat derived from eddy covariance, satellite, and meteorological observations. *Journal of Geophysical Research: Biogeosciences*, 116(3):1–16, 2011. doi: 10.1029/2010JG001566.

Kammesheidt, L., Kohler, P., and Huth, A. Sustainable timber harvesting in Venezuela: a modelling approach. *Journal of Applied Ecology*, 38(4):756–770, 2001. doi: 10.1046/j.1365-2664.2001.00629.x.

Kazmierczak, M., Wiegand, T., and Huth, A. A neutral vs. non-neutral parametrizations of a physiological forest gap model. *Ecological Modelling*, 288:94–102, 2014. doi: 10.1016/j.ecolmodel.2014.05.002.

Keeling, H. C. and Phillips, O. L. The global relationship between forest productivity and biomass. *Global Ecology and Biogeography*, 16(5):618–631, 2007. doi: 10.1111/j.1466-8238.2007.00314.x.

Keenan, T. F., Baker, I., Barr, A., Ciais, P., Davis, K., Dietze, M., Dragoni, D., Gough, C. M., Grant, R., Hollinger, D., Hufkens, K., Poulter, B., Mccaughey, H., Raczka, B., Ryu,

Y., Schaefer, K., Tian, H., Verbeeck, H., Zhao, M., and Richardson, A. D. Terrestrial biosphere model performance for inter-annual variability of land-atmosphere CO 2 exchange. *Global Change Biology*, 18(6):1971–1987, 2012. doi: 10.1111/j.1365-2486.2012.02678.x.

Kimball, J. S., White, M. a., and Running, S. W. BIOME-BGC simulations of stand hydrologic processes for BOREAS. *Journal of Geophysical Research*, 102(97):29043, 1997. doi: 10.1029/97JD02235.

Kirschbaum, M. The temperature dependence of organic-matter decomposition—still a topic of debate. *Soil Biology and Biochemistry*, 38(9):2510–2518, 2006. doi: 10.1016/j.soilbio.2006.01.030.

Köhler, P. and Huth, A. The effects of tree species grouping in tropical rainforest modelling: Simulations with the individual-based model Formind. *Ecological Modelling*, 109(3):301–321, 1998. doi: 10.1016/S0304-3800(98)00066-0.

Köhler, P. and Huth, A. Simulating growth dynamics in a South-East Asian rainforest threatened by recruitment shortage and tree harvesting. *Climatic Change*, 67(1):95–117, 2004. doi: 10.1007/s10584-004-0713-9.

Körner, C. Leaf Diffusive Conductances in the Major Vegetation Types of the Globe. In Schulze, E.-D. and Caldwell, M. M., editors, *Ecophysiology of Photosynthesis*. Springer Berlin Heidelberg, Berlin, Heidelberg, 1994. ISBN 978-3-540-58571-8. doi: 10.1007/978-3-642-79354-7.

Körner, C. and Paulsen, J. A world-wide study of high altitude treeline temperatures. *Journal of Biogeography*, 31(5):713–732, 2004. doi: 10.1111/j.1365-2699.2003.01043.x.

Krieger, G., Moreira, A., Fiedler, H., Hajnsek, I., Werner, M., Younis, M., and Zink, M. TanDEM-X: A Satellite Formation for High-Resolution SAR Interferometry. *IEEE Transactions on Geoscience and Remote Sensing*, 45(11):3317–3341, 2007. doi: 10.1109/TGRS.2007.900693.

Krinner, G., Viovy, N., de Noblet-Ducoudré, N., Ogée, J., Polcher, J., Friedlingstein, P., Ciais, P., Sitch, S., and Prentice, I. C. A dynamic global vegetation model for studies of the coupled atmosphere-biosphere system. *Global Biogeochemical Cycles*, 19(1):GB1015, 2005. doi: 10.1029/2003GB002199.

Kugler, F., Schulze, D., Hajnsek, I., Pretzsch, H., and Papathanassiou, K. P. TanDEM-X Pol-InSAR Performance for Forest Height Estimation. *IEEE Transactions on Geoscience and Remote Sensing*, 52(10):6404–6422, 2014. doi: 10.1109/TGRS.2013.2296533.

Kunert, N., Aparecido, L. M. T., Higuchi, N., Santos, J. D., and Trumbore, S. Higher tree transpiration due to road-associated edge effects in a tropical moist lowland for-

est. *Agricultural and Forest Meteorology*, 213(August):183–192, 2015. doi: 10.1016/j.agrformet.2015.06.009.

Kuzyakov, Y. Sources of CO2 efflux from soil and review of partitioning methods. *Soil Biology and Biochemistry*, 38(3):425–448, 2006. doi: 10.1016/j.soilbio.2005.08.020.

Landsberg, J. J. and Waring, R. H. A generalised model of forest productivity using simplified concepts ofradiation-use efficiency , carbon balance and partltlonlng. *Forest Ecology and Management*, 95:209–228, 1997. doi: 10.1016/S0378-1127(97)00026-1.

Larcher, W. *Ökophysiologie der Pflanzen*. Eugen Ullmer, Stuttgart, 6th edition, 2001. ISBN 9783825280741.

Lasslop, G., Reichstein, M., Papale, D., Richardson, A. D., Arneth, A., Barr, A., Stoy, P., and Wohlfahrt, G. Separation of net ecosystem exchange into assimilation and respiration using a light response curve approach: critical issues and global evaluation. *Global Change Biology*, 16(1):187–208, 2010. doi: 10.1111/j.1365-2486.2009.02041.x.

Laurance, W. F. Biomass Collapse in Amazonian Forest Fragments. *Science*, 278(5340):1117–1118, 1997. doi: 10.1126/science.278.5340.1117.

Lavigne, M. B. and Ryan, M. G. Growth and maintenance respiration rates of aspen, black spruce and jack pine stems at northern and southern BOREAS sites. *Tree Physiology*, 17(8-9):543–551, 1997. doi: 10.1093/treephys/17.8-9.543.

Le Quéré, C., Andrew, R. M., Canadell, J. G., Sitch, S., Korsbakken, J. I., Peters, G. P., Manning, A. C., Boden, T. A., Tans, P. P., Houghton, R. A., Keeling, R. F., Alin, S., Andrews, O. D., Anthoni, P., Barbero, L., Bopp, L., Chevallier, F., Chini, L. P., Ciais, P., Currie, K., Delire, C., Doney, S. C., Friedlingstein, P., Gkritzalis, T., Harris, I., Hauck, J., Haverd, V., Hoppema, M., Klein Goldewijk, K., Jain, A. K., Kato, E., Körtzinger, A., Landschützer, P., Lefèvre, N., Lenton, A., Lienert, S., Lombardozzi, D., Melton, J. R., Metzl, N., Millero, F., Monteiro, P. M. S., Munro, D. R., Nabel, J. E. M. S., Nakaoka, S.-i., O'Brien, K., Olsen, A., Omar, A. M., Ono, T., Pierrot, D., Poulter, B., Rödenbeck, C., Salisbury, J., Schuster, U., Schwinger, J., Séférian, R., Skjelvan, I., Stocker, B. D., Sutton, A. J., Takahashi, T., Tian, H., Tilbrook, B., van der Laan-Luijkx, I. T., van der Werf, G. R., Viovy, N., Walker, A. P., Wiltshire, A. J., and Zaehle, S. Global Carbon Budget 2016. *Earth System Science Data*, 8(2):605–649, 2016. doi: 10.5194/essd-8-605-2016.

Le Toan, T., Quegan, S., Davidson, M., Balzter, H., Paillou, P., Papathanassiou, K., Plummer, S., Rocca, F., Saatchi, S., Shugart, H., and Ulander, L. The BIOMASS mission: Mapping global forest biomass to better understand the terrestrial carbon cycle. *Remote Sensing of Environment*, 115(11):2850–2860, 2011. doi: 10.1016/j.rse.2011.03.020.

Leclerc, M. Y. and Thurtell, G. W. Footprint prediction of scalar fluxes using a Markovian analysis. *Boundary-Layer Meteorology*, 52(3):247–258, 1990. doi: 10.1007/BF00122089.

Lefsky, M. A., Cohen, W. B., Parker, G. G., and Harding, D. J. Lidar Remote Sensing for Ecosystem Studies. *BioScience*, 52(1):19–30, 2002. doi: 10.1641/0006-3568(2002)052[0019:LRSFES]2.0.CO;2.

Lefsky, M. A., Harding, D. J., Keller, M., Cohen, W. B., Carabajal, C. C., Del Bom Espirito-Santo, F., Hunter, M. O., and de Oliveira, R. Estimates of forest canopy height and aboveground biomass using ICESat. *Geophysical Research Letters*, 32(22):n/a–n/a, 2005. doi: 10.1029/2005GL023971.

Lehmann, S. and Huth, A. Fast calibration of a dynamic vegetation model with minimum observation data. *Ecological Modelling*, 301:98–105, 2015. doi: 10.1016/j.ecolmodel.2015.01.013.

Levin, S. A. The Problem of Pattern and Scale in Ecology: The Robert H. MacArthur Award Lecture. *Ecology*, 73(6):1943–1967, 1992. doi: 10.2307/1941447.

Lopez-Gonzalez, G., Lewis, S. L., Burkitt, M., and Phillips, O. L. ForestPlots.net: a web application and research tool to manage and analyse tropical forest plot data. *Journal of Vegetation Science*, 22(4):610–613, 2011. doi: 10.1111/j.1654-1103.2011.01312.x.

Los, S. O., Rosette, J. A. B., Kljun, N., North, P. R. J., Chasmer, L., Suárez, J. C., Hopkinson, C., Hill, R. A., van Gorsel, E., Mahoney, C., and Berni, J. A. J. Vegetation height and cover fraction between 60Deg S and 60Deg N from ICESat GLAS data. *Geoscientific Model Development*, 5(2):413–432, 2012. doi: 10.5194/gmd-5-413-2012.

Luyssaert, S., Inglima, I., Jung, M., Richardson, a. D., Reichstein, M., Papale, D., Piao, S. L., Schulze, E. D., Wingate, L., Matteucci, G., Aragao, L., Aubinet, M., Beer, C., Bernhofer, C., Black, K. G., Bonal, D., Bonnefond, J. M., Chambers, J., Ciais, P., Cook, B., Davis, K. J., Dolman, a. J., Gielen, B., Goulden, M., Grace, J., Granier, A., Grelle, A., Griffis, T., Grünwald, T., Guidolotti, G., Hanson, P. J., Harding, R., Hollinger, D. Y., Hutyra, L. R., Kolari, P., Kruijt, B., Kutsch, W., Lagergren, F., Laurila, T., Law, B. E., Le Maire, G., Lindroth, A., Loustau, D., Malhi, Y., Mateus, J., Migliavacca, M., Misson, L., Montagnani, L., Moncrieff, J., Moors, E., Munger, J. W., Nikinmaa, E., Ollinger, S. V., Pita, G., Rebmann, C., Roupsard, O., Saigusa, N., Sanz, M. J., Seufert, G., Sierra, C., Smith, M. L., Tang, J., Valentini, R., Vesala, T., and Janssens, I. a. CO 2 balance of boreal, temperate, and tropical forests derived from a global database. *Global Change Biology*, 13(12):2509–2537, 2007. doi: 10.1111/j.1365-2486.2007.01439.x.

Maidment, D. *Handbook of hydrology*. McGrawHill Inc, New York, 1993. ISBN 9780070397323.

Malhi, Y., Doughty, C. E., Goldsmith, G. R., Metcalfe, D. B., Girardin, C. a. J., Marthews, T. R., Del Aguila-Pasquel, J., Aragão, L. E. O. C., Araujo-Murakami, A., Brando, P., da Costa, A. C. L., Silva-Espejo, J. E., Farfán Amézquita, F., Galbraith, D. R., Quesada, C. a., Rocha, W., Salinas-Revilla, N., Silvério, D., Meir, P., and Phillips, O. L. The linkages between photosynthesis, productivity, growth and biomass in lowland Amazonian forests. *Global Change Biology*, 21(6):2283–95, 2015. doi: 10.1111/gcb.12859.

Malhi, Y., Phillips, O., Lloyd, J., Baker, T., Wright, J., Almeida, S., Arroyo, L., Frederiksen, T., Grace, J., Higuchi, N., Killeen, T., Laurance, W., Leaño, C., Lewis, S., Meir, P., Monteagudo, A., Neill, D., Núñez Vargas, P., Panfil, S., Patiño, S., Pitman, N., Quesada, C., Rudas-Ll., A., Salomão, R., Saleska, S., Silva, N., Silveira, M., Sombroek, W., Valencia, R., Vásquez Martínez, R., Vieira, I., and Vinceti, B. An international network to monitor the structure, composition and dynamics of Amazonian forests (RAINFOR). *Journal of Vegetation Science*, 13(3):439, 2002. doi: 10.1658/1100-9233(2002)013[0439:AINTMT]2.0.CO;2.

Malhi, Y., Wood, D., Baker, T. R., Wright, J., Phillips, O. L., Cochrane, T., Meir, P., Chave, J., Almeida, S., Arroyo, L., Higuchi, N., Killeen, T. J., Laurance, S. G., Laurance, W. F., Lewis, S. L., Monteagudo, A., Neill, D. a., Vargas, P. N., Pitman, N. C. a., Quesada, C. A., Salomao, R., Silva, J. N. M., Lezama, A. T., Terborgh, J., Martinez, R. V., and Vinceti, B. The regional variation of aboveground live biomass in old-growth Amazonian forests. *Global Change Biology*, 12(7):1107–1138, 2006. doi: 10.1111/j.1365-2486.2006.01120.x.

Martinez, J. and Letoan, T. Mapping of flood dynamics and spatial distribution of vegetation in the Amazon floodplain using multitemporal SAR data. *Remote Sensing of Environment*, 108(3):209–223, 2007. doi: 10.1016/j.rse.2006.11.012.

Marvin, D. C., Asner, G. P., Knapp, D. E., Anderson, C. B., Martin, R. E., Sinca, F., and Tupayachi, R. Amazonian landscapes and the bias in field studies of forest structure and biomass. *Proceedings of the National Academy of Sciences of the United States of America*, 111(48):E5224–32, 2014. doi: 10.1073/pnas.1412999111.

Meehl, G. A. and Tebaldi, C. More intense, more frequent, and longer lasting heat waves in the 21st century. *Science*, 305(5686):994–997, 2004. doi: 10.1126/science.1098704.

Meir, P., Kruijt, B., Broadmeadow, M., Barbosa, E., Kull, O., Carswell, F., Nobre, A., and Jarvis, P. G. Acclimation of photosynthetic capacity to irradiance in tree canopies in relation to leaf nitrogen concentration and leaf mass per unit area. *Plant, Cell and Environment*, 25(3):343–357, 2002. doi: 10.1046/j.0016-8025.2001.00811.x.

Mitchard, E. T. a., Feldpausch, T. R., Brienen, R. J. W., Lopez-Gonzalez, G., Monteagudo, A., Baker, T. R., Lewis, S. L., Lloyd, J., Quesada, C. a., Gloor, M., Ter Steege, H., Meir, P.,

Alvarez, E., Araujo-Murakami, A., Aragão, L. E. O. C., Arroyo, L., Aymard, G., Banki, O., Bonal, D., Brown, S., Brown, F. I., Cerón, C. E., Chama Moscoso, V., Chave, J., Comiskey, J. a., Cornejo, F., Corrales Medina, M., Da Costa, L., Costa, F. R. C., Di Fiore, A., Domingues, T. F., Erwin, T. L., Frederickson, T., Higuchi, N., Honorio Coronado, E. N., Killeen, T. J., Laurance, W. F., Levis, C., Magnusson, W. E., Marimon, B. S., Marimon Junior, B. H., Mendoza Polo, I., Mishra, P., Nascimento, M. T., Neill, D., Núñez Vargas, M. P., Palacios, W. a., Parada, A., Pardo Molina, G., Peña-Claros, M., Pitman, N., Peres, C. a., Poorter, L., Prieto, A., Ramirez-Angulo, H., Restrepo Correa, Z., Roopsind, A., Roucoux, K. H., Rudas, A., Salomão, R. P., Schietti, J., Silveira, M., de Souza, P. F., Steininger, M. K., Stropp, J., Terborgh, J., Thomas, R., Toledo, M., Torres-Lezama, A., van Andel, T. R., van der Heijden, G. M. F., Vieira, I. C. G., Vieira, S., Vilanova-Torre, E., Vos, V. a., Wang, O., Zartman, C. E., Malhi, Y., and Phillips, O. L. Markedly divergent estimates of Amazon forest carbon density from ground plots and satellites. *Global Ecology and Biogeography*, 23(8):935–946, 2014. doi: 10.1111/geb.12168.

Moffat, A. M., Papale, D., Reichstein, M., Hollinger, D. Y., Richardson, A. D., Barr, A. G., Beckstein, C., Braswell, B. H., Churkina, G., Desai, A. R., Falge, E., Gove, J. H., Heimann, M., Hui, D., Jarvis, A. J., Kattge, J., Noormets, A., and Stauch, V. J. Comprehensive comparison of gap-filling techniques for eddy covariance net carbon fluxes. *Agricultural and Forest Meteorology*, 147(3-4):209–232, 2007. doi: 10.1016/j.agrformet.2007.08.011.

Moorcroft, P. R., Hurtt, G. C., and Pacala, S. W. A Method for Scaling Vegetation Dynamics: the Ecosystem Demography Model (Ed). *Ecological Monographs*, 71(4):557–585, 2001.

Mopper, K., Zhou, X., Kieber, R. J., Kieber, D. J., Sikorski, R. J., and Jones, R. D. Photochemical degradation of dissolved organic carbon and its impact on the oceanic carbon cycle. *Nature*, 353(6339):60–62, 1991. doi: 10.1038/353060a0.

Moreira, A., Krieger, G., Hajnsek, I., Papathanassiou, K., Younis, M., Lopez-dekker, P., Huber, S., Eineder, M., Zan, F. D., and Parizzi, A. A Highly Innovative Bistatic SAR Mission for Global Observation of Dynamic Processes on the Earth ' s Surface. *Geoscience and Remote Sensing Magazine, IEEE*, 3(2):8–23, 2015.

Myneni, R. B., Dong, J., Tucker, C. J., Kaufmann, R. K., Kauppi, P. E., Liski, J., Zhou, L., Alexeyev, V., and Hughes, M. K. A large carbon sink in the woody biomass of Northern forests. *Proceedings of the National Academy of Sciences of the United States of America*, 98(26):14784–9, 2001. doi: 10.1073/pnas.261555198.

NASA. ISS Utilization: GEDI (Global Ecosystems Dynamics Investigation Lidar). 2017.

Nasset, E. and Gobakken, T. Estimating forest growth using canopy metrics derived from airborne laser scanner data. *Remote Sensing of Environment*, 96(3-4):453–465, 2005. doi: 10.1016/j.rse.2005.04.001.

Nguyen, C. Rhizodeposition of Organic C by Plant: Mechanisms and Controls. In *Sustainable Agriculture*, volume 23, pp. 97–123. Springer Netherlands, Dordrecht, 2009. doi: 10.1007/978-90-481-2666-8_9.

Nogueira, E. M., Fearnside, P. M., Nelson, B. W., and França, M. B. Wood density in forests of Brazil's 'arc of deforestation': Implications for biomass and flux of carbon from land-use change in Amazonia. *Forest Ecology and Management*, 248(3):119–135, 2007. doi: 10.1016/j.foreco.2007.04.047.

Nogueira, E. M., Nelson, B. W., Fearnside, P. M., França, M. B., and de Oliveira, Á. C. A. Tree height in Brazil's 'arc of deforestation': Shorter trees in south and southwest Amazonia imply lower biomass. *Forest Ecology and Management*, 255(7):2963–2972, 2008. doi: 10.1016/j.foreco.2008.02.002.

Numata, I., Cochrane, M. A., Roberts, D. A., Soares, J. V., Souza, C. M., and Sales, M. H. Biomass collapse and carbon emissions from forest fragmentation in the Brazilian Amazon. *Journal of Geophysical Research*, 115(G3):G03027, 2010. doi: 10.1029/2009JG001198.

Pacala, S. W., Canham, C. D., and Silander Jr., J. A. Forest models defined by field measurements: I. The design of a northeastern forest simulator. *Canadian Journal of Forest Research*, 23(10):1980–1988, 1993. doi: 10.1139/x93-249.

Pan, Y., Birdsey, R. a., Fang, J., Houghton, R., Kauppi, P. E., Kurz, W. a., Phillips, O. L., Shvidenko, A., Lewis, S. L., Canadell, J. G., Ciais, P., Jackson, R. B., Pacala, S. W., McGuire, a. D., Piao, S., Rautiainen, A., Sitch, S., and Hayes, D. A large and persistent carbon sink in the world's forests. *Science (New York, N.Y.)*, 333(6045):988–993, 2011. doi: 10.1126/science.1201609.

Paulick, S., Dislich, C., Homeier, J., Fischer, R., and Huth, A. The carbon fluxes in different successional stages: modelling the dynamics of tropical montane forests in South Ecuador. *Forest Ecosystems*, 4(1):5, 2017. doi: 10.1186/s40663-017-0092-0.

Phillips, O. L., Aragão, L. E. O. C., Lewis, S. L., Fisher, J. B., Lloyd, J., López-González, G., Malhi, Y., Monteagudo, A., Peacock, J., Quesada, C. a., van der Heijden, G., Almeida, S., Amaral, I., Arroyo, L., Aymard, G., Baker, T. R., Bánki, O., Blanc, L., Bonal, D., Brando, P., Chave, J., de Oliveira, A. C. A., Cardozo, N. D., Czimczik, C. I., Feldpausch, T. R., Freitas, M. A., Gloor, E., Higuchi, N., Jiménez, E., Lloyd, G., Meir, P., Mendoza, C., Morel, A., Neill, D. a., Nepstad, D., Patiño, S., Peñuela, M. C., Prieto, A., Ramírez, F., Schwarz, M., Silva, J., Silveira, M., Thomas, A. S., Steege, H. T., Stropp, J., Vásquez, R., Zelazowski, P., Alvarez Dávila, E., Andelman, S., Andrade, A., Chao, K.-J., Erwin,

T., Di Fiore, A., Honorio C, E., Keeling, H., Killeen, T. J., Laurance, W. F., Peña Cruz, A., Pitman, N. C. a., Núñez Vargas, P., Ramírez-Angulo, H., Rudas, A., Salamão, R., Silva, N., Terborgh, J., and Torres-Lezama, A. Drought sensitivity of the Amazon rainforest. *Science (New York, N.Y.)*, 323(5919):1344–7, 2009. doi: 10.1126/science.1164033.

Phillips, O. L., Baker, T. R., Arroyo, L., Higuchi, N., Killeen, T. J., Laurance, W. F., Lewis, S. L., Lloyd, J., Malhi, Y., Monteagudo, A., Neill, D. A., Nunez Vargas, P., Silva, J. N. M., Terborgh, J., Vasquez Martinez, R., Alexiades, M., Almeida, S., Brown, S., Chave, J., Comiskey, J. A., Czimczik, C. I., Di Fiore, A., Erwin, T., Kuebler, C., Laurance, S. G., Nascimento, H. E. M., Olivier, J., Palacios, W., Patino, S., Pitman, N. C. A., Quesada, C. A., Saldias, M., Torres Lezama, A., and Vinceti, B. Pattern and process in Amazon tree turnover, 1976-2001. *Philosophical Transactions of the Royal Society B: Biological Sciences*, 359(1443):381–407, 2004. doi: 10.1098/rstb.2003.1438.

Piao, S., Luyssaert, S., Ciais, P., Janssens, I. a., Chen, A., Cao, C., Fang, J., Friedlingstein, P., Luo, Y., and Wang, S. Forest annual carbon cost: a global-scale analysis of autotrophic respiration. *Ecology*, 91(3):652–661, 2010.

Poorter, L., Bongers, F., Aide, T. M., Almeyda Zambrano, A. M., Balvanera, P., Becknell, J. M., Boukili, V., Brancalion, P. H. S., Broadbent, E. N., Chazdon, R. L., Craven, D., de Almeida-Cortez, J. S., Cabral, G. a. L., de Jong, B. H. J., Denslow, J. S., Dent, D. H., DeWalt, S. J., Dupuy, J. M., Durán, S. M., Espírito-Santo, M. M., Fandino, M. C., César, R. G., Hall, J. S., Hernandez-Stefanoni, J. L., Jakovac, C. C., Junqueira, A. B., Kennard, D., Letcher, S. G., Licona, J.-C., Lohbeck, M., Marín-Spiotta, E., Martínez-Ramos, M., Massoca, P., Meave, J. a., Mesquita, R., Mora, F., Muñoz, R., Muscarella, R., Nunes, Y. R. F., Ochoa-Gaona, S., de Oliveira, A. a., Orihuela-Belmonte, E., Peña-Claros, M., Pérez-García, E. a., Piotto, D., Powers, J. S., Rodríguez-Velázquez, J., Romero-Pérez, I. E., Ruíz, J., Saldarriaga, J. G., Sanchez-Azofeifa, A., Schwartz, N. B., Steininger, M. K., Swenson, N. G., Toledo, M., Uriarte, M., van Breugel, M., van der Wal, H., Veloso, M. D. M., Vester, H. F. M., Vicentini, A., Vieira, I. C. G., Bentos, T. V., Williamson, G. B., and Rozendaal, D. M. a. Biomass resilience of Neotropical secondary forests. *Nature*, 530(7589):211–4, 2016. doi: 10.1038/nature16512.

Poorter, L., van der Sande, M. T., Thompson, J., Arets, E. J. M. M., Alarcón, A., Álvarez-Sánchez, J., Ascarrunz, N., Balvanera, P., Barajas-Guzmán, G., Boit, A., Bongers, F., Carvalho, F. a., Casanoves, F., Cornejo-Tenorio, G., Costa, F. R. C., de Castilho, C. V., Duivenvoorden, J. F., Dutrieux, L. P., Enquist, B. J., Fernández-Méndez, F., Finegan, B., Gormley, L. H. L., Healey, J. R., Hoosbeek, M. R., Ibarra-Manríquez, G., Junqueira, a. B., Levis, C., Licona, J. C., Lisboa, L. S., Magnusson, W. E., Martínez-Ramos, M., Martínez-Yrizar, A., Martorano, L. G., Maskell, L. C., Mazzei, L., Meave, J. a., Mora, F., Muñoz, R., Nytch, C., Pansonato, M. P., Parr, T. W., Paz, H., Pérez-García, E. a., Rentería, L. Y., Rodríguez-Velazquez, J., Rozendaal, D. M. a., Ruschel, a. R., Sakschewski, B., Salgado-Negret, B., Schietti, J., Simões, M., Sinclair, F. L., Souza, P. F., Souza, F. C., Stropp, J.,

ter Steege, H., Swenson, N. G., Thonicke, K., Toledo, M., Uriarte, M., van der Hout, P., Walker, P., Zamora, N., and Peña-Claros, M. Diversity enhances carbon storage in tropical forests. *Global Ecology and Biogeography*, 24(11):1314–1328, 2015. doi: 10.1111/geb.12364.

Poulter, B., Heyder, U., and Cramer, W. Modeling the Sensitivity of the Seasonal Cycle of GPP to Dynamic LAI and Soil Depths in Tropical Rainforests. *Ecosystems*, 12(4):517–533, 2009. doi: 10.1007/s10021-009-9238-4.

Prentice, I. C., Sykes, M. T., and Cramer, W. A simulation model for the transient effects of climate change on forest landscapes. *Ecological Modelling*, 65(1-2):51–70, 1993. doi: 10.1016/0304-3800(93)90126-D.

Pretzsch, H. *Forest Dynamics, Growth and Yield*. Springer Berlin Heidelberg, Berlin, Heidelberg, 2010. ISBN 978-3-540-88306-7. doi: 10.1007/978-3-540-88307-4.

Pütz, S., Groeneveld, J., Henle, K., Knogge, C., Martensen, A. C., Metz, M., Metzger, J. P., Ribeiro, M. C., de Paula, M. D., and Huth, A. Long-term carbon loss in fragmented Neotropical forests. *Nature Communications*, 5:5037, 2014. doi: 10.1038/ncomms6037.

Quesada, C. a., Phillips, O. L., Schwarz, M., Czimczik, C. I., Baker, T. R., Patiño, S., Fyllas, N. M., Hodnett, M. G., Herrera, R., Almeida, S., Alvarez Dávila, E., Arneth, A., Arroyo, L., Chao, K. J., Dezzeo, N., Erwin, T., di Fiore, A., Higuchi, N., Honorio Coronado, E., Jimenez, E. M., Killeen, T., Lezama, a. T., Lloyd, G., López-González, G., Luizão, F. J., Malhi, Y., Monteagudo, A., Neill, D. a., Núñez Vargas, P., Paiva, R., Peacock, J., Peñuela, M. C., Peña Cruz, A., Pitman, N., Priante Filho, N., Prieto, A., Ramírez, H., Rudas, A., Salomão, R., Santos, a. J. B., Schmerler, J., Silva, N., Silveira, M., Vásquez, R., Vieira, I., Terborgh, J., and Lloyd, J. Basin-wide variations in Amazon forest structure and function are mediated by both soils and climate. *Biogeosciences*, 9(6):2203–2246, 2012. doi: 10.5194/bg-9-2203-2012.

Rammig, A., Jupp, T., Thonicke, K., Tietjen, B., Heinke, J., Ostberg, S., Lucht, W., Cramer, W., and Cox, P. Estimating the risk of Amazonian forest dieback. *New Phytologist*, 187(3):694–706, 2010. doi: 10.1111/j.1469-8137.2010.03318.x.

Ranson, K. J., Sun, G., Knox, R. G., Levine, E. R., Weishampel, J. F., and Fifer, S. T. Northern forest ecosystem dynamics using coupled models and remote sensing. *Remote Sensing of Enviromental*, 75(00):291–302, 2001.

Rebmann, C., Zeri, M., Lasslop, G., Mund, M., Kolle, O., Schulze, E.-D., and Feigenwinter, C. Treatment and assessment of the CO2-exchange at a complex forest site in Thuringia, Germany. *Agricultural and Forest Meteorology*, 150(5):684–691, 2010. doi: 10.1016/j.agrformet.2009.11.001.

Reich, P. B., Walters, M. B., and Ellsworth, D. S. From tropics to tundra: global convergence in plant functioning. *Proceedings of the National Academy of Sciences of the United States of America*, 94(25):13730–4, 1997.

Reichstein, M., Falge, E., Baldocchi, D., Papale, D., Aubinet, M., Berbigier, P., Bernhofer, C., Buchmann, N., Gilmanov, T., Granier, A., Grunwald, T., Havrankova, K., Ilvesniemi, H., Janous, D., Knohl, A., Laurila, T., Lohila, A., Loustau, D., Matteucci, G., Meyers, T., Miglietta, F., Ourcival, J.-M., Pumpanen, J., Rambal, S., Rotenberg, E., Sanz, M., Tenhunen, J., Seufert, G., Vaccari, F., Vesala, T., Yakir, D., and Valentini, R. On the separation of net ecosystem exchange into assimilation and ecosystem respiration: review and improved algorithm. *Global Change Biology*, 11(9):1424–1439, 2005. doi: 10.1111/j.1365-2486.2005.001002.x.

Réjou-Méchain, M., Muller-Landau, H. C., Detto, M., Thomas, S. C., Le Toan, T., Saatchi, S. S., Barreto-Silva, J. S., Bourg, N. a., Bunyavejchewin, S., Butt, N., Brockelman, W. Y., Cao, M., Cárdenas, D., Chiang, J.-M., Chuyong, G. B., Clay, K., Condit, R., Dattaraja, H. S., Davies, S. J., Duque, A., Esufali, S., Ewango, C., Fernando, R. H. S., Fletcher, C. D., Gunatilleke, I. a. U. N., Hao, Z., Harms, K. E., Hart, T. B., Hérault, B., Howe, R. W., Hubbell, S. P., Johnson, D. J., Kenfack, D., Larson, a. J., Lin, L., Lin, Y., Lutz, J. a., Makana, J.-R., Malhi, Y., Marthews, T. R., McEwan, R. W., McMahon, S. M., McShea, W. J., Muscarella, R., Nathalang, A., Noor, N. S. M., Nytch, C. J., Oliveira, a. a., Phillips, R. P., Pongpattananurak, N., Punchi-Manage, R., Salim, R., Schurman, J., Sukumar, R., Suresh, H. S., Suwanvecho, U., Thomas, D. W., Thompson, J., Uríarte, M., Valencia, R., Vicentini, A., Wolf, a. T., Yap, S., Yuan, Z., Zartman, C. E., Zimmerman, J. K., and Chave, J. Local spatial structure of forest biomass and its consequences for remote sensing of carbon stocks. *Biogeosciences*, 11(23):6827–6840, 2014. doi: 10.5194/bg-11-6827-2014.

Rödig, E., Cuntz, M., Heinke, J., Rammig, A., and Huth, A. Spatial heterogeneity of biomass and forest structure of the Amazon rain forest: Linking remote sensing, forest modelling and field inventory. *Global Ecology and Biogeography*, 26(11):1292–1302, 2017a. doi: 10.1111/geb.12639.

Rödig, E., Huth, A., Bohn, F., Rebmann, C., and Cuntz, M. Estimating the carbon fluxes of forests with an individual-based forest model. *Forest Ecosystems*, 4(1):4, 2017b. doi: 10.1186/s40663-017-0091-1.

Rosette, J., Suárez, J., Nelson, R., Los, S., Cook, B., and North, P. Lidar Remote Sensing for Biomass Assessment. In Fatoyinbo, L., editor, *Remote Sensing of Biomass - Principles and Applications*, volume 24, pp. 3–27. InTech, 2012. ISBN 978-953-51-0313-4. doi: 10.5772/696.

Running, S. W., Nemani, R. R., Heinsch, F. A., Zhao, M., Reeves, M., and Hashimoto, H. A Continuous Satellite-Derived Measure of Global Terrestrial Primary Production.

BioScience, 54(6):547, 2004. doi: 10.1641/0006-3568(2004)054[0547:ACSMOG]2.0.CO;2.

Ryan, M. G. A simple method for estimating gross carbon budgets for vegetation in forest ecosystems. *Tree Physiology*, 9(1-2):255–266, 1991. doi: 10.1093/treephys/9.1-2.255.

Saatchi, S., Asefi-Najafabady, S., Malhi, Y., Aragão, L. E. O. C., Anderson, L. O., Myneni, R. B., and Nemani, R. Persistent effects of a severe drought on Amazonian forest canopy. *Proceedings of the National Academy of Sciences of the United States of America*, 110(2):565–70, 2013. doi: 10.1073/pnas.1204651110.

Saatchi, S., Mascaro, J., Xu, L., Keller, M., Yang, Y., Duffy, P., Espírito-Santo, F., Baccini, A., Chambers, J., and Schimel, D. Seeing the forest beyond the trees. *Global Ecology and Biogeography*, 24(5):606–610, 2015. doi: 10.1111/geb.12256.

Saatchi, S. S., Harris, N. L., Brown, S., Lefsky, M., Mitchard, E. T. a., Salas, W., Zutta, B. R., Buermann, W., Lewis, S. L., Hagen, S., Petrova, S., White, L., Silman, M., and Morel, A. Benchmark map of forest carbon stocks in tropical regions across three continents. *Proceedings of the National Academy of Sciences of the United States of America*, 108(24):9899–904, 2011. doi: 10.1073/pnas.1019576108.

Saatchi, S. S., Houghton, R. A., Dos Santos Alvalá, R. C., Soares, J. V., and Yu, Y. Distribution of aboveground live biomass in the Amazon basin. *Global Change Biology*, 13(4):816–837, 2007. doi: 10.1111/j.1365-2486.2007.01323.x.

Sakschewski, B., von Bloh, W., Boit, A., Poorter, L., Peña-Claros, M., Heinke, J., Joshi, J., and Thonicke, K. Resilience of Amazon forests emerges from plant trait diversity. *Nature Climate Change*, 6(11):1032–1036, 2016. doi: 10.1038/nclimate3109.

Sakschewski, B., von Bloh, W., Boit, A., Rammig, A., Kattge, J., Poorter, L., Penuelas, J., and Thonicke, K. Leaf and stem economics spectra drive diversity of functional plant traits in a dynamic global vegetation model. *Global Change Biology*, pp. 1–15, 2015. doi: 10.1111/gcb.12870.

Saleska, S. R., Miller, S. D., Matross, D. M., Goulden, M. L., Wofsy, S. C., da Rocha, H. R., de Camargo, P. B., Crill, P., Daube, B. C., de Freitas, H. C., Hutyra, L., Keller, M., Kirchhoff, V., Menton, M., Munger, J. W., Pyle, E. H., Rice, A. H., and Silva, H. Carbon in Amazon forests: unexpected seasonal fluxes and disturbance-induced losses. *Science (New York, N.Y.)*, 302(5650):1554–7, 2003. doi: 10.1126/science.1091165.

Samaniego, L., Kumar, R., and Attinger, S. Multiscale parameter regionalization of a grid-based hydrologic model at the mesoscale. *Water Resources Research*, 46(5):n/a–n/a, 2010. doi: 10.1029/2008WR007327.

Sato, H., Itoh, A., and Kohyama, T. SEIB–DGVM: A new Dynamic Global Vegetation Model using a spatially explicit individual-based approach. *Ecological Modelling*, 200(3-4):279–307, 2007. doi: 10.1016/j.ecolmodel.2006.09.006.

Scherstjanoi, M., Kaplan, J. O., Thürig, E., and Lischke, H. GAPPARD: A computationally efficient method of approximating gap-scale disturbance in vegetation models. *Geoscientific Model Development*, 6(5):1517–1542, 2013. doi: 10.5194/gmd-6-1517-2013.

Schimel, D. Terrestrial ecosystems and the carbon cycle. *Global Change Biology*, 1(October 1994):77–91, 1995. doi: 10.1111/j.1365-2486.1995.tb00008.x.

Schimel, D., Pavlick, R., Fisher, J. B., Asner, G. P., Saatchi, S., Townsend, P., Miller, C., Frankenberg, C., Hibbard, K., and Cox, P. Observing terrestrial ecosystems and the carbon cycle from space. *Global Change Biology*, 21(5):1762–1776, 2015. doi: 10.1111/gcb.12822.

Schulze, E.-D. CLIMATE CHANGE: Managing Forests After Kyoto. *Science*, 289(5487):2058–2059, 2000. doi: 10.1126/science.289.5487.2058.

Schumacher, S., Bugmann, H., and Mladenoff, D. J. Improving the formulation of tree growth and succession in a spatially explicit landscape model. *Ecological Modelling*, 180(1):175–194, 2004. doi: 10.1016/j.ecolmodel.2003.12.055.

Seidl, R., Rammer, W., Scheller, R. M., and Spies, T. a. An individual-based process model to simulate landscape-scale forest ecosystem dynamics. *Ecological Modelling*, 231:87–100, 2012. doi: 10.1016/j.ecolmodel.2012.02.015.

Sellers, P., Berry, J., Collatz, G., Field, C., and Hall, F. Canopy reflectance, photosynthesis, and transpiration. III. A reanalysis using improved leaf models and a new canopy integration scheme. *Remote Sensing of Environment*, 42(3):187–216, 1992. doi: 10.1016/0034-4257(92)90102-P.

Shugart, H. H. *A Theory of Forest Dynamics*. The Blackburn Press, New Jersey, 1984.

Shugart, H. H., Asner, G. P., Fischer, R., Huth, A., Knapp, N., Le Toan, T., and Shuman, J. K. Computer and remote-sensing infrastructure to enhance large-scale testing of individual-based forest models. *Frontiers in Ecology and the Environment*, 13(9):503–511, 2015. doi: 10.1890/140327.

Simard, M., Pinto, N., Fisher, J. B., and Baccini, A. Mapping forest canopy height globally with spaceborne lidar. *Journal of Geophysical Research*, 116(G4):G04021, 2011. doi: 10.1029/2011JG001708.

Sitch, S., Huntingford, C., Gedney, N., Levy, P. E., Lomas, M., Piao, S. L., Betts, R., Ciais, P., Cox, P., Friedlingstein, P., Jones, C. D., Prentice, I. C., and Woodward, F. I.

Evaluation of the terrestrial carbon cycle, future plant geography and climate-carbon cycle feedbacks using five Dynamic Global Vegetation Models (DGVMs). *Global Change Biology*, 14(9):2015–2039, 2008. doi: 10.1111/j.1365-2486.2008.01626.x.

Sitch, S., Smith, B., Prentice, I. C., Arneth, A., Bondeau, A., Cramer, W., Kaplan, J. O., Levis, S., Lucht, W., Sykes, M. T., Thonicke, K., and Venevsky, S. Evaluation of ecosystem dynamics, plant geography and terrestrial carbon cycling in the LPJ dynamic global vegetation model. *Global Change Biology*, 9(2):161–185, 2003. doi: 10.1046/j.1365-2486.2003.00569.x.

Slatyer, R. O. The Significance of the Permanent Wilting Percentage in Studies of Plant and Soil Water Relations. *Botanical Review*, 23(10):585–636, 1957.

Smith, B., Prentice, I. C., and Sykes, M. T. Representation of vegetation dynamics in the modelling of terrestrial ecosystems: comparing two contrasting approaches within European climate space. *Global Ecology and Biogeography*, 10(6):621–637, 2008. doi: 10.1046/j.1466-822X.2001.t01-1-00256.x.

Sonntag, M. *Klimaveraenderung und Waldwachstum: TREEDYN3- Simulationen mit einer Analyse modellstruktureller Unsicherheiten*. PhD thesis. Universitaet Gesamthochschule Kassel., 1998.

Sperry, J. S., Hacke, U. G., Oren, R., and Comstock, J. P. Water deficits and hydraulic limits to leaf water supply. *Plant, Cell and Environment*, 25(2):251–263, 2002. doi: 10.1046/j.0016-8025.2001.00799.x.

ter Steege, H., Pitman, N. C. A., Sabatier, D., Baraloto, C., Salomao, R. P., Guevara, J. E., Phillips, O. L., Castilho, C. V., Magnusson, W. E., Molino, J., Monteagudo, A., Nunez Vargas, P., Montero, J. C., Feldpausch, T. R., Coronado, E. N. H., Killeen, T. J., Mostacedo, B., Vasquez, R., Assis, R. L., Terborgh, J., Wittmann, F., Andrade, A., Laurance, W. F., Laurance, S. G. W., Marimon, B. S., Marimon, B., Guimaraes Vieira, I. C., Amaral, I. L., Brienen, R., Castellanos, H., Cardenas Lopez, D., Duivenvoorden, J. F., Mogollon, H. F., Matos, F. D. d. A., Davila, N., Garcia-Villacorta, R., Stevenson Diaz, P. R., Costa, F., Emilio, T., Levis, C., Schietti, J., Souza, P., Alonso, A., Dallmeier, F., Montoya, A. J. D., Fernandez Piedade, M. T., Araujo-Murakami, A., Arroyo, L., Gribel, R., Fine, P. V. A., Peres, C. A., Toledo, M., Aymard C., G. A., Baker, T. R., Ceron, C., Engel, J., Henkel, T. W., Maas, P., Petronelli, P., Stropp, J., Zartman, C. E., Daly, D., Neill, D., Silveira, M., Paredes, M. R., Chave, J., Lima Filho, D. d. A., Jorgensen, P. M., Fuentes, A., Schongart, J., Cornejo Valverde, F., Di Fiore, A., Jimenez, E. M., Penuela Mora, M. C., Phillips, J. F., Rivas, G., van Andel, T. R., von Hildebrand, P., Hoffman, B., Zent, E. L., Malhi, Y., Prieto, A., Rudas, A., Ruschell, A. R., Silva, N., Vos, V., Zent, S., Oliveira, A. A., Schutz, A. C., Gonzales, T., Trindade Nascimento, M., Ramirez-Angulo, H., Sierra, R., Tirado, M., Umana Medina, M. N., van der Heijden, G., Vela, C. I. A., Vilanova Torre, E., Vriesendorp, C., Wang, O., Young, K. R., Baider, C., Balslev, H.,

Ferreira, C., Mesones, I., Torres-Lezama, A., Urrego Giraldo, L. E., Zagt, R., Alexiades, M. N., Hernandez, L., Huamantupa-Chuquimaco, I., Milliken, W., Palacios Cuenca, W., Pauletto, D., Valderrama Sandoval, E., Valenzuela Gamarra, L., Dexter, K. G., Feeley, K., Lopez-Gonzalez, G., and Silman, M. R. Hyperdominance in the Amazonian Tree Flora. *Science*, 342(6156):1243092–1243092, 2013. doi: 10.1126/science.1243092.

Tang, H. and Dubayah, R. Light-driven growth in Amazon evergreen forests explained by seasonal variations of vertical canopy structure. *Proceedings of the National Academy of Sciences*, 114(10):2640–2644, 2017. doi: 10.1073/pnas.1616943114.

Tans, P. and Keeling, R. Trends in Atmospheric Carbon Dioxide. www.esrl.noaa.gov/gmd/ccgg/trends/. 2017.

Taubert, F. *Modelling and analysing the structure and dynamics of species-rich grasslands and forests. Universität Osnabrück. PhD Dissertation*. Helmholtz-Zentrum für Umweltforschung - UFZ, Leipzig, 2014.

Thornley, J. and Johnson, I. *Plant and crop modelling: a mathematical approach to plant and crop physiology*, volume 37. Oxford University Press, 1990. doi: https://doi.org/10.1016/0308-521X(91)90064-H.

Tietjen, B. and Huth, A. Modelling dynamics of managed tropical rainforests—An aggregated approach. *Ecological Modelling*, 199(4):421–432, 2006. doi: 10.1016/j.ecolmodel.2005.11.045.

Tjoelker, M. G., Oleksyn, J., and Reich, P. B. Modelling respiration of vegetation: evidence for a general temperature-dependent Q10. *Global Change Biology*, 7(2):223–230, 2001. doi: 10.1046/j.1365-2486.2001.00397.x.

Tucker, C. J., Townshend, J. R., and Goff, T. E. African Land-Cover Classification Using Satellite Data. *Science*, 227(4685):369–375, 1985. doi: 10.1126/science.227.4685.369.

Turner, W., Spector, S., Gardiner, N., Fladeland, M., Sterling, E., and Steininger, M. Remote sensing for biodiversity science and conservation. *Trends in Ecology & Evolution*, 18(6):306–314, 2003. doi: 10.1016/S0169-5347(03)00070-3.

Verbeeck, H., Peylin, P., Bacour, C., Bonal, D., Steppe, K., and Ciais, P. Seasonal patterns of CO 2 fluxes in Amazon forests: Fusion of eddy covariance data and the ORCHIDEE model. *Journal of Geophysical Research*, 116(G2):G02018, 2011. doi: 10.1029/2010JG001544.

Vermeulen, M. H., Kruijt, B., and Kabat, P. Modelling short term variability in carbon and water exchange in a Dutch pine forest. *Earth System Dynamics*, 14(2):5575, 2015. doi: 10.5194/esd-6-485-2015.

Weedon, G. P., Balsamo, G., Bellouin, N., Gomes, S., Best, M. J., and Viterbo, P. The WFDEI meteorological forcing data set: WATCH Forcing Data methodology applied to ERA-Interim reanalysis data. *Water Resources Research*, 50(9):7505–7514, 2014. doi: 10.1002/2014WR015638.

van der Werf, G. R., Morton, D. C., DeFries, R. S., Olivier, J. G. J., Kasibhatla, P. S., Jackson, R. B., Collatz, G. J., and Randerson, J. T. CO2 emissions from forest loss. *Nature Geoscience*, 2(11):737–738, 2009. doi: 10.1038/ngeo671.

Wieder, W., Boehnert, J., Bonan, G., and Langseth, M. Regridded Harmonized World Soil Database v1.2. Data set. Available on-line [http://daac.ornl.gov] from Oak Ridge National Laboratory Distributed Active Archive Center, Oak Ridge, Tennessee, USA. 2014. doi: http://dx.doi.org/10.3334/ORNLDAAC/1247.

Wilson, A. M. and Jetz, W. Remotely Sensed High-Resolution Global Cloud Dynamics for Predicting Ecosystem and Biodiversity Distributions. *PLOS Biology*, 14(3):e1002415, 2016. doi: 10.1371/journal.pbio.1002415.

Zaitchik, B. F., Macalady, A. K., Bonneau, L. R., and Smith, R. B. Europe's 2003 heat wave: A satellite view of impacts and land - Atmosphere feedbacks. *International Journal of Climatology*, 26(6):743–769, 2006. doi: 10.1002/joc.1280.

Zhao, M., Heinsch, F. A., Nemani, R. R., and Running, S. W. Improvements of the MODIS terrestrial gross and net primary production global data set. *Remote Sensing of Environment*, 95(2):164–176, 2005. doi: 10.1016/j.rse.2004.12.011.

Zhao, M. and Running, S. W. Drought-Induced Reduction in Global. *Science*, 329(5994):940–943, 2010. doi: 10.1126/science.1192666.

Erklärung über die Eigenständigkeit der erbrachten wissenschaftlichen Leistung

Ich erkläre hiermit, dass ich die vorliegende Arbeit ohne unzulässige Hilfe Dritter und ohne Benutzung anderer als der angegebenen Hilfsmittel angefertigt habe. Die aus anderen Quellen direkt oder indirekt übernommenen Daten und Konzepte sind unter Angabe der Quelle gekennzeichnet.

Bei der Auswahl und Auswertung folgenden Materials haben mir die nachstehend aufgeführten Personen in der jeweils beschriebenen Weise unentgeltlich geholfen.

Kapitel 1: Kommentare und Sprachliche Korrekturen: Andreas Huth.

Kapitel 2: Ko-Autoren des Manuskripts: Andreas Huth, Friedrich Bohn, Corinna Rebmann, Matthias Cuntz.

Kapitel 3: Ko-Autoren des Manuskripts: Matthias Cuntz, Jens Heinke, Anja Rammig, Andreas Huth.

Kapitel 4: Ko-Autoren des Manuskripts: Matthias Cuntz, Anja Rammig, Rico Fischer, Jens Heinke, Franziska Taubert, Andreas Huth.

Kapitel 5: Kommentare und Sprachliche Korrekturen: Andreas Huth.

Weitere Personen waren an der inhaltlichen materiellen Erstellung der vorliegenden Arbeit nicht beteiligt. Insbesondere habe ich hierfür nicht die entgeltliche Hilfe von Vermittlungs- bzw. Beratungsdiensten (Promotionsberater oder andere Personen) in Anspruch genommen. Niemand hat von mir unmittelbar oder mittelbar geldwerte Leistungen für Arbeiten erhalten, die im Zusammenhang mit dem Inhalt der vorgelegten Dissertation stehen.

Die Arbeit wurde bisher weder im In- noch im Ausland in gleicher oder ähnlicher Form einer anderen Prüfungsbehörde vorgelegt.

_____ _____

Ort, Datum Unterschrift